Title
THE ROLE OF ORGANIC CATION TRANSPORTERS IN THE PHARMACOKINETICS AND PHARMACODYNAMICS OF METFORMIN

Author
Chen, Eugene Chia-Te

Publication Date
2015

Peer reviewed|Thesis/dissertation

THE ROLE OF ORGANIC CATION TRANSPORTERS IN THE PHARMACOKINETICS AND PHARMACODYNAMICS OF METFORMIN

by

Eugene Chia-Te Chen

DISSERTATION

Submitted in partial satisfaction of the requirements for the degree of

DOCTOR OF PHILOSOPHY

in

Pharmaceutical Sciences and Pharmacogenomics

in the

GRADUATE DIVISION

To my parents, Pwu and Lydia — for their endless love and support.

To my wife, Ivy, who makes my life worthwhile.

ACKNOWLEDGEMENTS

I would never have been able to finish my dissertation without the guidance of my committee members, help from colleagues and collaborators, and support from my family and friends.

First and foremost, I would like to express my deepest gratitude to my advisor, Dr. Kathy Giacomini, for her encouragement, patience, support, and guidance over the past 5 years. I've learned so much from Dr. Giacomini, yet I know it would take my lifetime to learn everything she has to offer. All I can do is to absorb as much as I can. Besides my parents, no body has ever done so much for me. I am eternally grateful to Dr. Giacomini, and she has my greatest respect. I am honored and proud to be her student. I would also like to thank the members of my thesis committee, Dr. Les Benet and Dr. Kaveh Ashrafi, for the assistance and critique they provided of my research projects.

I must also acknowledge colleagues and collaborators, without whom I would not be able to finish my projects. I would like to thank Dr. Natalia Khuri for her brilliant computational work for the OCT1 project, and Dr. Pär Matsson for his computational analysis on the OCT3 screening project. I would also like to thank all the past and current members of the Giacomini lab, particularly Dr. Sook Wah Yee for all her help and Dr. Kari Morrissey for the encouragement.

I would like to thank my friends who helped me through this sometimes stressful but overall wonderful experience. Peter Westcott and I became fast friend after the new student orientation, and he is an integral part of my graduate career. I will forever treasure all our discussions, debates, and the late-night pondering of our existence and place in the universe. I would also like to thank Dr. Ethan Geier and Xiaomin Liang. I really appreciate your friendship and enjoyed our time working together.

Finally, I recognize that this research would not have been possible without the financial support from National Institute of Health, Center for Drug Evaluation and Research, and the University of California, San Francisco, and express my gratitude to these agencies.

ABSTRACT

The Role of Organic Cation Transporters in the Pharmacokinetics and Pharmacodynamics of Metformin

Eugene Chia-Te Chen

Metformin, the most widely prescribed anti-diabetic drug, requires transporters to enter tissues involved in its pharmacologic action, including liver, kidney and peripheral tissues. Although membrane transporters responsible for the liver and kidney uptake of metformin have been identified, the mechanism in which metformin enters peripheral tissues is not completely understood. Organic cation transporter 3 (OCT3, *SLC22A3*) transports metformin *in vitro* and is expressed ubiquitously. The goals of this research are to determine the role of OCT3 in metformin disposition and response, identify OCT3 inhibitors that could potentially result in clinical drug-drug interactions when co-administered with metformin, and develop a method to predict competitive and non-competitive inhibitors of transporters.

In this dissertation, we showed that ablation of *Oct3* in mice results in dramatic changes in the pharmacokinetics of metformin. In particular, the apparent volume of distribution, clearance and bioavailability of metformin were decreased in Oct3 knockout mice. We also showed that *Oct3* knockout mice had reduced response to

metformin. Notably, the effect of metformin on glucose tolerance is reduced in mice lacking *Oct3*, and that a likely explanation for this is reduced metformin accumulation in peripheral sites such as adipose tissue. Analysis of data from healthy volunteers receiving metformin revealed that a reduced function *OCT3* genetic variant associated with attenuated response to metformin. In addition, we developed and conducted a high-throughput screen (HTS) against a large library of 2,556 prescription drugs and bioactive compounds for OCT3 inhibitors. We identified 210 potent OCT3 inhibitors, 23 of which could potentially cause drug-drug interactions with metformin. In order to enhance our currently limited understanding of inhibitor-transporter interactions, we developed a methodology combining structure-based and cell-based HTS to rapidly identify competitive and non-competitive inhibitors of OCT1, a paralog of OCT3, which plays a critical role in metformin disposition and response. Our method has broad implications for using combined *in silico* and HTS methods to not only identify ligands of transporters, but to understand their mechanisms of interaction with transporters.

Our findings have important implications for understanding metformin disposition and pharmacologic response, and pave the way for future studies of OCT3-mediated drug-drug interactions. Additionally, the combined modeling and HTS methodology we developed can accelerate transporter inhibition studies that are mandated by regulatory agencies during drug development.

TABLE OF CONTENTS

LIST OF TABLES

LIST OF FIGURES

CHAPTER 1

The Physiological and Pharmacological Role of Organic Cation Transporter 3

INTRODUCTION

Organic cation transporter 3 (OCT3, *SLC22A3*) is a member of the polyspecific organic cation transporters (OCTs). Unlike many members of the solute carriers (SLC) superfamily, which transport specific nutrients or endogenous compounds, OCTs mediate the transport of a wide variety of endogenous compounds and xenobiotics[1]. Studies have shown that organic cation transporter 1 (OCT1, *SLC22A1*) and organic cation transporter 2 (OCT2, *SLC22A2*) transport drugs and play a role in the disposition and efficacy of their substrates *in vivo*, but less is known about OCT3 in this regard. Like OCT1 and OCT2, OCT3 mediates the bi-directional transport of small (less than 500 dalton) cationic compounds independent of sodium and proton gradients in an electrogenic manner[2]. Studies have also shown that OCT3 is capable of transporting many drugs *in vitro* or in animal models, suggesting an emerging role of OCT3 in drug development.

OCT3 is closely related to OCT1 and OCT2 based on sequence similarity[1]. It is predicted to consist of 12 transmembrane domains (TMDs), a large extracellular loop between TMD 1 and 2, and a large intracellular loop between TMD 6 and 7. Unlike OCT1 and OCT2, which are primarily expressed in the liver and kidney, the mRNA of

OCT3 is detected in almost all tissues and at higher levels in adipose tissue, lung, prostate, and skeletal muscle. Notably, OCT3 is expressed in the blood brain barrier and term placenta, implicating a role in regulating the movement of environmental chemicals, endogenous compounds, and drugs across these protective barriers[3,4].

OCT3 was first cloned and characterized in 1998, and the first *Oct3* knockout mouse strain was generated in 2001. Originally considered to be the extraneuronal monoamine transporter, OCT3 has since been implicated in many biological processes, diseases, and in drug disposition and response. This chapter will summarize our current understanding of OCT3, with particular emphasis on its physiological and pharmacological roles.

PHYSIOLOGICAL FUNCTION OF OCT3

Brain

Catecholamines are monoamines that serve as neurotransmitters in the central nervous system and as hormones in tissues innervated by the sympathetic nervous system[5]. In the brain, the released catecholamines are recycled at the presynaptic cleft by high-affinity, low-capacity reuptake transporters, including the dopamine transporter (DAT)[6], noradrenaline transporter (NET)[7], and serotonin transporter (SERT)[8]. In the peripheral tissues, the actions of catecholamines are terminated by catechol-O-methyltraferase (COMT)[9] and monoamine oxidases[10]. It has been hypothesized that a

different set of transporters that work in conjunction with these metabolizing enzymes exists to regulate levels of circulating catecholamines. In contrast to the reuptake transporters in the brain, the proposed transporters should transport catecholamines in a low-affinity, high-capacity manner, consistent with their lower levels in peripheral tissues, and be inhibited by corticosterone, which has been shown to inhibit tissue uptake of catecholamines[11]. Indeed, OCTs fit this profile, and OCT3, in particular, has been proposed to be the major component of this alternative catecholamine transport system, because of its broad peripheral tissue distribution and capacity to transport adrenaline, noradrenaline, serotonin (5-HT), and the neurotoxin MPP^{+}[12]. Interestingly, several studies using different methodologies showed that OCT3 is expressed in neuronal cells in the brain[5,13,14], thus raising the possibility for a physiological role of the transporter in the reuptake of neurotransmitters in the central nervous system.

It has been hypothesized that OCT3 acts as a scavenger and transports catecholamines that escape the high-affinity, low-capacity reuptake transporters. Furthermore, OCT3 has been shown to partly co-localize with a catecholamine-metabolizing enzyme, MAOB[15]. Based on this observation, OCT3 may play a role in modulating neurotransmitter levels in the brain. Indeed, it has been proposed that the delayed action of norepinephrine reuptake inhibitors is caused by the compensatory action of OCT3. Therefore, an antidepressant that also inhibits OCT3 could speed up the pharmacological effect by preventing catecholamine uptake and increasing the local levels of norepinephrine[16]. Several studies have investigated the role of OCT3 in the brain using animal models. Using antisense oligodeoxynucleotide to knockdown

OCT3 in mice, Kitaichi *et al.* showed that mice with reduced OCT3 expression exhibit increased locomotor activity in both a forced swimming test and psychostimulant-induced hyperlocomotion. The authors hypothesized that the observations were the result of an increased level of monoamines in the brain[17]. Further support for a physiological role of OCT3 in the brain was provided by studies that showed that *Oct3* knockout mice exhibit increased activity and less anxiety in elevated-maze and open field tests, arguing for a role of OCT3 in regulation of fear and anxiety, presumably by modulating serotonin levels[18]. In a separate study, Cui *et al.* showed that *Oct3* knockout mice have difficulties clearing excess extracellular dopamine induced by methamphetamine, resulting in dopaminergic cell death[19]. Collectively, these results support the hypothesized role of OCT3 as a catecholamine scavenger in the central nervous system, and OCT3 as a possible target for pharmaceutical agents.

Immune Response

In addition to its presumed role in the central nervous system, OCT3 appears to play an important role in immune function, and in particular in basophils. Basophils are the least common of the peripheral blood leukocytes. Since their discovery by light microscopy more than 150 years ago, basophils were considered to be a minor and redundant player in immune response, partly due to the low number and the difficulty inherent in isolating these cells. Basophils did not receive much attention until the 1990s when it was discovered that they release large amounts of cytokines and play an important role in allergic disease and parasitic infections[20]. Basophils synthesize many

interleukins (ILs) and histamine, which they release when induced by various stimuli. Interestingly, exogenous histamine inhibits its own production, as well as that of IL-4, IL-6, and IL-13, by basophils. Schneider *et al.* showed that this inhibitory effect is not mediated by histamine receptors, yet nevertheless requires the uptake of histamine into basophils[21]. In this study, the authors identified OCT3 as the transporter responsible for the uptake of histamine. Basophils isolated from *Oct3* knockout mice have significantly reduced histamine uptake, and the inhibitory effect of histamine on IL production was lost in basophils lacking OCT3, consistent with an intracellular target of histamine. Although it has been proposed that basophils store histamine in granules and release them by exocytosis[22], Schneider *et al.* showed increased intracellular histamine levels and reduced histamine release in basophils deficient in OCT3. These results suggest that OCT3 works bi-directionally in basophils, modulating the uptake of exogenous histamine and the release of histamine synthesized within basophils. These findings led to the proposal of targeting OCT3 as a way of fine tuning the innate immune response or alleviating the symptoms of certain allergic diseases[23].

Adipose Tissue

Although *OCT3* is expressed ubiquitously, mRNA transcript levels of *OCT3* vary from tissue to tissue. In human and mouse, *OCT3* is expressed at high levels in the adipose tissue, ranked at 81st percentile vs. pool and 92nd percentile vs. pool, respectively[24,25]. In fact, *OCT3* is the most highly expressed organic cation transporter in human[24] and mouse adipose tissue (see Chapter 2, Fig. 1). Currently, there is no

published research exploring the physiological role of OCT3 in adipose tissue, despite its high expression in this tissue. However, analyses of microarray data from two separate studies in mice suggest a role of OCT3 in diet-induced obesity. In one study[25], inbred male C57BL/6J mice were fed a high-fat diet beginning at 8 weeks of age, and adipose tissues were harvested from the top 10% weight gainers and the bottom 10% weight gainers after 14 weeks. *OCT3* expression was found to be significantly higher in the high weight gainer group compared with the low weight gainer group (Fig. 1.1A). In another study[26], gene expression patterns of mice fed normal diets and high-fat diets were analyzed. Interestingly, the transcript level of *OCT3* was more than 6 fold higher in mice fed a high-fat diet (Fig. 1.1B).

Motivated by these observations, a series of preliminary studies were conducted in our laboratory. Wildtype mice and *Oct3* knockout mice were maintained on a high-fat diet for 12 weeks, beginning at 6 weeks of age. We found that knockout mice had significantly attenuated weight gain and significantly smaller epididymal fat pads compared to wildtype mice (Fig. 1.2A, B). Since histamine can induce adipogenesis and lipolysis[27,28], immunohistochemical analysis of histamine was performed. We found that the extracellular level of histamine was higher in the knockout mice, supporting the hypothesis that OCT3 is involved in the elimination of peripheral catecholamines. However, further studies are needed to confirm these preliminary observations and to determine the role of OCT3 in adipose tissue and to investigate the possible involvement of central histamine in the phenotype we observed.

Regulation of OCT3

Recently, it was reported that there are multiple phosphorylation sites on the intracellular loop and the C-terminal tail of OCT1, and that phosphorylation by protein kinase C (PKC) stimulates OCT1 activity[29]. Because of the structure and sequence similarity, it is likely that OCT3 activity could be regulated by phosphorylation as well. Indeed, studies in an OCT3 overexpressing cell line showed that the activity of the transporter was significantly reduced by mitogen-activated protein kinase (MAPK) inhibitors[30]. However, the study did not determine whether the reduced activity directly resulted from reduced phosphorylation of OCT3 by MAPK or from one of its downstream effectors. In contrast to OCT1, the activity of OCT3 was not altered by PKC activators, or pan-inhibitors of PKA, PKC, and PKG. In addition, similar to many transporters[31–33], the activity of OCT3 was modulated by CA^{2+}/calmodulin mediated pathway[30].

Several studies have looked into the epigenetic and genetic regulation of OCT3. In mice, the *Igf2* gene cluster (*Igf2, Oct2, Oct3)* is a target of gene imprinting. The genes are silenced in a *cis*-acting mechanism and the silencing is mediated by the paternally expressed non-coding *Air* RNA[34]. A homolog of the *Air* RNA was found in human and certain features of the *IGF2* regulatory element were shown to be evolutionary conserved, however *IGF2* imprinting is believed to be rare and polymorphic in human[35]. A study from our laboratory also showed that common genetic variants in the promoter region of OCT3 exhibited stronger transcription factor-binding affinities and resulted in increased expression of the transporter[36]. Furthermore,

the study also showed that higher methylation level of the OCT3 promoter in prostate tumor samples was associated with lower OCT3 expression, indicating that OCT3 expression can be modulated by DNA methylation. Lastly, post-transcriptional control of OCT3 was also observed. OCT3 has a 3.9 kb 3'UTR region and, to date, more than 15 polymorphisms in the region are registered in the dbSNP database. One of the SNPs has been shown to be associated with lower OCT3 expression levels in liver samples[37]. In chapter 2, we also report a SNP in the 3'UTR region that is associated with lower OCT3 expression levels in adipose tissue samples. Future studies are needed to systematically investigate the SNPs in the 3'UTR region, and their role in the expression and function of OCT3.

PHARMACOLOGICAL ROLE OF OCT3

Metformin

Metformin is a widely prescribed biguanide and is the first-line oral therapy for type 2 diabetes. Although the mechanism of metformin is not yet fully understood, AMP-activated protein kinase (AMPK) activation has been proposed to mediate many of its actions. At least in part due to the activation of AMPK, metformin decreases hepatic glucose output and enhances glucose utilization in peripheral tissues, particularly skeletal muscle and adipose tissues[38]. Metformin has been shown *in vitro* to be a substrate of organic cation transporters (OCTs). Two members of the OCTs, OCT1 and OCT2, are expressed mainly in the liver and kidney, respectively, and their

roles in the disposition of metformin are well characterized[39,40]. However, less is known about the role of OCT3 in the disposition of metformin. A recent study showed that the C_{MAX} of metformin was significantly different between wildtype and *Oct3* knockout mice after oral administration[41]. This study also showed differences in metformin accumulation in several tissues between wildtype and knockout mice, including salivary gland and heart. The authors concluded that OCT3 contributes to the taste disturbance side-effect of metformin. However, this study did not address whether OCT3 plays a role in metformin accumulation in adipose tissue, and whether OCT3 plays a role in the pharmacological actions of metformin. In this dissertation research, studies are presented that do address these key issues related to metformin pharmacology.

Platinum Containing Antineoplastic

Platinum containing antineoplastics (platins) are powerful antitumor agents first approved by the FDA in 1978. Cisplatin was the first of its class and, thirty years after its approval, remains one of the most potent antitumor agents and is particularly beneficial for the treatment of ovarian and testicular cancer[42]. Since its approval, many analogues of cisplatin have been introduced, seeking to reduce toxicity or expand efficacy across a wider spectrum of cancers. One example is oxaliplatin, a third generation cisplatin analogue, effective in the treatment of colorectal cancer[43]. Several studies have investigated the role of organic cation transporters in the antitumor activity of platins. OCT1 and OCT2 have been shown to be major determinants of

oxaliplatin accumulation and cytotoxicity in cell lines over-expressing these transporters[44]. However, the role of OCT3 in the activity of platins remains controversial.

Zhang *et al.* first reported the involvement of OCT1 and OCT2 in oxaliplatin activity, but concluded that OCT3 does not transport oxaliplatin and cisplatin[44]. In the same year, another study reported that OCT3 is capable of transporting oxaliplatin and modulating oxaliplatin toxicity in cell lines over-expressing this transporter, albeit to a lesser degree compared to OCT2[45]. The two studies did agree that OCT3 does not transport cisplatin. Interestingly, Li *et al.* reported that OCT3 expression is down regulated in a cisplatin-resistant cervical cancer cell line. While OCT3 does not transport cisplatin in OCT3 over-expressing cell lines, shRNA knockdown of OCT3 in the parent cisplatin-sensitive cell line provided a small but significant degree of resistance to cisplatin[46]. However, this study did not address the mechanism of resistance or the clinical relevance of the slight increase in cisplatin resistance. The specificity of the shRNA was also not reported. Recently, Yookoo *et al.* showed that colorectal cancer cell lines expressing high levels of OCT3 accumulated more oxaliplatin and were more susceptible to its cytotoxic effect[47]. Finally, over-expression of OCT3 in colorectal cancer cell lines with low endogenous expression of OCT3 significantly increased oxaliplatin accumulation and sensitivity[47]. These results support the role of OCT3 in the accumulation and cytotoxicity of oxaliplatin. In addition, human colon cancer samples had significantly higher OCT3 expression compared to normal colon[47]. Since colorectal cancer is one of the main indications of oxaliplatin, these

findings have led to the proposal that OCT3 expression level in colorectal tumors could be used as a marker for oxaliplatin chemotherapy.

Long-Acting β_2-agonist

While the mRNA level of *OCT3* is high in human lung tissue relative to other tissues, OCT3 protein has been shown to localize to specific cell types or membranes[48]. Low levels of *OCT3* mRNA have been detected in airway epithelial cells[49], and immunohistochemical analysis revealed low levels of OCT3 in ciliated cells[48]. However, OCT3 was detected at high levels in the airway smooth muscle cells, basal cells, intermediate cells, and bronchial and pulmonary vessels[49,50]. Currently, our knowledge of OCT3 in the lung and its role in the disposition of inhaled drugs is limited, but a study by Horvath *et al.* proposed an interesting synergistic drug-drug interaction mediated by OCT3[50]. It was observed that asthmatic patients treated with the combination of inhaled corticosteroid and long-acting β_2-agonists responded better than those treated with either drug alone. Using cultured bronchial and vascular smooth muscle cells, the authors showed that the uptake of formoterol, a cationic β_2-agonist, was mediated by OCT3. The OCT3 mediated uptake in smooth muscle cells was inhibited by commonly co-administered inhaled corticosteroids, such as budesonide and fluticasone. Thus, the authors proposed that inhaled corticosteroids potentiate the effect of formoterol by inhibiting OCT3 and therefore interfering with the vascular clearance of the drug. While further studies are needed to confirm this effect

in vivo, these findings raise the interesting possibility of manipulating transporter activity in order to modulate inhaled drug delivery.

Figure 1.1

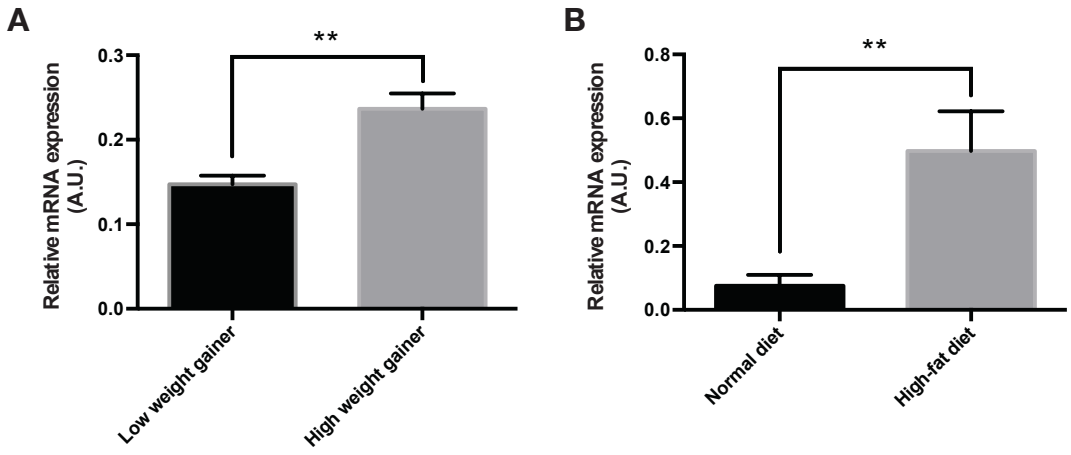

Figure 1.1. *OCT3* expression is increased in mice fed high-fat diet[25,26]. (A) *OCT3* mRNA levels in low and high weight gaining mice on high fat-diet for 8 weeks. (B) *OCT3* mRNA levels in mice fed with normal and high-fat diet for 11 weeks. Data represent mean ± SD, $n = 3$ mice per group, $^{**}P < 0.01$. The mRNA level of *OCT3* was normalized to beta-actin level in both analyses.

Figure 1.2

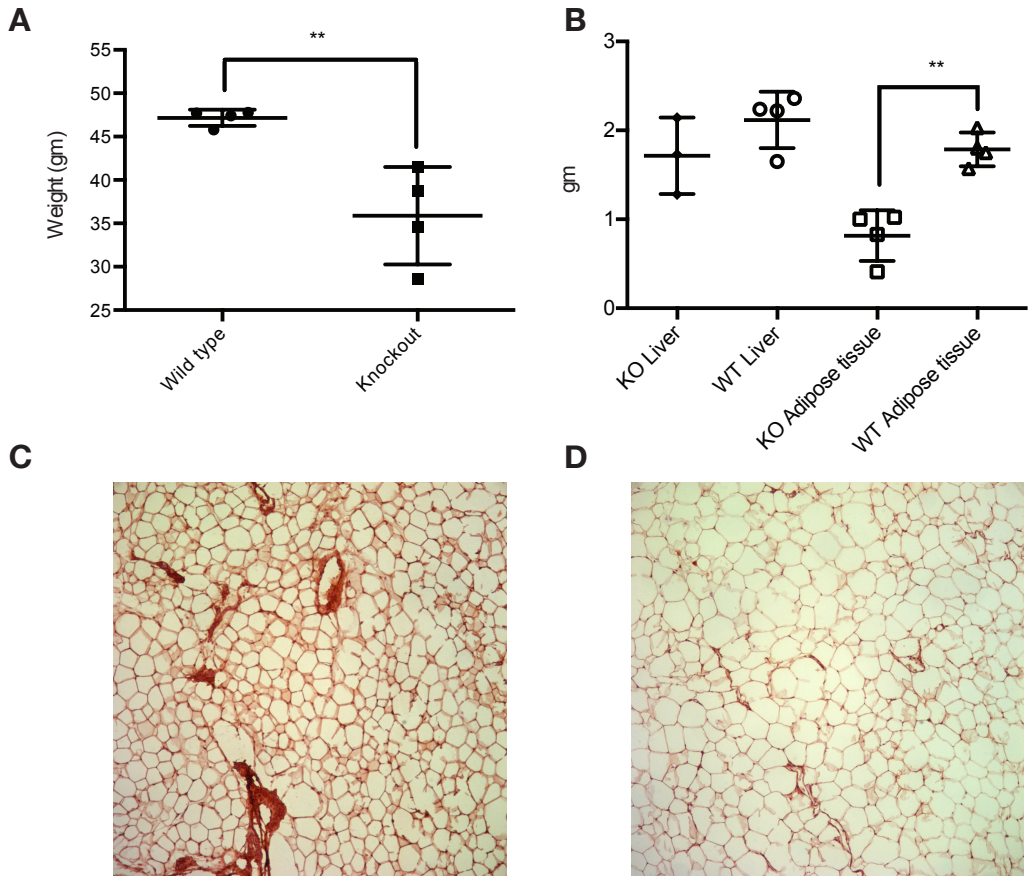

Figure 1.2. Attenuated weight gain in *Oct3* knockout mice. Wildtype and *Oct3* knockout mice were maintained on a high-fat diet for 12 weeks. (A) Wildtype mice gained significantly more weight than *Oct3* knockout mice. (B) The weight of epididymal adipose tissue in wildtype mice was significantly heavier than that in *Oct3* knockout mice. Immunohistochemistry of adipose tissue sections from *Oct3* knockout (C) and wildtype (D) mice reveals that extracellular histamine levels are higher in the adipose tissue of *Oct3* knockout mice. Data represent mean ± SD, $n = 4$ mice per group, $^{**}P < 0.01$.

CONCLUSION AND FUTURE DIRECTIONS

Since its discovery in 1998, many studies have explored the endogenous role of OCT3 because of its wide tissue expression and ability to transport catecholamines. These studies have revealed novel roles of OCT3 in normal physiology and implicated the transporter in many biological processes. However, these studies have largely focused on the central nervous system and the immune system, even though OCT3 is widely expressed and could play a role in the elimination of catecholamines in peripheral tissues innervated by the sympathetic nervous system, such as the adipose tissue where OCT3 is highly expressed. Preliminary studies have revealed that in adipose tissue, OCT3 is expressed primarily in mature adipocytes. *Oct3* knockout mice fed with high-fat diet gained less weight compared with wildtype mice and had smaller epididymal white adipose tissue depots. Immunohistochemical analysis revealed higher histamine levels in the adipose tissue of *Oct3* knockout mice, suggesting that Oct3 can modulate catecholamine levels in the peripheral tissues as well. Future studies are needed to confirm the findings and investigate the endogenous role of OCT3 in the adipose tissue.

In 2010, the International Transporter Consortium (ITC) published a recommendation detailing methodologies, data interpretations, and decision trees to guide clinical drug-drug interactions for key transporters, based on the available information at the time. Among the transporters recommended for testing in the ITC paper are OCT1 and OCT2, both of which are expressed primarily in the liver and kidney, respectively, and mediate the uptake of metformin, a widely prescribed

antidiabetic biguanide. Studies have shown that OCT1 and OCT2 could play a role in the disposition and efficacy of metformin *in vivo*[39,40]. Inhibitors of OCT1 and OCT2 therefore could potentially cause clinical drug-drug interactions when co-administered with metformin. Emerging evidence suggests that OCT3 could also play an important role in the pharmacokinetics and pharmacodynamics of metformin. First, OCT3 is capable of transporting metformin *in vitro*. Second, OCT3 is expressed ubiquitously, unlike OCT1 and OCT2. The large volume of distribution of metformin suggests wide tissue distribution, and OCT3 is expressed in many tissues implicated in the peripheral effect of metformin, such as skeletal muscle and adipose tissue [REF]. Further studies are needed to understand the role of OCT3 in the disposition and efficacy of metformin, and have been a focus on this dissertation research, which will be described next.

SUMMARY OF DISSERTATION CHAPTERS

Metformin is the recommended first-line oral therapy for type 2 diabetes, yet much remains to be understood regarding its mechanism of action. It has been proposed that metformin works by inhibiting gluconeogenesis centrally in the liver and increasing glucose utilization in the peripheral tissues, such as skeletal muscle and adipose tissue. While studies have shown that OCT1 and OCT2 transport metformin in the liver and kidney, respectively, the transporters responsible for the peripheral uptake of metformin remain to be identified. OCT3 transports metformin *in vitro* and is expressed at high levels in the proposed peripheral action sites of metformin. The goal of this research is to test the hypothesis that OCT3 plays a role in the pharmacokinetics and pharmacodynamics of metformin, and to identify potent OCT inhibitors that could potentially cause drug-drug interactions with metformin when co-administered. The results of this research are addressed in the following chapters.

Chapter 2. Targeted Disruption of Organic Cation Transporter 3 (Oct3) Attenuates the Pharmacologic Response to Metformin

Metformin, the most widely prescribed anti-diabetic drug, requires transporters to enter tissues involved in its pharmacological action including liver, kidney and peripheral tissues. Organic cation transporter 3 (OCT3, *SLC22A3*) transports metformin and is expressed ubiquitously, but its *in vivo* role in metformin response is not known. Using *Oct3* knockout mice, the role of the transporter in metformin pharmacokinetics and pharmacodynamics was determined. After an intravenous dose of metformin, a 2-

fold decrease in the apparent volume of distribution and clearance was observed in knockout compared to wildtype mice ($p < 0.001$), indicating an important role of OCT3 in tissue distribution and elimination of the drug. Following oral doses, a significantly lower bioavailability was observed in knockout compared to wildtype mice (0.28 versus 0.58, $p < 0.001$). Importantly, metformin's effect on oral glucose tolerance was reduced in knockout compared with wildtype mice (30% versus 12% reduction, $p < 0.05$), along with its accumulation in skeletal muscle and adipose tissue ($p < 0.05$). Furthermore, the effect of metformin on phosphorylation of AMP activated protein kinase (AMPK) and expression of glucose transporter type 4 was absent in the adipose tissue of *Oct3* knockout mice. Additional analysis revealed that an *OCT3* 3'UTR variant was associated with reduced activity in luciferase assays and reduced response to metformin in 57 healthy volunteers. These findings suggest that OCT3 plays an important role in the absorption and elimination of metformin, and that the transporter is a critical determinant of metformin bioavailability, clearance, and pharmacologic action.

Chapter 3. High-throughput Screening of a Prescription Library for Inhibitors of Organic Cation Transporter 3

Transporter mediated drug-drug interactions may lead to problems in drug toxicity and efficacy. The goal of this study was to use high-throughput screening methods to identify drugs and dietary supplements that may potentially inhibit OCT3 at clinically relevant concentrations. Previous work suggested that OCT3 may play a role

in the pharmacological action of metformin (see Chapter 2), and inhibitors of OCT3 could potentially decrease its therapeutic effect. In this study, a large prescription drug and nutraceutical library was screened for inhibitors of OCT3 that may cause clinical drug interactions. A robust high-throughput screen (HTS) using the fluorescent substrate 4-Di-1-ASP (ASP^+) was developed for measuring OCT3 activity. Out of the 2556 unique compounds screened, 210 inhibited more than 50% ASP^+ uptake by OCT3. Potent inhibitors such as papaverine (IC_{50}=4.0μM) and trazodone (IC_{50}=5.1μM) were identified. Among the inhibitors identified, 23 compounds had an *in vivo* IC_{50} (predicted) / C_{MAX} value over 0.1 and therefore may inhibit OCT3 at clinically relevant drug concentrations. Furthermore, 50 compounds could potentially inhibit OCT3 in the intestine based on their maximum expected concentrations in the intestine lumen. A predictive Structure-activity relationship model was developed and validated, and which can be used to test new molecular entities to inform future *in vitro* studies in drug development.

Chapter 4. Comparative Modeling and High-throughput Screening Reveals the Mechanism of Ligand Interaction with OCT1

Organic cation transporter 1 (OCT1; *SLC22A1*) plays a critical role in the hepatocellular uptake of structurally diverse endogenous compounds and xenobiotics, including the anti-diabetic drug, metformin and the opiate analog, morphine. Here, we identified OCT1 orthosteric and allosteric ligands in a library of 1,780 prescription drugs by combining *in silico* and *in vitro* methods. Ligands were predicted by docking

against a comparative model based on the atomic structure of a eukaryotic homolog. In parallel, high-throughput screening (HTS) was conducted using the fluorescent probe substrate 4-Di-1-ASP (ASP^+) in OCT1 overexpressing cells. Thirty OCT1 orthosteric ligands, defined as ligands predicted *in silico* as well as found by HTS, were identified. An additional 137 ligands were identified using HTS, but not *in silico*; thus, some of these compounds might be allosteric ligands. A competition assay confirmed the orthostery and allostery for 2 selected ligands from each group. Of the 167 ligands identified experimentally, six were predicted to potentially cause clinical drug interactions based on *in vitro* potencies. Comparing HTS data from two other hepatic transporters, OATP1B1 and OATP1B3, we showed that a structure-guided approach predicted OCT1 selectivity with 87% accuracy. Finally, virtual screening of 29,332 metabolites against comparative and structure-activity relationship models identified 146 orthosteric OCT1 ligands; one of them, an endogenous neurotoxin, 1-benzyl-1,2,3,4-tetrahydroisoquinoline, was experimentally validated. In conclusion, we showed that combining *in silico* docking and *in vitro* HTS approaches can accurately and comprehensively predict whether a ligand binds orthosterically or allosterically, and the selectivity of membrane transporter inhibitors.

Chapter 5. Conclusions and Perspectives

In this chapter, we summarize the results of the studies in this dissertation, highlighting major findings. In addition, future studies necessary to further understand the pharmacological role of membrane transporters are discussed.

REFERENCES

1. Koepsell, H., Lips, K. & Volk, C. Polyspecific organic cation transporters: structure, function, physiological roles, and biopharmaceutical implications. *Pharm. Res.* **24,** 1227–51 (2007).
2. Koepsell, H., Schmitt, B. M. & Gorboulev, V. Organic cation transporters. *Rev. Physiol. Biochem. Pharmacol.* **150,** 36–90 (2003).
3. Kekuda, R. *et al.* Cloning and functional characterization of a potential-sensitive, polyspecific organic cation transporter (OCT3) most abundantly expressed in placenta. *J. Biol. Chem.* **273,** 15971–9 (1998).
4. Geier, E. G. *et al.* Profiling solute carrier transporters in the human blood-brain barrier. *Clin. Pharmacol. Ther.* **94,** 636–9 (2013).
5. Wu, X. *et al.* Identity of the organic cation transporter OCT3 as the extraneuronal monoamine transporter (uptake2) and evidence for the expression of the transporter in the brain. *J. Biol. Chem.* **273,** 32776–86 (1998).
6. Morrissey, K. M., Stocker, S. L., Wittwer, M. B., Xu, L. & Giacomini, K. M. Renal transporters in drug development. *Annu. Rev. Pharmacol. Toxicol.* **53,** 503–29 (2013).
7. Amara, S. G. & Kuhar, M. J. Neurotransmitter transporters: recent progress. *Annu. Rev. Neurosci.* **16,** 73–93 (1993).
8. Murphy, D. L. & Lesch, K.-P. Targeting the murine serotonin transporter: insights into human neurobiology. *Nat. Rev. Neurosci.* **9,** 85–96 (2008).

9. Craddock, N., Owen, M. J. & O'Donovan, M. C. The catechol-O-methyl transferase (COMT) gene as a candidate for psychiatric phenotypes: evidence and lessons. *Mol. Psychiatry* **11,** 446–58 (2006).

10. Youdim, M. B. H., Edmondson, D. & Tipton, K. F. The therapeutic potential of monoamine oxidase inhibitors. *Nat. Rev. Neurosci.* **7,** 295–309 (2006).

11. Eisenhofer, G. The role of neuronal and extraneuronal plasma membrane transporters in the inactivation of peripheral catecholamines. *Pharmacol. Ther.* **91,** 35–62 (2001).

12. Gründemann, D., Schechinger, B., Rappold, G. A. & Schömig, E. Molecular identification of the corticosterone-sensitive extraneuronal catecholamine transporter. *Nat. Neurosci.* **1,** 349–51 (1998).

13. Schmitt, A. *et al.* Organic cation transporter capable of transporting serotonin is up-regulated in serotonin transporter-deficient mice. *J. Neurosci. Res.* **71,** 701–9 (2003).

14. Vialou, V., Amphoux, A., Zwart, R., Giros, B. & Gautron, S. Organic cation transporter 3 (Slc22a3) is implicated in salt-intake regulation. *J. Neurosci.* **24,** 2846–51 (2004).

15. Haag, C. *et al.* The localisation of the extraneuronal monoamine transporter (EMT) in rat brain. *J. Neurochem.* **88,** 291–7 (2004).

16. Schildkraut, J. J. & Mooney, J. J. Toward a rapidly acting antidepressant: the normetanephrine and extraneuronal monoamine transporter (uptake 2) hypothesis. *Am. J. Psychiatry* **161,** 909–11 (2004).

17. Kitaichi, K. *et al.* Behavioral changes following antisense oligonucleotide-induced reduction of organic cation transporter-3 in mice. *Neurosci. Lett.* **382,** 195–200 (2005).

18. Wultsch, T. *et al.* Decreased anxiety in mice lacking the organic cation transporter 3. *J. Neural Transm.* **116,** 689–97 (2009).

19. Cui, M. *et al.* The organic cation transporter-3 is a pivotal modulator of neurodegeneration in the nigrostriatal dopaminergic pathway. *Proc. Natl. Acad. Sci. U. S. A.* **106,** 8043–8 (2009).

20. Karasuyama, H., Mukai, K., Tsujimura, Y. & Obata, K. Newly discovered roles for basophils: a neglected minority gains new respect. *Nat. Rev. Immunol.* **9,** 9–13 (2009).

21. Schneider, E. *et al.* Organic cation transporter 3 modulates murine basophil functions by controlling intracellular histamine levels. *J. Exp. Med.* **202,** 387–93 (2005).

22. Chirumbolo, S. State-of-the-art review about basophil research in immunology and allergy: is the time right to treat these cells with the respect they deserve? *Blood Transfus.* **10,** 148–64 (2012).

23. Schneider, E. *et al.* Downregulation of basophil-derived IL-4 and in vivo T(H)2 IgE responses by serotonin and other organic cation transporter 3 ligands. *J. Allergy Clin. Immunol.* **128,** 864–871.e2 (2011).

24. Bleasby, K. *et al.* Expression profiles of 50 xenobiotic transporter genes in humans and pre-clinical species: a resource for investigations into drug disposition. *Xenobiotica* **36,** 963–88 (2006).

25. Koza, R. A. *et al.* Changes in gene expression foreshadow diet-induced obesity in genetically identical mice. *PLoS Genet.* **2,** e81 (2006).

26. Ichimura, A. *et al.* Dysfunction of lipid sensor GPR120 leads to obesity in both mouse and human. *Nature* **483,** 350–4 (2012).

27. Kawazoe, Y., Tanaka, S. & Uesugi, M. Chemical genetic identification of the histamine H1 receptor as a stimulator of insulin-induced adipogenesis. *Chem. Biol.* **11,** 907–13 (2004).

28. Iffiú-Soltész, Z., Wanecq, E., Prévot, D., Grès, S. & Carpéné, C. Histamine oxidation in mouse adipose tissue is controlled by the AOC3 gene-encoded amine oxidase. *Inflamm. Res.* **59 Suppl 2,** S227–9 (2010).

29. Ciarimboli, G. *et al.* Individual PKC-phosphorylation sites in organic cation transporter 1 determine substrate selectivity and transport regulation. *J. Am. Soc. Nephrol.* **16,** 1562–70 (2005).

30. Martel, F. *et al.* Regulation of human extraneuronal monoamine transporter (hEMT) expressed in HEK293 cells by intracellular second messenger systems. *Naunyn. Schmiedebergs. Arch. Pharmacol.* **364,** 487–495 (2014).

31. Fog, J. U. *et al.* Calmodulin kinase II interacts with the dopamine transporter C terminus to regulate amphetamine-induced reverse transport. *Neuron* **51,** 417–29 (2006).

32. Cetinkaya, I. *et al.* Regulation of human organic cation transporter hOCT2 by PKA, PI3K, and calmodulin-dependent kinases. *Am. J. Physiol. Renal Physiol.* **284,** F293–302 (2003).

33. Jayanthi, L. D., Ramamoorthy, S., Mahesh, V. B., Leibach, F. H. & Ganapathy, V. Calmodulin-dependent regulation of the catalytic function of the human serotonin transporter in placental choriocarcinoma cells. *J. Biol. Chem.* **269,** 14424–9 (1994).

34. Sleutels, F., Zwart, R. & Barlow, D. P. The non-coding Air RNA is required for silencing autosomal imprinted genes. *Nature* **415,** 810–3 (2002).

35. Monk, D. *et al.* Limited evolutionary conservation of imprinting in the human placenta. *Proc. Natl. Acad. Sci. U. S. A.* **103,** 6623–8 (2006).

36. Chen, L. *et al.* Genetic and epigenetic regulation of the organic cation transporter 3, SLC22A3. *Pharmacogenomics J.* **13,** 110–20 (2013).

37. Nies, A. T. *et al.* Expression of organic cation transporters OCT1 (SLC22A1) and OCT3 (SLC22A3) is affected by genetic factors and cholestasis in human liver. *Hepatology* **50,** 1227–40 (2009).

38. Kirpichnikov, D., McFarlane, S. I. & Sowers, J. R. Metformin: an update. *Ann. Intern. Med.* **137,** 25–33 (2002).

39. Chen, Y. *et al.* Effect of genetic variation in the organic cation transporter 2 on the renal elimination of metformin. *Pharmacogenet. Genomics* **19,** 497–504 (2009).

40. Shu, Y. *et al.* Effect of genetic variation in the organic cation transporter 1 (OCT1) on metformin action. *J. Clin. Invest.* **117,** 1422–31 (2007).

41. Chen, L. *et al.* Role of organic cation transporter 3 (SLC22A3) and its missense variants in the pharmacologic action of metformin. *Pharmacogenet. Genomics* **20,** 687–99 (2010).

42. Siddik, Z. H. Cisplatin: mode of cytotoxic action and molecular basis of resistance. *Oncogene* **22,** 7265–79 (2003).

43. Misset, J. L., Bleiberg, H., Sutherland, W., Bekradda, M. & Cvitkovic, E. Oxaliplatin clinical activity: a review. *Crit. Rev. Oncol. Hematol.* **35,** 75–93 (2000).

44. Zhang, S. *et al.* Organic cation transporters are determinants of oxaliplatin cytotoxicity. *Cancer Res.* **66,** 8847–57 (2006).

45. Yonezawa, A., Masuda, S., Yokoo, S., Katsura, T. & Inui, K. Cisplatin and oxaliplatin, but not carboplatin and nedaplatin, are substrates for human organic cation transporters (SLC22A1-3 and multidrug and toxin extrusion family). *J. Pharmacol. Exp. Ther.* **319,** 879–86 (2006).

46. Li, Q., Peng, X., Yang, H., Rodriguez, J. & Shu, Y. Contribution of organic cation transporter 3 to cisplatin cytotoxicity in human cervical cancer cells. *J. Pharm. Sci.* **101,** 394–404 (2012).

47. Yokoo, S. *et al.* Significance of organic cation transporter 3 (SLC22A3) expression for the cytotoxic effect of oxaliplatin in colorectal cancer. *Drug Metab. Dispos.* **36,** 2299–306 (2008).

48. Lips, K. S. *et al.* Polyspecific cation transporters mediate luminal release of acetylcholine from bronchial epithelium. *Am. J. Respir. Cell Mol. Biol.* **33,** 79–88 (2005).

49. Horvath, G. *et al.* Epithelial organic cation transporters ensure pH-dependent drug absorption in the airway. *Am. J. Respir. Cell Mol. Biol.* **36,** 53–60 (2007).

50. Horvath, G. *et al.* The effect of corticosteroids on the disposal of long-acting beta2-agonists by airway smooth muscle cells. *J. Allergy Clin. Immunol.* **120,** 1103–9 (2007).

CHAPTER 2

Targeted Disruption of Organic Cation Transporter 3 (Oct3) Attenuates the Pharmacologic Response to Metformin

INTRODUCTION

In 2012, approximately 20 million people in the United States had been diagnosed with type 2 diabetes mellitus, resulting in a substantial toll on health in the country[1]. Among the array of pharmacological agents aimed at the treatment of type 2 diabetes, the biguanide, metformin is recommended for first-line oral therapy and is particularly beneficial for overweight diabetic patients[2]. Although metformin has been used for decades, its mechanism of action is not completely understood. However, the drug clearly reduces the rate of ATP synthesis, and results in higher AMP/ATP ratios[3]. One of the outcomes from the altered energy status of the cell is activation of AMP-activated protein kinase, AMPK. At least in part due to activation of AMPK, metformin decreases glucose output by the liver, which is widely considered to be the primary site of metformin action. In addition, the drug enhances glucose utilization in peripheral tissues, particularly skeletal muscle and adipose tissues[4]. These changes ultimately contribute to the therapeutic effect of metformin: improved insulin sensitivity and glycemic control.

Because of its low hydrophobicity, metformin requires membrane transporters to cross biological membranes and enter and exit cells. Previously, studies from our laboratory and others have shown that organic cation transporters 1 and 2, OCT1 (*SLC22A1*) and OCT2 (*SLC22A2*), transport metformin in the liver and kidney, respectively[5–8]. For example, in *Oct1* knockout mice, the accumulation of metformin is significantly reduced in the liver compared to wild-type mice[9]. Further, healthy volunteers with reduced function variants of OCT1 exhibit reduced pharmacologic response to metformin compared to those with reference OCT1[9]. On the other hand, significantly altered systemic exposure and renal clearance were observed in healthy volunteers with genetic variants of OCT2[10,11]. OCT2 mediated drug-drug interactions have also been described[12,13], though recent studies suggest that transporters in the multi-drug and toxin extrusion protein family, MATE (*SLC47A*) play more important roles in these interactions. Because of their interactions with many drugs, OCT1 and OCT2 along with MATEs have been included in drug-drug interaction guidances from regulatory authorities in Europe and the U.S.

In contrast to our knowledge of OCT1 and OCT2, much less is known about the third member of the SLC22 family, organic cation transporter 3, OCT3. The transporter exhibits overlapping substrate specificity with OCT1 and OCT2[14], and in particular is an excellent transporter for metformin. However unlike OCT1 and OCT2, OCT3 is expressed ubiquitously in most tissues. Originally thought to be a major component of the extraneuronal monoamine transporter system, scavenging neurotransmitters that escaped reuptake in the central nervous system, OCT3 has been shown to play an

important role in the homeostasis and neuropharmacology of monoamines[15–18]. Alhough OCT3 is widely expressed in many tissues and has been shown to be the most highly expressed organic cation transporter in skeletal muscle and adipose tissue[19], little is known about its biological or pharmacological roles in peripheral tissues. A recent study shows that OCT3 is important in the salivary accumulation of metformin, suggesting that it plays a role in the taste-altering effects of the drug[20]. In this study, we hypothesized that OCT3 plays a critical role in the pharmacologic response to the drug.

Using knockout mice, the role of OCT3 in the pharmacokinetics and pharmacodynamics of metformin was determined. In particular, the pharmacokinetic profiles and tissue accumulation of metformin were compared between wildtype and *Oct3* knockout mice after intravenous and oral doses. The glucose lowering effect of metformin after an oral glucose tolerance test (OGTT) was investigated in mice, and the role of OCT3 in metformin action in adipose tissues was further examined. Finally, the effect of OCT3 genetic polymorphisms on the pharmacologic effects of metformin was assessed in healthy volunteers.

RESULTS

Murine OCT3, mOCT3, transports metformin and is expressed in tissues implicated in metformin action.

A previous study has shown that human OCT3 transports metformin and its missense variants affect metformin uptake *in vitro*[21]. To understand whether mOCT3 plays a role in metformin pharmacokinetics and pharmacodynamics *in vivo*, we first determined the kinetics of metformin uptake by mOCT3 and the tissue distribution of *Oct3* in mice. In cells stably transfected with *Oct3* (HEK-mOCT3), the initial rate of metformin uptake increased with concentration and was saturable (Fig. 2.1A). Compared to kinetics of uptake in HEK cells overexpressing human OCT3, the kinetics of metformin uptake in HEK-mOCT3 exhibited a lower K_m and a significantly higher V_{max} (1.1 mM vs. 1.5 mM and 67 nmol/min/mg protein vs. 11 nmol/min/mg protein, $p < 0.01$, respectively. Fig. 2.2).

To assess the expression pattern of *Oct3* in C57BL/6 mice, the mRNA levels of *Oct3* in tissues were determined by quantitative real-time PCR. As shown in Figure 1B, *Oct3* mRNA was detected in all tissues tested and at significantly higher levels in lung and adipose tissue compared with other tissues. Further analyses were performed in important tissues for metformin response including the liver, kidney, skeletal muscle, and adipose tissue to compare the mRNA levels of *Oct1, Oct2,* and *Oct3* (Fig. 2.1C-F).

In the skeletal muscle and the adipose tissue, *Oct3* mRNA transcript levels were the highest among the three organic cation transporters. However, the mRNA levels of *Oct3* were lower than the levels of *Oct1* in the liver, and both *Oct1* and *Oct2* in the kidney.

Metformin pharmacokinetics and tissue accumulation are altered in Oct3 knockout mice

The pharmacokinetics of metformin in wildtype and *Oct3* knockout mice were evaluated after an intravenous bolus dose of 50 mg/kg via tail vein injection (Fig. 2.3A, Table 2.1). The plasma concentrations of metformin were significantly higher in knockout mice at five time points up to 60 minutes after dosing. The systemic exposure, area under the plasma concentration time curve (AUC), was 2.1-fold higher in knockout mice compared to wild-type mice (5340 ± 775 min·mcg·ml^{-1} in knockout mice versus 2500 ± 257 min·mcg·ml^{-1} in wildtype mice, $p < 0.001$). Consistent with the significantly greater exposure, the systemic clearance of metformin was significantly lower in *Oct3* knockout mice in comparison to their wildtype counterparts (8.96 ± 0.85 ml·min^{-1}·kg^{-1} in knockout mice versus 18.6 ± 1.8 ml·min^{-1}·kg^{-}1 in wildtype mice, $p < 0.001$). In addition, *Oct3* deletion modulated the distribution of metformin. In particular, the apparent volume of distribution of metformin was substantially reduced in *Oct3* knockout mice (550 ± 60 ml·kg^{-1} in knockout mice versus 1480 ± 218 ml·kg^{-1} in wild-type mice, $p < 0.001$). Consistent with its reduced volume of distribution, metformin tissue-to-plasma ratios (2 hours after intravenous dosing) were significantly lower in the

liver and adipose tissue in knockout mice (Fig. 2.3B). However, the ratio was similar in the skeletal muscle between wildtype and knockout mice. Unexpectedly, *Oct3* deletion resulted in a significantly higher tissue-to-plasma ratio of metformin in the kidney.

The pharmacokinetics of metformin after oral dosing was also studied in wildtype and *Oct3* knockout mice (Fig. 2.4A, Table 2.1). After a bolus dose of 50 mg/kg of metformin via oral gavage, the plasma concentrations were not significantly different between wildtype and knockout mice when followed for 4 hours after dosing, although a trend for a higher Cmax was observed in the knockout mice. Oral exposure was not significantly different between wildtype and knockout mice. Interestingly, oral bioavailability calculated from the intravenous and oral area under the curve (AUC) showed a 2.1-fold decrease in the knockout mice (0.28 in knockout mice versus 0.58 in wildtype mice, $p < 0.001$) suggesting that Oct3 contributes to metformin absorption. Tissue-to-plasma ratios were determined 4 hours after oral administration. The ratios in knockout mice were significantly lower in the liver, kidney, adipose tissue, and skeletal muscle (Fig. 2.4B-F).

The effect of metformin on oral glucose tolerance is reduced in Oct3 knockout mice

The glucose lowering effect of metformin after an oral glucose tolerance test was determined in wildtype and knockout mice. In wildtype mice, the effect of metformin was apparent, i.e., the drug significantly reduced blood glucose levels at

various times (i.e., at 15, 30, 60, 90, and 120 minutes) after oral glucose administration (Fig. 2.5A). In contrast, though slight decreases in blood glucose levels were observed in knockout mice following metformin administration, the blood glucose levels were not significantly reduced at any of the time points tested (Fig. 2.5B). *Oct3* deletion had no effect on baseline glucose tolerance as the blood glucose AUCs in saline treated groups were comparable between wildtype and knockout mice. On average, metformin significantly decreased glucose AUC in wildtype mice by 30% (18600 ± 2080 $mg \cdot min \cdot dl^{-1}$ in metformin treated mice versus 26000 ± 1450 $mg \cdot min \cdot dl^{-1}$ in saline treated mice, $p < 0.01$). While it did not reach significance, metformin on average decreased glucose AUC in knockout mice by 12%.

To investigate the mechanisms by which *Oct3* deletion modulated the effect of metformin on oral glucose tolerance, tissue accumulation of metformin was determined 30 minutes after oral administration of metformin (150 mg/kg). No significant difference in accumulation was observed in the liver between wildtype and knockout mice (Fig. 2.5C). On the other hand, tissue accumulation of metformin was significantly decreased in skeletal muscle and adipose tissue (Fig. 2.5E,F). The effect was most prominent in the adipose tissue, where the absolute exposure was decreased by 3.2-fold. Decreased accumulation of metformin in the kidney was also observed at 30 minutes in knockout mice, however it did not reach statistical significance (Fig. 2.5D). No significant differences were found in the intestinal accumulation of metformin between *Oct3* knockout and wildtype mice (Fig. 2.6).

We performed further experimentation to understand the impact of reduced metformin accumulation in the adipose tissue on pharmacologic action. Wildtype and knockout mice were treated with intraperitoneal doses of metformin (100 mg/kg) for 5 days. On day 5, adipose tissues were collected, and selected proteins level and phosphorylation status were analyzed with Western blot (Fig. 2.5G). In wildtype, but not knockout mice treated with metformin, an increase in the level of phosphorylated AMPK was observed, consistent with metformin's known effects on AMPK. No difference was observed in phosphorylated ACC level among all groups of mice. The glucose transporter, GLUT4, also showed an increase in protein level in wildtype mice treated with metformin, but not in metformin treated knockout mice. These data suggest that mOCT3 modulates the pharmacologic action of metformin on AMPK and GLUT4 in adipose tissue, and are consistent with the observed effects of metformin on oral glucose tolerance in wildtype and *Oct3* knockout mice.

The OCT3 3'UTR variant (C>G) in healthy human volunteers is linked to change in metformin pharmacodynamics.

Luciferase assays were used to determine the effect of human genetic variants in the 3'UTR region of *OCT3*. The entire length of the 3'UTR region of *OCT3* was cloned into a luciferase reporter vector. Single nucleotide polymorphisms (SNPs) were introduced into vectors, and vectors were then used to transfect human colorectal carcinoma cell line, HCT-116, and human hepatocellular carcinoma cell line, HepG2. Luciferase activity was used as a surrogate for gene expression level. Of 11 SNPs

tested (data not shown), rs2076828 had an effect on luciferase activity, where the minor allele, G, exhibited significantly lower activity compared with the reference allele in HCT-116 cell line ($p < 0.01$, Figure 2.7A). A similar trend was observed in HepG2 cell line, but the activity differences between the minor and major alleles did not reach statistical significance. The effect of the SNP on *OCT3* expression level was confirmed in expression quantitative trait loci (eQTL) analysis from previously published data[22], where the mRNA level of *OCT3* was significantly lower in adipose tissues of subjects with the minor allele ($p < 0.01$, Figure 2.7B).

We then analyzed the impact of rs2076828 on metformin pharmacokinetics and pharmacodynamics using previously published data from a healthy human cohort (N = 57) [23]. The variant had no significant effect on metformin pharmacokinetic parameters, even after adjusting for creatinine clearance, age and sex (data not shown). However, analysis of pharmacodynamic data showed that the variant was associated with reduced response to metformin in the healthy volunteers (Figure 2.7C). The healthy volunteers with the minor G allele had significantly smaller changes in their glucose AUC (mean ± SD, CC, -88±40 mg/dl/h; CG, -34±51 mg/dl/h; GG, -41±72 mg/dl/h; One-way ANOVA $p < 0.001$). We also noted that volunteers with the minor allele had significantly lower glucose AUC even before metformin dosing (mean ± SD, CC, 376±62 mg/dl/h; CG, 348±55 mg/dl/h; GG, 330±41 mg/dl/h; $p < 0.05$) suggesting an effect of *OCT3* on baseline oral glucose tolerance. However, after adjusting for the difference in glucose AUC before metformin dosing, the linear regression analysis

showed that the variant remained significantly associated with metformin response ($p < 0.05$).

DISCUSSION

The major findings of this study are that mOCT3 modulates the pharmacokinetics and pharmacologic effects of metformin. In particular, *Oct3* deletion in mice affected metformin absorption and clearance as well as its accumulation in tissues, notably skeletal muscle and adipose tissue. The decreased accumulation of metformin in these tissues may have accounted for the strikingly reduced effects of metformin on blood glucose levels after an oral glucose challenge in *Oct3* knockout mice compared with wildtype mice. Consistent with our studies in mice, our analysis also showed that a reduced function genetic polymorphism in the 3'UTR of *OCT3* was associated with decreased response to metformin in healthy volunteers. To the best of our knowledge, this is the first study that demonstrates a critical role of OCT3 in the bioavailability, clearance, and pharmacodynamics of metformin.

Unlike many hydrophilic compounds that distribute primarily into body water spaces[24], the volume of distribution of metformin reported in the literature is large and variable (63-276L), consistent with extensive tissue accumulation[25]. Because of its hydrophilicity, metformin requires transporters to cross plasma membranes and enter body tissues. Transporters implicated in metformin tissue distribution include OCT1, which is expressed primarily in the liver, and OCT2, expressed largely in the kidney[5,7]. In addition, knockout mouse studies indicate that MATE1 plays an important role in renal and hepatic distribution of the drug[26]. A recent study showing that OCT3 is involved in the salivary gland accumulation of metformin suggests that the transporter

plays a role in the taste-altering effects of the drug[20]. In this study, we reaffirm the hypothesis that OCT3 is an important metformin transporter *in vivo*. The wide tissue distribution of OCT3 in mice (see Figure 2.1B) including adipose tissue and skeletal muscle suggests a mechanism for tissue uptake of metformin. Indeed, after intravenous administration of the drug, *Oct3* knockout mice exhibited a 2 -fold reduction in V_d (Table 2.1), suggesting a lower overall tissue accumulation of metformin. The reduced tissue accumulation of metformin in the knockout mice was confirmed in the liver and adipose tissue collected 2 hours after intravenous administration (Figure 2.2B,D). In addition to its effect on metformin tissue distribution, *Oct3* deletion also resulted in a notable reduction in metformin clearance (Table 2.1). Interestingly, there was a significant increase in the renal accumulation of metformin in the *Oct3* knockout mice after the intravenous metformin dose (Figure 2.2C). These data are similar to data obtained for metformin in *Mate1* knockout mice, that is, there is increased renal accumulation of metformin in the kidney of the *Mate1* knockout mice[26]. Our parallel results suggest that similar to mouse Mate1, mOCT3 may act as an efflux transporter for the drug in the kidney.

In contrast to the striking differences in the pharmacokinetics of metformin after intravenous administration of the drug, no significant differences in AUC, CL/F and V/F between knockout and wildtype mice were observed after oral administration (Table 2.1). Since AUC is determined by both oral bioavailability and systemic clearance, the data may be explained by an effect of *Oct3* on both bioavailability and clearance. That is, *Oct3* deletion results in a reduced clearance of metformin as noted after intravenous

doses (Table 2.1), and a reduced bioavailability of the drug. In particular, a mean oral bioavailability of 0.58 was estimated for the wildtype mice, a value that closely matches data from a previously published study[27]. In contrast, a mean oral bioavailability of 0.28 was estimated in knockout mice, suggesting that mOCT3 plays an important role in the absorption of metformin. In fact, OCT3 has been localized to the brush border membrane of the small intestine[28], consistent with a role in metformin absorption. The dual effects of *Oct3* deletion on both bioavailability and clearance resulted in no apparent effect of gene deletion on AUC of metformin after oral administration of the drug.

Though no differences in the systemic plasma levels of metformin were observed after the oral dose, tissue levels of metformin were significantly lower in liver, kidney, adipose tissue and muscle of the knockout mice in comparison to the wildtype mice (Figure 2.3). Interestingly, in contrast to the higher kidney levels of metformin observed after the intravenous dose, renal accumulation of metformin was significantly lower in the *Oct3* knockout mice in comparison to the wildtype mice after the oral dose. These differences may reflect kinetic differences since tissue levels, which were measured at 4 hours after the oral dose, were substantially lower than those measured at 2 hours after the intravenous dose. Thus at low metformin levels, OCT3 may contribute primarily to renal uptake whereas at high metformin levels, OCT3 may contribute to metformin efflux in the kidney.

Several studies have used knockout mice to determine the role of membrane transporters in metformin disposition. However, few have used knockout mice to evaluate the impact of transporters on the therapeutic action of metformin. Shu *et al.* reported lowered fasting plasma glucose levels in wildtype but not *Oct1* knockout mice after metformin treatment and suggested that reduced hepatic accumulation of metformin due to *Oct1* deletion resulted in reduced effects on gluconeogenesis in the liver[9]. In our study, metformin treatment significantly reduced blood glucose AUC after an oral glucose tolerance test in wildtype but not *Oct3* knockout mice (Figures 2.4A and B), suggesting an important role for *Oct3* in the glucose lowering effect of metformin. These differences could not be explained by differences in systemic plasma levels, since those were virtually identical in the knockout and wildtype mice (Figure 2.3A). However, the differences could be explained by substantial differences in metformin levels in peripheral tissues that are sites of glucose uptake and utilization (adipose tissue and skeletal muscle) between wildtype and knockout mice (Figure 2.4E,F). Correspondingly, phosphorylated AMPK and expression levels of the insulin-sensitive glucose transporter, GLUT4, increased in response to metformin in wildtype mice, but with barely detectable increases in knockout mice (Figure 2.4G). Taken together, our data suggest that OCT3 plays a major role in the uptake of metformin into adipose tissue thereby modulating the therapeutic effect of metformin.

Based on our finding that mOCT3 played a role in metformin disposition and response, we hypothesized that functional genetic polymorphisms of *SLC22A3 (OCT3)* affect metformin disposition and response. We selected an *OCT3* 3'UTR variant for

the association study because it exhibited reduced function in *in vitro* luciferase assays and was associated with expression level differences in *OCT3* in eQTL analysis of adipose tissue[22]. We observed that the minor allele G was associated with reduced response to metformin in healthy volunteers (Figure 2.5C), consistent with lower *OCT3* mRNA levels observed previously in adipose tissue[22] and lower luciferase activity in cell lines (Figure 2.5A). The fact that we did not observe a significant effect of this 3'UTR variant on metformin disposition after oral doses is also consistent with our *in vivo* studies in the mice suggesting no effect of *Oct3* deletion on the overall drug levels of metformin after oral administration. Collectively, the data in healthy volunteers support the findings in mice and indicate that OCT3 is an important determinant of metformin response. Similar to OCT1, OCT2 and MATEs[29–31], our results suggest that OCT3 is an important site for drug-drug interactions and that future studies examining OCT3-mediated drug interactions with metformin should be performed.

In conclusion, this study demonstrates that murine OCT3 plays a critical role in the clearance and bioavailability of metformin as well as its accumulation in various tissues, notably skeletal muscle and adipose tissue. The transporter has route-dependent effects on the systemic plasma levels of metformin because of dual effects on the bioavailability and clearance of the drug. Importantly, our study shows that OCT3 plays a major role in the pharmacologic response to metformin in both mice and humans.

METHODS

Animals and materials

Oct3 knockout mice were generated as previously described in C57BL/6J background[32] and wildtype mice were obtained from Jackson Laboratories. Animal studies described here were conducted in male *Oct3* knockout and wildtype mice (12-16 weeks old), and were reviewed and approved by UCSF IACUC. Metformin and glucose were purchased from Sigma Chemical (St. Louis, MO). Cell culture media were purchased from Life Technologies (Carlsbad, CA). All other chemicals were commercially available.

Uptake study

The stably overexpressing human or mouse OCT3 (pcDNA5/FRT vector) cell lines were generated from HEK FlpIn-293 cells (Life Technologies, Carlsbad, CA) according to the manufacturer's protocol. The cells were maintained in Dulbecco's Modified Eagle's Medium (DMEM H-21) supplemented with 75 μg/ml of hygromycin B penicillin (100 U/ml), streptomycin (100 mg/ml), and 10% fetal bovine serum. For the uptake studies, cells were cultured on poly-D-lysine coated 24-well plates to 95% confluence. The cells were washed once with warm Hank's balanced salt solution (HBSS) and then incubated in the uptake buffer with various concentrations of unlabeled metformin and [^{14}C] metformin (American Radiolabeled Chemicals, St. Louis, MO) in HBSS. The uptake was performed at 37°C for 3 minutes; then the cells were

washed 3 times with ice-cold HBSS. The cells were lysed with lysis buffer containing 0.1 N NaOH and 0.1% SDS, and the radioactivity in the lysate was determined by liquid scintillation counting. The K_m and V_{max} were calculated by fitting the data to Michaelis-Menten equations using GraphPad Prism software (La Jolla, CA).

Real time RT-PCR analysis of mRNA level in tissues

Total RNA from various C57BL/6J mouse tissues was isolated using RNeasy Mini kit (Qiagen, Valencia, CA) according to the manufacturer's protocol. Two μg of total RNA from each sample was reverse transcribed into cDNA using SuperScript VILO cDNA Synthesis kit (Life Technologies, Carlsbad, CA) according to the manufacturer's protocol. Quantitative real-time PCR was carried out in 384-well reaction plates using 2X Taqman Fast Universal Master Mix (Applied Biosystems, Foster City, CA), 20X Taqman specific gene expression probes and 10 ng of the cDNA template. The reactions were carried out on an Applied Biosystems 7500 Fast Real-Time PCR System (Applied Biosystems, Foster City, CA). The relative expression level of each mRNA transcript was calculated by the comparative method (ΔΔCt method) normalized to the housekeeping gene glyceraldhydes-3-phospate dehydrogenase (*Gapdh*).

Pharmacokinetic study and tissue distribution of metformin

Mice were fasted for 16 hours then given a dose of 50 mg/kg metformin in saline with 0.2 μCi/g of [^{14}C]metformin via oral gavage or tail vein injection. Blood samples were collected at specific time points by tail bleeding into heparinized microhematocrit

capillary tubes (Fisher Scientific, Waltham MA). The capillary tubes were centrifuged to obtain the plasma portion. Mice were sacrificed at the end of the study and tissues were collected immediately. All tissues were weighed and homogenized in Solvable (PerkinElmer, Waltham MA) overnight. The amount of metformin in tissue homogenates and plasma were measured by liquid scintillation counting. The pharmacokinetic parameters were obtained by fitting the raw data using noncompartmental methods with WinNonlin (Pharsight, Princeton, NJ).

Oral glucose tolerance test

Age-matched *Oct3* knockout and wildtype mice were fasted overnight for 16 hours, then given saline via oral gavage followed by an oral dose of glucose (3 g/kg) 15 minutes after. Blood samples were collected at specific time points by tail bleeding, and blood glucose levels were measured with FreeStyle Lite glucometer (Abbott, Abbott Park, IL). Three days after the saline treatment, mice were fasted again for 16 hours, then given an oral dose of metformin (150 mg/kg) followed by an oral dose of glucose (3 g/kg) 15 minutes later. Blood samples and blood glucose levels were collected as described.

Western blotting and analysis

Age-matched *Oct3* knockout and wildtype mice (N = 3) were treated with metformin (100 mg/kg) or saline via intraperitoneal injection for 5 days. On day 5, mice were sacrificed and epididymal adipose tissues were collected. The tissues were lysed and homogenized with a tissue homogenizer in Cellytic MT buffer with cOmplete mini

protease inhibitor and PhosSTOP phosphatase inhibitor following the manufacturer's protocol (Sigma Chemical, St. Louis, MO; Roche Diagnostic, Indianapolis, IN). The tissue lysates from each group were combined and stored at - 80ºC. The proteins were separated on 4-20% SDS PAGE gels and transferred to PVDF membrane (Bio-Rad, Hercules, CA). The membranes were blocked overnight at 4ºC with Tris-buffered saline containing 0.05% Tween 20 and 5% nonfat milk. Immunoblotting was performed following standard procedures, and signals were detected by ECL chemiluminescence reagent (GE healthcare, Piscataway, NJ). All antibodies used were purchased from Cell Signaling Technologies following manufacturer's recommendation for dilution and incubation time (Danvers, MA). Quantification analysis was conducted with ImageJ program (*http://imagej.nih.gov/ij/*) following the software manual.

Luciferase reporter assay

The complete 3'UTR sequence of *OCT3* was cloned into the MCR site downstream of firefly luciferase gene in the pmirGLO vector (Promega, Madison WI). Single nucleotide polymorphisms were introduced into the reference sequence using site-directed mutagenesis with QuikChange kit (Stratagene, La Jolla CA). HCT-116 and HepG2 cells were double transfected with pmirGLO containing *OCT3* 3'UTR sequence and pGL4.73 containing Renilla luciferase gene using Lipofectamine 2000 (Life Technologies, Carlsbad CA). After 24 hours incubation period, luminescence from firefly and Renilla luciferase were measured according to manufacturer's protocol (Promega, Madison WI) as previously described[33].

Association analysis of 3'UTR variant in *OCT3* with metformin response

Previously, we have described the healthy human cohort that was used to determine the effects of functional variants on metformin disposition and response[23]. Using the same cohort, which has been genotyped using Illumina OmniExpress1.0 as described in our previous study[34], we evaluated the effect of a functional *OCT3* variant, rs2076828, on metformin disposition and response in healthy volunteers. Using the pharmacokinetic and pharmacodynamic parameters that have been ascertained previously, we determined the association of rs2076828 with (i) metformin plasma AUC (area under the curve), (ii) metformin renal clearance, (iii) metformin secretory clearance and (iv) metformin effects on oral glucose tolerance test as quantified by changes in area under the curve of plasma glucose between 0 and 2 hours after oral glucose administration. We used linear regression analysis to test the effect of the variant with each of the parameters above assuming an additive genetic effect.

Statistical analysis

Unless otherwise noted, statistical analysis was performed by Student's *t* test to identify significant differences between various treatment groups. In general, four mice were used per treatment group. Numbers are specified in the figure and table legends.

Table 2.1 Pharmacokinetic parameters of metformin in *Oct3* knockout and wildtype mice.

IV Parameter	**Wild-type**	***Oct3* Knockout**
C_0 (mcg/ml)	70.9 ± 11.7	148 ± 19 **
AUC (min*mcg/ml)	2500 ± 257	5340 ± 775 *
V (ml/kg)	1480 ± 218	550 ± 60 *
CL(ml/min/kg)	18.6 ± 1.8	8.96 ± 0.85 ***
Oral Parameter	**Wild-type**	***Oct3* Knockout**
Cmax (mcg/ml)	9.70 ± 0.77	11.2 ± 0.4
AUC (min*mcg/ml)	1460 ± 184	1480 ± 45
V/F (ml/kg)	4240 ± 698	3670 ± 293
CL/F (ml/min/kg)	27.4 ± 2.3	28.0 ± 0.5
F (AUC Oral/AUC IV)	0.58	0.28

Oral bioavailability was obtained by dividing AUC_{oral} by AUC_{IV}. Each value represents the mean ± S.D. for four mice.

* $P < 0.05$, significantly different from wildtype mice.

** $P < 0.01$, significantly different from wildtype mice.

*** $P < 0.001$, significantly different from wildtype mice.

Figure 2.1

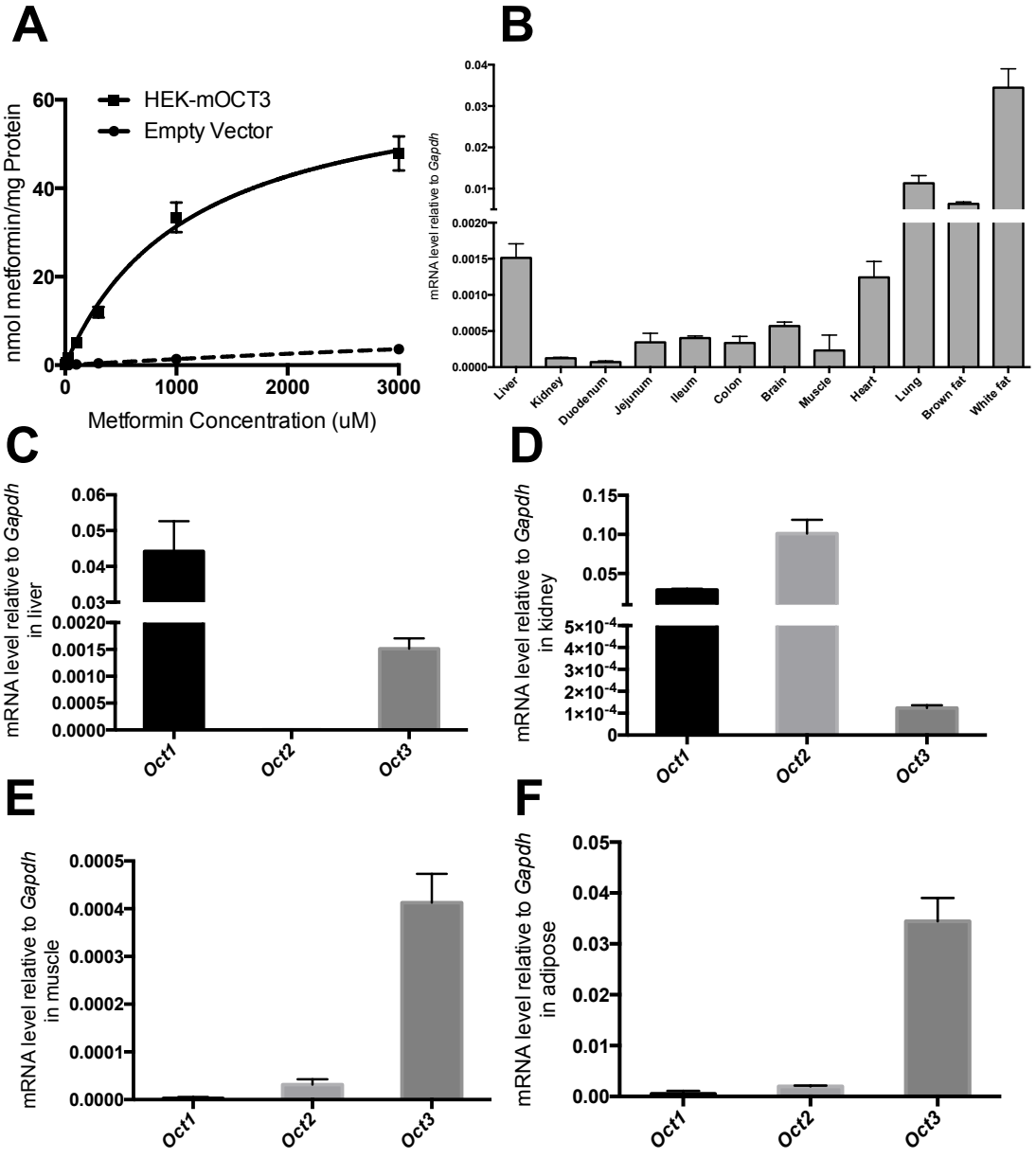

Figure 2.1. Characterization of the kinetics and tissue levels of mouse OCT3. (A) Overexpressing mouse OCT3 increases metformin uptake in HEK cells. Metformin uptake studies were conducted in HEK cells overexpressing mouse OCT3 or empty vector. Cells were incubated with increasing concentrations of metformin for 3

minutes. The uptake kinetic parameters (see Results section) were calculated using the difference in accumulation between OCT3 overexpressing and empty vector cells. (B) *Oct3* mRNA expression pattern was assessed in C57/B6J mice. The relative mRNA levels of *Oct3* were determined by real-time PCR. The mRNA levels of *Oct1, Oct2* and *Oct3* were determined in the liver (C), kidney (D), adipose tissue (E), and skeletal muscle (F). Data represent mean ± SD, n = 3 mice per group.

Figure 2.2

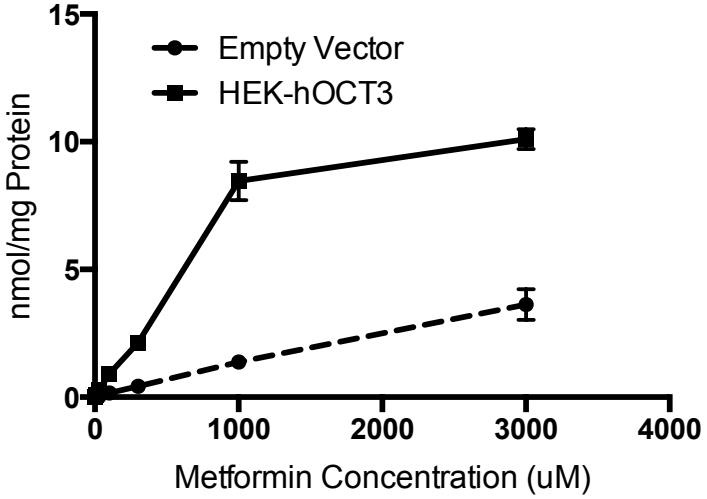

Figure 2.2. Characterization of the kinetics of metformin transport by human OCT3. Metformin uptake studies were conducted in HEK cells overexpressing human OCT3 or empty vector. Cells were incubated with increasing concentrations of metformin for 3 minutes, and uptake kinetic parameters (see Results section) were calculated using the difference in accumulation between OCT3 overexpressing and empty vector cells. Data represent mean ± SD.

Figure 2.3

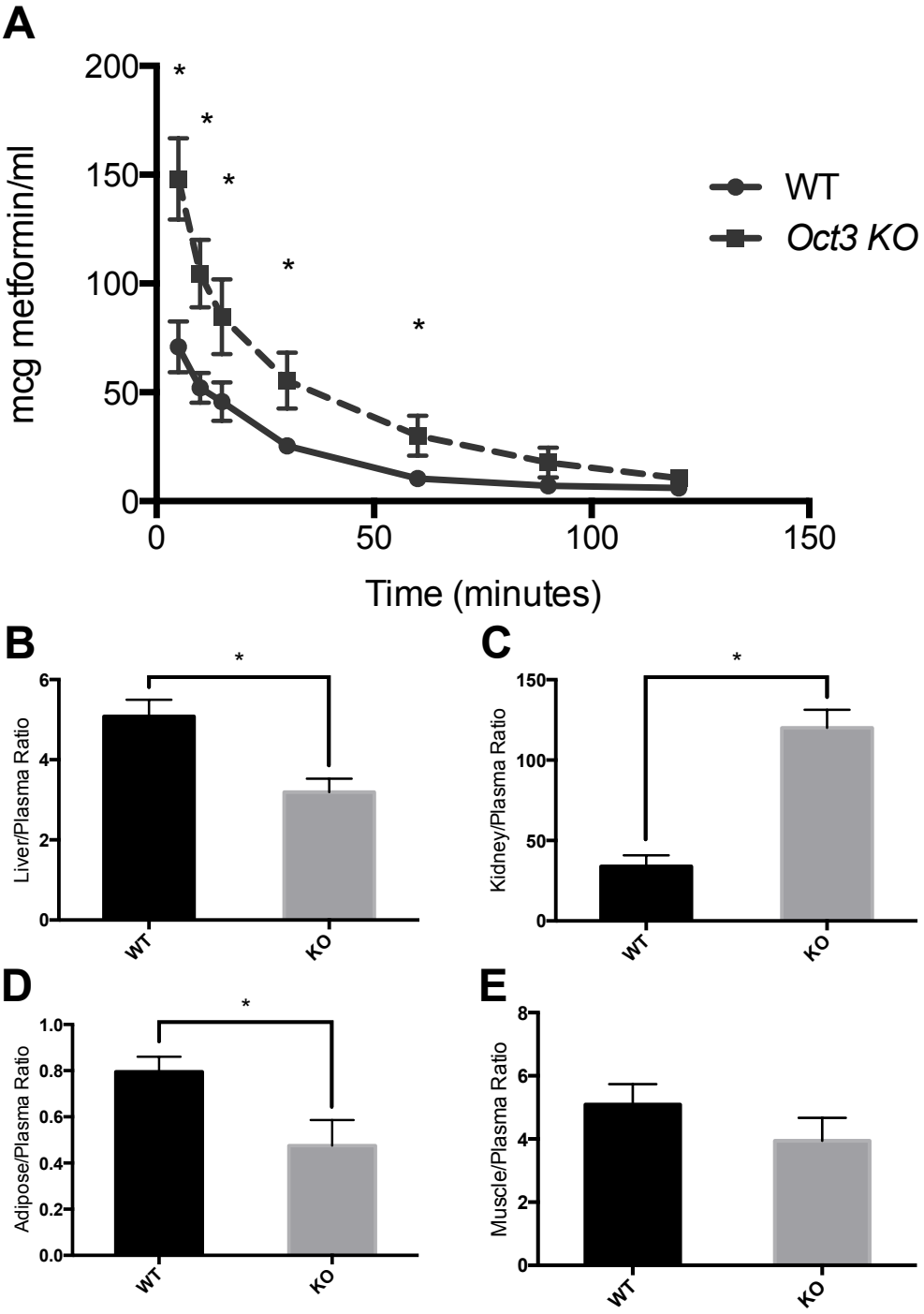

Figure 2.3. *Oct3* deletion resulted in altered pharmacokinetics and tissue accumulation of metformin in mice. (A) The plasma metformin concentration-time profiles in wild-type

and knockout mice after an i.v. dose (50mg/kg metformin containing 0.2mCi/Kg [^{14}C]metformin via tail vein). Significantly higher plasma concentrations were observed in knockout mice at 5, 10, 15, 30, 60 minutes after injection. (B-E) Tissue distribution of metformin in wildtype and knockout mice. Two hours after dosing, mice were sacrificed and tissues were collected. Radioactivity in tissue homogenates were determined and converted to mass amounts. Tissue accumulation was significantly reduced in liver and adipose tissue of knockout mice. Metformin accumulation was higher in kidney of knockout mice. Data represent mean ± SD, n = 4 mice per group, *$P < 0.05$ wild-type versus knockout mice.

Figure 2.4

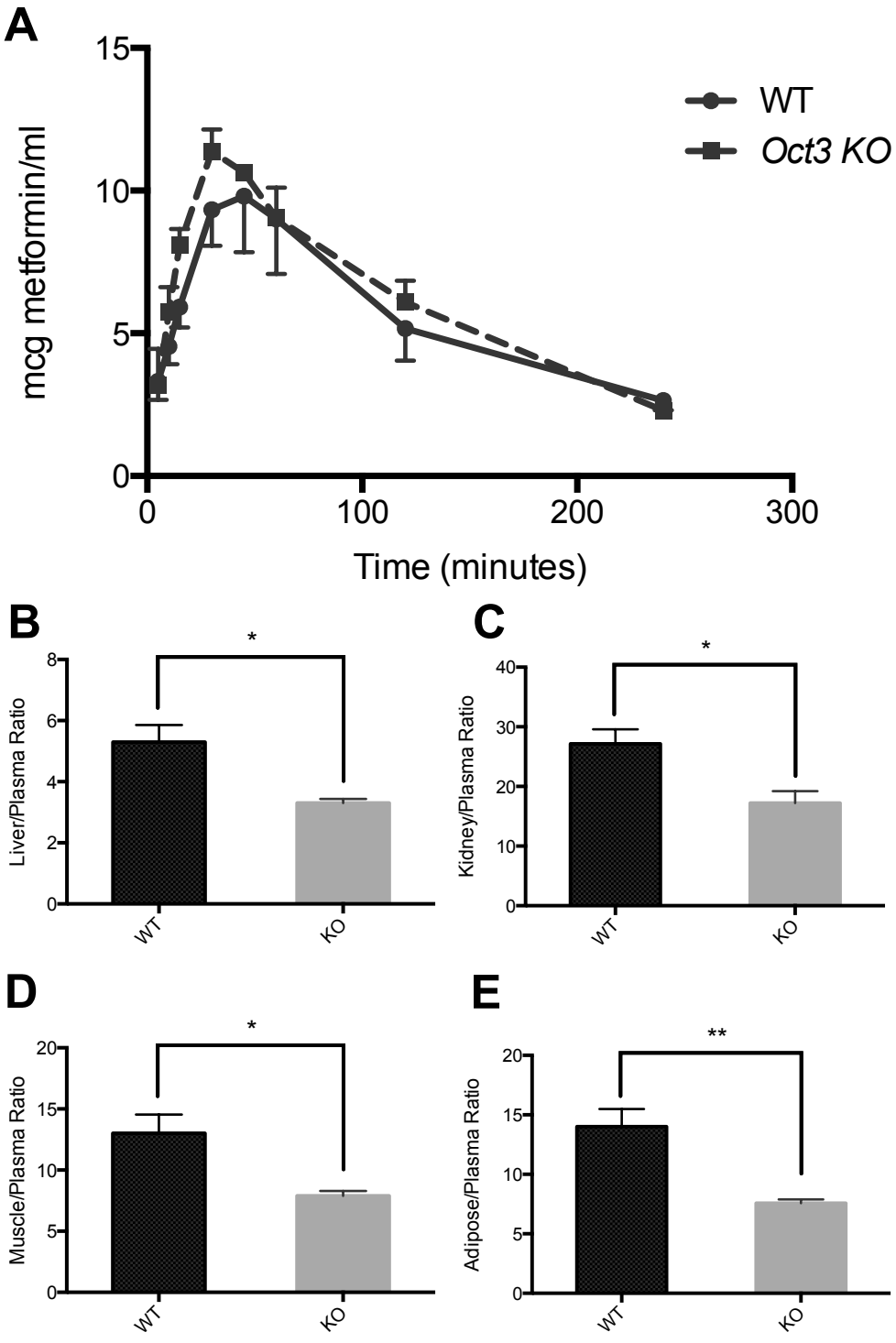
A
15
10
5
0
mcg metformin/ml
0
100
200
300
Time (minutes)
WT
Oct3 KO
B
Liver/Plasma Ratio
8
6
4
2
0
*
WT
KO
C
Kidney/Plasma Ratio
40
30
20
10
0
*
WT
KO
D
Muscle/Plasma Ratio
20
15
10
5
0
*
WT
KO
E
Adipose/Plasma Ratio
20
15
10
5
0
**
WT
KO

Figure 2.4. *Oct3* deletion resulted in altered tissue accumulation of metformin after an oral dose. (A) The plasma metformin concentration-time profiles in wild-type and knockout mice after an oral dose (50 mg/kg metformin containing 0.2mCi/Kg [^{14}C]metformin via oral gavage). Radioactivity in the plasma is determined and converted to mass amounts. (B-E) Tissue distribution of metformin in wildtype and knockout mice. Four hours after administration, mice were sacrificed and tissues were collected. Radioactivity in tissue homogenates were determined and converted to mass amounts. Metformin accumulation was significantly reduced in skeletal muscle and adipose tissue of knockout mice. Data represent mean ± SD, $n = 4$ mice per group, $^{*}P < 0.05$, $^{**}P < 0.01$ wildtype versus knockout mice.

Figure 2.5

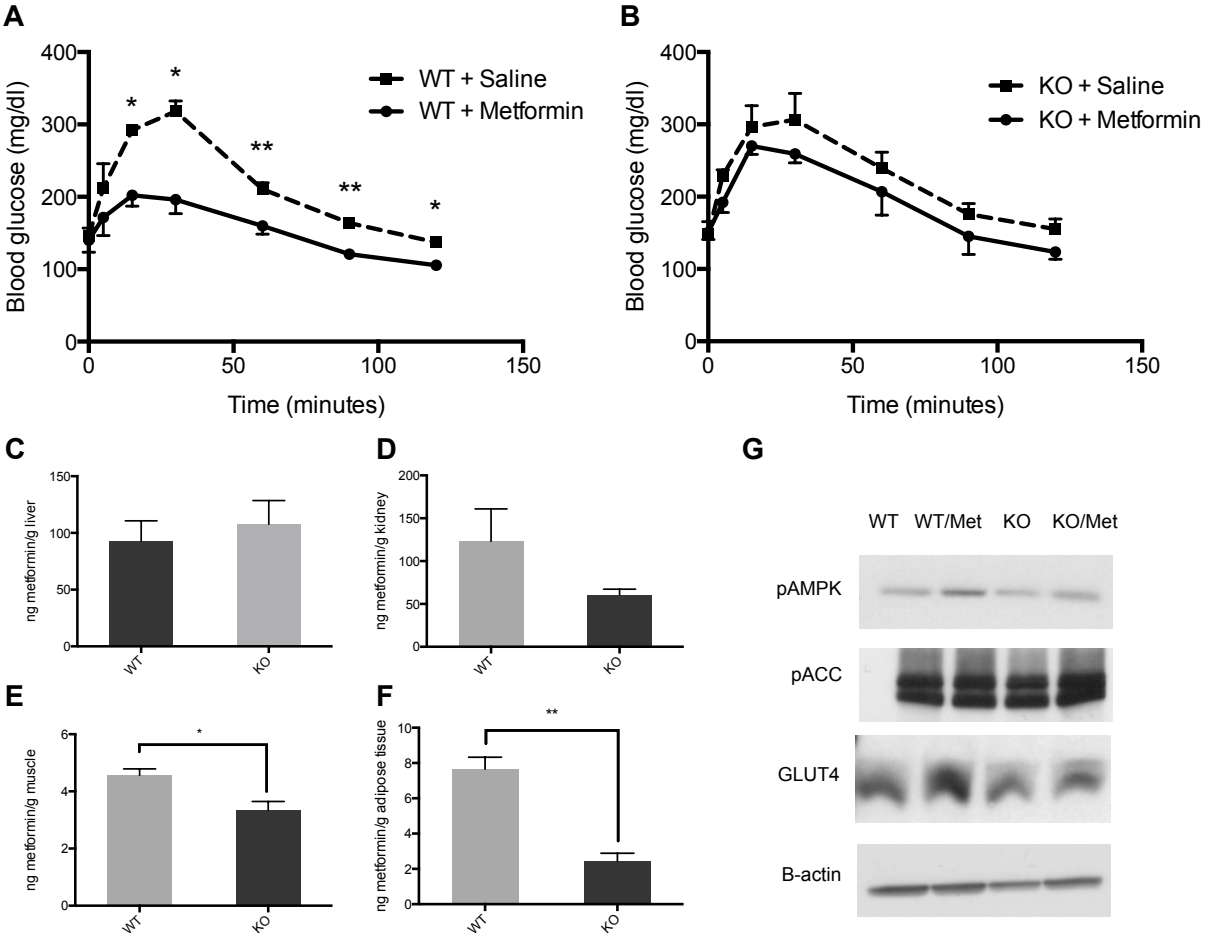

Figure 2.5. *Oct3* deletion resulted in reduced pharmacologic effects of metformin. The blood glucose concentration-time profiles of wildtype mice treated with metformin or saline (A) and knockout mice treated with metformin or saline (B). Mice were given metformin (150 mg/kg) or saline orally followed by glucose (3g/kg) orally after 15 minutes. Data represent mean ± SE, $n = 4$ mice per group, $^*P < 0.05$ metformin treated group versus saline treated group. (B-E) Tissue distribution of metformin in wildtype and knockout mice. Thirty minutes after metformin (150 mg/kg p.o.), mice were

sacrificed and tissues were collected. Radioactivity in tissue homogenates were determined and converted to mass amounts. Data represent mean ± SD, $n = 4$ mice per group, $^{*}P < 0.05$ wildtype versus knockout mice. (G) Representative Western blots of adipose tissues from knockout and wildtype mice treated with i.p 100mg/kg metformin or saline for 5 days.

Figure 2.6

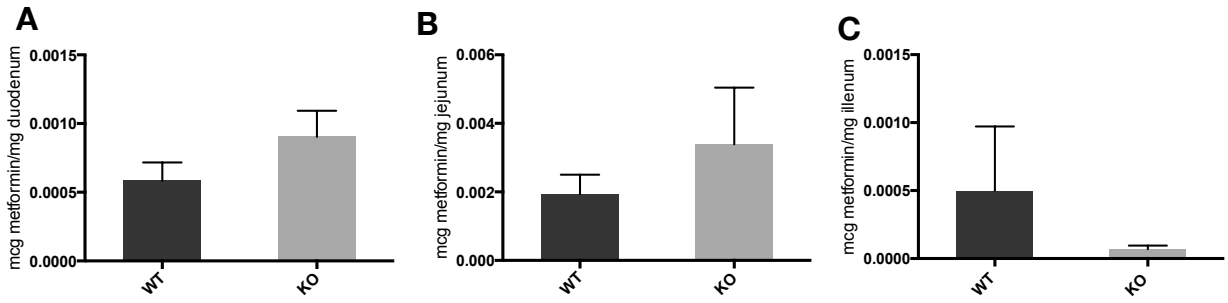

Figure 2.6. Tissue distribution of metformin in wildtype and knockout mice in the intestine. Thirty minutes after metformin (150 mg/kg p.o.), mice were sacrificed and tissues were collected. Radioactivity in duodenum, jejunum, and illenum homogenates (A, B, and C, respectively) were determined and converted to mass amounts. Data represent mean ± SD, n = 4 mice per group. No statistically significant changes were observed between groups.

Figure 2.7

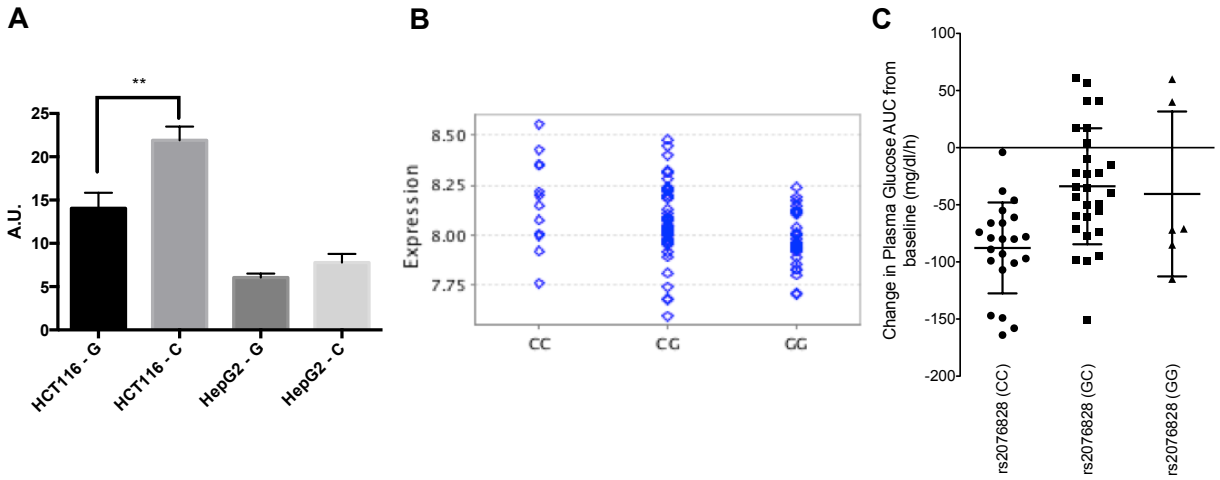

Figure 2.7. The OCT3 3'UTR variant (C>G) in healthy human volunteers is associated with changes in metformin pharmacodynamics. (A) Luciferase reporter assay of rs2076828. Luciferase activity was significantly lower in HCT-116 cell line transfected with a reporter construct containing the minor allele (G) compared with the reference allele. Data represent mean ± SD, $n = 3$ per cell line, $^{**}P < 0.01$. (B) E-QTL analysis of rs2076828 in healthy human cohorts revealed lower mRNA levels of OCT3 in adipose tissues of subjects with the minor allele (G), $p < 0.01$. (C) The change in glucose exposure following an oral glucose tolerance test (OGTT) (area under the curve, AUC) after metformin treatment in healthy volunteers. Change in glucose AUC was calculated as glucose AUC after metformin dosing minus glucose AUC before metformin dosing. Healthy volunteers with the minor allele had lower response to metformin ($p < 0.05$). The dot plot displays the mean ± SD.

REFERENCES

1. H.H.S. *National Diabetes Statistics Report: Estimates of Diabetes and Its Burden in the United States, 2014.* 2009–2012 (Atlanta, GA, 2014).

2. Boyle, J. G., Salt, I. P. & McKay, G. A. Metformin action on AMP-activated protein kinase: a translational research approach to understanding a potential new therapeutic target. *Diabet. Med.* **27,** 1097–106 (2010).

3. Pernicova, I. & Korbonits, M. Metformin--mode of action and clinical implications for diabetes and cancer. *Nat. Rev. Endocrinol.* **10,** 143–56 (2014).

4. Kirpichnikov, D., McFarlane, S. I. & Sowers, J. R. Metformin: an update. *Ann. Intern. Med.* **137,** 25–33 (2002).

5. Jonker, J. W. *et al.* Reduced hepatic uptake and intestinal excretion of organic cations in mice with a targeted disruption of the organic cation transporter 1 (Oct1 [Slc22a1]) gene. *Mol. Cell. Biol.* **21,** 5471–7 (2001).

6. Wang, D. *et al.* Involvement of organic cation transporter 1 in hepatic and intestinal distribution of metformin. *J. Pharmacol. Exp. Ther.* **302,** 510–5 (2002).

7. Jonker, J. W., Wagenaar, E., Van Eijl, S. & Schinkel, A. H. Deficiency in the organic cation transporters 1 and 2 (Oct1/Oct2 [Slc22a1/Slc22a2]) in mice abolishes renal secretion of organic cations. *Mol. Cell. Biol.* **23,** 7902–8 (2003).

8. Chen, L. *et al.* OCT1 is a high-capacity thiamine transporter that regulates hepatic steatosis and is a target of metformin. *Proc. Natl. Acad. Sci. U. S. A.* **111,** 9983–8 (2014).

9. Shu, Y. *et al.* Effect of genetic variation in the organic cation transporter 1 (OCT1) on metformin action. *J. Clin. Invest.* **117,** 1422–31 (2007).

10. Song, I. S. *et al.* Genetic variants of the organic cation transporter 2 influence the disposition of metformin. *Clin. Pharmacol. Ther.* **84,** 559–62 (2008).

11. Chen, Y. *et al.* Effect of genetic variation in the organic cation transporter 2 on the renal elimination of metformin. *Pharmacogenet. Genomics* **19,** 497–504 (2009).

12. Somogyi, A. & Muirhead, M. Pharmacokinetic interactions of cimetidine 1987. *Clin. Pharmacokinet.* **12,** 321–66 (1987).

13. Somogyi, a, Stockley, C., Keal, J., Rolan, P. & Bochner, F. Reduction of metformin renal tubular secretion by cimetidine in man. *Br. J. Clin. Pharmacol.* **23,** 545–51 (1987).

14. Koepsell, H., Schmitt, B. M. & Gorboulev, V. Organic cation transporters. *Rev. Physiol. Biochem. Pharmacol.* **150,** 36–90 (2003).

15. Zwart, R., Verhaagh, S., Buitelaar, M., Popp-Snijders, C. & Barlow, D. P. Impaired activity of the extraneuronal monoamine transporter system known as uptake-2 in Orct3/Slc22a3-deficient mice. *Mol. Cell. Biol.* **21,** 4188–96 (2001).

16. Zhu, H.-J., Appel, D. I., Gründemann, D. & Markowitz, J. S. Interaction of organic cation transporter 3 (SLC22A3) and amphetamine. *J. Neurochem.* **114,** 142–9 (2010).

17. Wultsch, T. *et al.* Decreased anxiety in mice lacking the organic cation transporter 3. *J. Neural Transm.* **116,** 689–97 (2009).

18. Horton, R. E. *et al.* Decynium-22 enhances SSRI-induced antidepressant-like effects in mice: uncovering novel targets to treat depression. *J. Neurosci.* **33,** 10534–43 (2013).

19. Bleasby, K. *et al.* Expression profiles of 50 xenobiotic transporter genes in humans and pre-clinical species: a resource for investigations into drug disposition. *Xenobiotica* **36,** 963–88 (2006).

20. Lee, N. *et al.* Taste of a pill: organic cation transporter-3 (OCT3) mediates metformin accumulation and secretion in salivary glands. *J. Biol. Chem.* **289,** 27055–64 (2014).

21. Chen, L. *et al.* Role of organic cation transporter 3 (SLC22A3) and its missense variants in the pharmacologic action of metformin. *Pharmacogenet. Genomics* **20,** 687–99 (2010).

22. Grundberg, E. *et al.* Mapping cis- and trans-regulatory effects across multiple tissues in twins. *Nat. Genet.* **44,** 1084–9 (2012).

23. Stocker, S. L. *et al.* The effect of novel promoter variants in MATE1 and MATE2 on the pharmacokinetics and pharmacodynamics of metformin. *Clin. Pharmacol. Ther.* **93,** 186–94 (2013).

24. Rowland, M. & Tozer, T. N. *Clinical Pharmacokinetics and Pharmacodynamics Concepts and Applications*. 4th ed. (Wolters Kluwer Health/Lippincott William & Wilkins, Philadelphia, PA, 1995).

25. Graham, G. G. *et al.* Clinical pharmacokinetics of metformin. *Clin. Pharmacokinet.* **50,** 81–98 (2011).

26. Tsuda, M. *et al.* Targeted disruption of the multidrug and toxin extrusion 1 (mate1) gene in mice reduces renal secretion of metformin. *Mol. Pharmacol.* **75,** 1280–6 (2009).

27. Higgins, J. W., Bedwell, D. W. & Zamek-Gliszczynski, M. J. Ablation of both organic cation transporter OCT1 and OCT2 alters metformin pharmacokinetics but has no effect on tissue drug exposure and pharmacodynamics. *Drug Metab. Dispos.* **40,** 1170–7 (2012).

28. Müller, J. *et al.* Drug specificity and intestinal membrane localization of human organic cation transporters (OCT). *Biochem. Pharmacol.* **70,** 1851–60 (2005).

29. Jonker, J. W. & Schinkel, A. H. Pharmacological and physiological functions of the polyspecific organic cation transporters: OCT1, 2, and 3 (SLC22A1-3). *J. Pharmacol. Exp. Ther.* **308,** 2–9 (2004).

30. Koepsell, H. Polyspecific organic cation transporters: their functions and interactions with drugs. *Trends Pharmacol. Sci.* **25,** 375–81 (2004).

31. Becker, M. L. *et al.* Genetic variation in the multidrug and toxin extrusion 1 transporter protein influences the glucose-lowering effect of metformin in patients with diabetes: a preliminary study. *Diabetes* **58,** 745–9 (2009).

32. Vialou, V. *et al.* Altered aminergic neurotransmission in the brain of organic cation transporter 3-deficient mice. *J. Neurochem.* **106,** 1471–82 (2008).

33. Choi, J. H. *et al.* A common 5'-UTR variant in MATE2-K is associated with poor response to metformin. *Clin. Pharmacol. Ther.* **90,** 674–84 (2011).

34. Goswami, S. *et al.* Genetic variants in transcription factors are associated with the pharmacokinetics and pharmacodynamics of metformin. *Clin. Pharmacol. Ther.* **96,** 370–9 (2014).

CHAPTER 3

High-Throughput Screening of a Prescription Drug Library for Inhibitors of the Organic Cation Transporter 3, OCT3

INTRODUCTION

Obesity has reached epidemic proportion globally. Estimates of the United States population suggest that 33.8% of adults and 17% of children are obese[1,2]. As one of the major risk factors for type 2 diabetes, obesity is expected to contribute to the increasing prevalence of diabetes and impose tremendous economic costs on society. As many diabetic patients are obese, which contributes to insulin resistance, drugs that can treat both diabetes and obesity are especially beneficial. For this and other reasons, among the array of pharmacological agents aimed at the treatment of type 2 diabetes, metformin is now first-line therapy and is considered particularly beneficial for overweight diabetics[3].

Although the mechanism of metformin action is not yet fully understood, AMPK activation, a well-described effect of metformin, has been proposed to mediate many of its actions. At least in part due to the activation of AMPK, metformin decreases hepatic glucose output and enhances glucose utilization in peripheral tissues, particularly skeletal muscle and adipose tissues[4]. While the beneficial effects of weight loss with the use of metformin is still debated, several studies have shown that metformin significantly increases weight loss, especially the reduction of total body and

visceral fat, in patients on a controlled, hypocaloric diet[5–7]. Metformin is also especially useful in treating diabetes in patients with higher body mass indices, BMIs[8]. Because of its effects on body weight and on diabetic patients with high BMIs, it is reasonable to propose that metformin may target adipose tissue. Indeed, AMPK has been implicated in glucose uptake and glucose oxidation in adipocytes, and the loss of AMPKα2 resulted in increased body weight and adiposity in mice[9,10]. A recent study also showed that metformin activates AMPK in isolated human adipocytes[11].

In chapter 2, we demonstrated that murine OCT3 (mOCT3) is expressed in most tissues and is capable of transporting metformin *in vitro*, similar to human OCT3 (hOCT3) protein. We showed that metformin pharmacokinetics were altered by *Oct3* deletion in mice. The results indicated that mOCT3 plays an important role in the bioavailability and clearance of metformin as well as metformin accumulation in tissues, especially in the adipose tissue. The pharmacologic response to metformin was also reduced in *Oct3* knockout mice. Consistent with these results in mice, humans harboring a reduced function 3'UTR variant of *OCT3* also exhibited reduce response to metformin. Collectively, our data suggested that reduced OCT3 function is associated with altered pharmacokinetics and pharmacodynamics of metformin.

OCT3 function may be modulated by reduced function polymorphisms, but also by concomitant medications. Twenty-five percent of the U.S. population over 65 has a diagnosis of diabetes[12] and polypharmacy is common among the elderly[13]. It is therefore important to identify inhibitors that could interact with OCT3 and may

potentially reduce the efficacy of metformin. To this end, we developed a high-throughput screen (HTS) using the fluorescent substrate, 4-Di-1-ASP (ASP^+), to identify inhibitors of OCT3 activity in cell line overexpressing the transporter. Our HTS identified 210 compounds as OCT3 inhibitors out of 2,556 structurally diverse prescription drugs, natural products, and bioactive molecules screened. Most of inhibitors that were identified in the screen were previously not known to inhibit OCT3. Twenty-three of the 210 inhibitors were potent inhibitors and could potentially cause clinical relevant drug-drug interactions based on their predicted IC_{50} and reported plasma C_{MAX} values. Additionally, 50 compounds could inhibit OCT3 in the intestine based on their maximum expected concentrations in the intestine lumen. Using the data from the screen, a predictive structure-activity relationship (SAR) model was developed to inform future *in vitro* studies in drug development.

RESULTS

HTS identified novel OCT3 inhibitors.

A HTS assay was developed using the fluorescent probe, ASP^+, in HEK cells overexpressing OCT3 as a measurement of transporter activity[14,15]. OCT3 transported ASP^+ in a time dependent manner and the uptake was linear until 5 minutes. The K_m of OCT3-mediated ASP^+ uptake was 33.3 μM (Fig. 3.1A, B). Thus, an incubation time of 2 minutes was used to measure the initial rate of ASP^+ uptake and an ASP^+ concentration of 2 μM was used to minimize the effect of substrate concentration on the IC_{50} values[16]. In our HTS assay, an inhibitor was defined as any compound that inhibited 50% or more of the ASP^+ uptake at 20 μM. Of the 2,556 compounds in the Spectrum library, we identified 210 (8.4%) OCT3 inhibitors (Figure 3.1C). Most inhibitors identified were previously not known to interact with OCT3. Based on predicted IC_{50} and reported maximum plasma levels, C_{MAX}, we also predicted that 23 of the 210 inhibitors could potentially cause drug-drug interactions (Table 3.1). In addition, 50 of the 210 inhibitors could potentially inhibit OCT3 in the intestine based on their maximum expected concentrations in the intestine lumen. The average Z-prime of the HTS was 0.73, indicating an excellent HTS assay[17].

Inhibitors were grouped into pharmacological classes, and several of these drug classes were enriched in our HTS (Fig. 3.1D). Similar to inhibitors of OCT1, steroids, antihistamines, and α adrenergic receptor antagonists were more likely to inhibit OCT3[14]. In addition, we identified OCT3 inhibitors in other classes as well, including β

adrenergic receptor agonists/antagonists, sodium/calcium channel blockers, 5-HT receptor agonists/antagonists, and dopamine receptor agonists/antagonists. However, tricyclic antidepressants that commonly inhibit OCT1 and OCT2[14,15] were not enriched in our HTS. In fact, none of the eight TCAs tested inhibit 50% or more OCT3 mediated ASP^+ uptake at 20 μM.

Select compounds previously not known to inhibit OCT3 were validated by determining their IC_{50} in inhibition studies (Fig 3.3). *In vitro* studies showed that their IC_{50} values were below 20 μM when tested against OCT3 mediated ASP^+ uptake. Interestingly, when the inhibition potencies were tested against OCT3 mediated [^{14}C] metformin uptake, the determined IC_{50} values were generally lower than those of ASP^+ uptake (Fig. 3.3). For example, the IC_{50} values against ASP^+ uptake for telmisartan and amiloride were determined to be 12.0 μM and 14.5 μM, respectively (Fig. 3.2A,B). When tested against OCT3 mediated [^{14}C] metformin uptake, the IC_{50} values for telmisrtan and amiloride were determined to be 3.9 μM and 3.0 μM, respectively (Fig. 3.3A,B). The result suggests that for these two compounds, the inhibition potency was greater for OCT3-mediated metformin uptake than OCT3-mediated ASP^+ uptake.

Structure-activity relationship, SAR, modeling

Next, we generated an SAR model capable of discriminating OCT3 inhibitors from noninhibitors. The 2,556 compounds were first classified as inhibitors or noninhibitors of OCT3 based on their ability to inhibit >50% of ASP^+ uptake at 20 μM. Molecular descriptors were generated for each compound and were used to develop

the model. Using partial least square (PLS) projection, we were able to identify descriptors that could classify inhibitors and noninhibitors. After optimization through an iterative variable procedure (i.e. descriptors with low influence on the model were removed in a step-wise manner, removing smaller and smaller chunks as the selection progressed), we arrived at a set of important descriptors used in the final model (Fig. 3.4A). As expected, cationic compounds were more likely to interact with OCT3. Inhibitors are also more likely to be larger (topological diameter), spherical (asphericity), and with less freely rotatable bounds. Lastly, a double-loop cross-validation procedure was used to evaluate the SAR model, since this gives an unbiased estimate of external model predictivity (Table 3.3). The final SAR model had an average accuracy of 0.76, and an average precision of 0.58. The receiver operating characteristic (ROC) curve (Fig. 3.4B), a graphical representation of the performance of a model, showed an area under the curve (AUC) of 0.77, indicating a good binary classifier SAR model.

Virtual Screening by SAR model of a drug library

In this study, we screened a large compound library, the Spectrum library, for OCT3 inhibitors. While the library contains 2,556 compounds, only 60% of the compounds are drugs and the rest are bioactives and natural products. In order to identify additional OCT3 inhibitors among registered drugs, we applied our SAR model against all registered drugs in the KEGG drug database (2,643 drugs) to predict OCT3 inhibitors *in silico*. Each drug in the database was assigned a probability value of interacting with OCT3. Using 75% as the cutoff, 6.4% of the 2,643 compounds were

predicted to interact with OCT3; many of these drugs were novel OCT3 inhibitors and were not included in Spectrum library. Selected compounds were validated by determining their IC_{50} in inhibition studies. From the *in silico* model, carvedilol, doxazosin, and risperidone had probabilities of 86%, 93%, and 82%, respectively, of inhibiting OCT3. Experimental studies confirmed the predictions, and the IC_{50} values of the three compounds were determined to be 19.7 μM, 5.6 μM, and 1.9 μM, respectively; Fig. 3.5A, B, C). In contrast, desipramine had a probability of 55% of inhibiting OCT3, below the cutoff value, and did not inhibit 50% or more OCT3 activity at 20 μM (Fig. 3.5D).

DISCUSSION

In chapter two, we showed that murine OCT3 is involved in metformin disposition and response. We also showed that a reduced function variant of OCT3 was associated with response to metformin in healthy volunteers. These results suggest that inhibitors of OCT3 could potentially cause drug-drug interactions when co-administered with metformin. The goals of this study were to develop a HTS to identify OCT3 inhibitors and to develop a predictive SAR model capable of distinguishing between OCT3 inhibitors and noninhibitors. Our key findings are described below.

HTS identified prescription drugs that were predicted to cause clinical drug-drug interactions.

We developed a HTS assay using ASP^+ as a measure of OCT3 activity in cell line overexpressing the transporter. Our HTS of a large compound library consisting of 2,556 prescription drugs, bioactive, and natural products, identified 210 inhibitors that inhibit 50% or more OCT3 activity at 20 μM (Fig 3.1C). Since this is the first large-scale inhibitor screen against OCT3, most of the inhibitors identified were novel, i.e., not previously known to interact with OCT3. We grouped the inhibitors into pharmacological classes and identified drug classes that were more likely to contain inhibitors of OCT3 (Figure 3.1D). Drugs in several of the classes have also been found to inhibit OCT1 and OCT2[14,15]. Surprisingly, tricyclic antidepressants (TCAs), many of which are well-

established inhibitors of OCT1 and OCT2, were not included among the classes of drugs that are enriched for inhibitors of OCT3. Notably, none of the TCAs tested were inhibitors of OCT3. The observation could be explained by the structural differences between the three OCTs. Based on the recently solved structure of a eukaryotic SLC22 homolog[18], a preliminary alignment of the predicted binding sites suggested that OCT3 is more dissimilar to OCT1 and OCT2 (data not shown). While OCT1 and OCT2 share many residues predicted to be important in substrate binding, OCT3 differs significantly in some of the important residues shared between OCT1 and OCT2. Our data also showed that drugs that interact with monoamine receptors such as receptors for histamine, adrenergic agents, serotonin (5-HT), and dopamine often interact with OCT3. OCT3 transports many neurotransmitters and is expressed in regions of the brain[19]. Future studies are needed to explore the impact of OCT3 in the pharmacological actions of these inhibitors.

Based on the predicted IC_{50} values, we identified 23 drugs that could potentially cause drug-drug interactions with metformin at clinical relevant concentrations (Table 3.1). As the unbound drug is often considered the active form of the drug, we compared the predicted IC_{50} values of the drugs with their maximum unbound concentration in plasma, which was obtained from the literature or predicted from their total maximum plasma concentration and their percent unbound in plasma. Nine of the 23 drugs had predicted IC_{50} values less than 10 times their unbound C_{MAX} values after therapeutic doses, suggesting that these nine compounds have the potential to cause clinical drug-drug interactions with metformin. Fourteen of the 23 compounds

had IC_{50} value less than 10 times their total C_{MAX} values. These compounds may potentially inhibit OCT3 at clinical concentrations, but would be less likely to than the nine compounds. The IC_{50} values were determined experimentally *in vitro* for selected drugs, and the values were in range of their predicted IC_{50} values. For example, telmisartan and trazodone were predicted to have IC_{50} values of 5 μM, and their IC_{50} were determined to be 12.0 μM and 5.2 μM, respectively (Figure 3.2A, E).

OCT3 gene deletion was shown in chapter 2 to result in reduced bioavailability of metformin. Given its localization on the apical membrane of the intestine[20], OCT3 activity could potentially modulate the absorption of OCT3 substrates into the systemic circulation. Thus, inhibitors of OCT3 may decrease the uptake of OCT3 substrates from the intestinal lumen and reduce their bioavailability. In Table 3.2, we identified 50 inhibitors of OCT3 whose predicted IC_{50} values was smaller than their maximum expected concentrations in the intestine lumen (0.1 – fold the maximum dose on one occasion / 250 ml). Based on the estimation, these prescription drugs could potentially inhibit OCT3 in the intestine and cause drug-drug interactions related to absorption. These 50 compounds meet the criteria recommended by regulatory agencies to initiate *in vivo* drug-drug interaction studies[21].

Finally, we compared the potencies of select inhibitors against ASP^+ with their potencies against metformin. Interestingly, all inhibitors tested had a lower IC_{50} value against OCT3 mediated metformin uptake (Fig 3.3). One possible explanation is that multiple binding sites exist in OCT3, and ASP^+ and metformin interact differently with

one or more of the binding sites. Therefore, inhibitors have substrate-dependent potencies based on how substrates interact with the transporter. However, it is also possible that differences in the experimental procedures resulted in this discrepancy (fluorescent probe uptake *versus* isotopic uptake procedures). For example, although the concentrations of probe substrates were lower than their K_m values and should not significantly alter K_i based on the Cheng-Prusoff equation[16], the concentration of metformin used in isotopic uptake (1 μM) was at least 0.001 – fold lower than its K_m (1.5mM), significantly lower than the ratio of the concentration of ASP^+ (2 μM) to its K_m (33.3 μM).

Virtual screening using a SAR model identified novel OCT3 inhibitors.

In light of the inclusion of transporters in the FDA draft guidance on drug interactions[22], increasingly the requirements to identify transporter inhibitors and substrates will be expanded. Predictive models for both substrates and inhibitors are needed to inform *in vitro* studies carried out during drug discovery and development to assess drug-drug interaction liabilities. Here, we developed an SAR model using data generated by our HTS. The predictive SAR model is capable of identifying OCT3 inhibitors and noninhibitors (Figure 3.4). A virtual screen using the SAR model against all current registered drugs showed that our SAR model was able to accurately identify known inhibitors and predict novel OCT3 inhibitors. Until recently, it was often assumed that transporter inhibitors interact with the protein in a competitive manner only. Studies now suggest that the inhibition can occur by other mechanisms as well (competitive inhibition, non-competitive inhibition, mixed inhibition)[23]. This is especially

true for polyspecific transporters, where multiple substrate binding sites may exist. The International Transporter Consortium recently acknowledged that our lack of understanding of the inhibition mechanism is a limiting factor in transporter studies[24]. However, our HTS and SAR model would not be able to identify or predict the mechanism of inhibition.

It is possible to predict whether an inhibitor binds to the binding site of a transporter, therefore identifying the mechanism of inhibition, with the use of a structure-based model. Because of their multiple transmembrane domains and relatively low affinity to substrates, it is notoriously difficult to crystalize polyspecific transporters and obtain accurate structure information. A prokaryotic homolog of the SLC family protein, LeuT, had been solved and was used to generate comparative models of human SLC transporters[25–27]. However, its low sequence similarity to OCTs casts doubt on comparative models generated based on LeuT structure. Recently, the structure of a phosphate transporter from *Piriformospora indica* (PipT) was solved[18]. It shares homology with SLC transporters, especially the SLC22 family in which OCTs belong, and could be used for comparative modeling. In chapter 4, we successfully constructed a comparative model of OCT1 based on the structure of PipT, and we demonstrate its accuracy in predicting orthosteric ligands and selective inhibitors. New technology, such as the cryo-transmission electron microscopy, is also promising in solving membrane transporter structures. Future studies are needed to explore these options to generate structure-based models for polyspecific transporters.

OCT3 shares significant sequence homology with OCT1 and OCT2[28]. However, the predicted binding site of OCT3 is more dissimilar to OCT1 and OCT2 based on comparative models built with PipT structure (data not shown). The predicted differences agree with the observed substrate specificity of OCTs, for example, the differential substrate selectivity for platins (see chapter 1). In Figure 3.6, we compared HTS data of OCT1, OCT2, and OCT3 to investigate inhibitor selectivity among the three OCTs. Of the 717 compounds with inhibition data for all three transporters, 25 compounds are identified as pan-inhibitors of OCTs. OCT1 and OCT2 share 78 inhibitors, while OCT3 shares significantly less inhibitors with OCT1 and OCT2 (58 inhibitors and 28 inhibitors, respectively). The result agrees with the predicted differences in binding sites and suggests that a comparative model could be used to predict selective inhibitors among OCTs.

In conclusion, we developed and conducted a HTS against a large compound library for OCT3 inhibitors. We identified 210 OCT3 inhibitors, most of them previously not known to interact with OCT3. Using the HTS data, we generated a predictive SAR model capable of discriminating OCT3 inhibitors from noninhibitors. Virtual screen using of a comprehensive prescription drug library against the SAR model identified additional OCT3 inhibitors. Of the inhibitors identified in this study, 23 compounds can potentially inhibit OCT3 at clinically relevant drug concentrations, and lead to pharmacodynamic as well as pharmacokinetic drug-drug interactions with metformin.

METHODS

Chemicals

The MicroSource Spectrum compound library (Gaylordsville, CT) was obtained through the Small Molecular Discovery Center at University of California, San Francisco (San Francisco, CA). 4-Di-1-ASP was purchased from Molecular Probes (Grand Island, NY). All other chemicals were purchased from Sigma-Aldrich (St. Louis, MO). All cell culture media and supplements were purchased from Life Technologies (Carlsbad, CA) except fetal bovine serum, which was purchased from GE Healthcare Life Sciences (South Logan, UT).

Cell culture

A Human embryonic kidney (HEK-293) cell line stably overexpressing OCT3 was established previously in our laboratory[29]. The cells were maintained in Dulbecco's Modified Eagle's Medium (DMEM H-21) supplemented with 75 μg/ml of hygromycin B, penicillin (100 U/ml), streptomycin (100 mg/ml), and 10% fetal bovine serum in a humidified atmosphere with 5% CO_2 at 37°C.

In vitro uptake studies

HEK-293 cells overexpressing OCT3 were seeded in black, clear bottom poly-D-lysine coated 96-well plates (Greiner Bio-One, Monroe, NC) and allowed to grow for 48 hours until approximately 90% confluency. For uptake kinetic studies, cells were incubated with HBSS containing serial dilution of ASP^+ for 2 minutes at 37°C. At the end of experiments, the media were aspirated and the cells were washed twice with ice-cold HBSS containing 50 μM corticosterone. The K_m and V_{max} were calculated by fitting the data to Michaelis-Menten equations. For time course studies, cells were incubated with HBSS containing 2 μM ASP^+ at 37°C. At various time points, the experiment was stopped as previously described. For IC_{50} determination, cells were incubated with HBSS containing 2 μM ASP^+ or 1 μM metformin with 0.5 μCi/ml [^{14}C] metformin, and serial dilution of inhibitors for 2 minutes at 37°C. IC_{50} values were determined using appropriate curve fitting. The signal of ASP^+ was measured using an Analyst AD plate reader (Molecular Devices, Sunnyvale, CA) with excitation and emission filters tuned at 485 and 585 nm wavelength, respectively. All statistical analysis and curve fitting were done using GraphPad Prism software (La Jolla, CA).

High-throughput screening

The high throughput screen was performed at the Small Molecule Discovery Center at the University of California, San Francisco. HEK-293 cells overexpressing OCT3 were seeded in black, clear bottom poly-D-lysine coated 96-well plates (Greiner Bio-One, Monroe, NC) and allowed to grow for 48 hours until approximately 90% confluency.

Cells were incubated with HBSS containing 2mM ASP^+ and 20μM of test compounds at ambient temperature for approximately 2 minutes. At the end of the experiment, media were aspirated and cells were washed twice with HBSS containing 50 μM corticosterone. Nonspecific transport was determined in wells on each assay plate using 100 μM corticosterone as OCT3 inhibitor. The screen was carried out with a Biomek FXp liquid handler (Beckman Coulter, Brea, CA). Fluorescence was measured as previously described.

Molecular descriptor generation

The molecular descriptor generation was performed as previously described[15]. Three-dimensional molecular structures were generated from SMILES representations using Corina, version 3.0 (Molecular Networks, Erlangen, Germany), keeping the lowest energy conformation of a maximum of 100 alternative ring conformations, and were used as input for molecular descriptor calculation with DragonX, version 1.4 (Talete, Milan, Italy), ADMETPredictor, version 5.0 (SimulationsPlus, Lancaster, CA), and MAREA, version 3.02[30]. After removal of replicate molecular descriptors and descriptors having zero variance, the remaining descriptors were used for cluster analyses and as the starting point for structure-activity model development.

Structure-activity modeling

The structure-activity modeling was generated as previously described[15]. Partial least-squares discriminant analysis (PLS-DA) was used to develop computational models that differentiate between OCT1 inhibitors and noninhibitors based on differences in

molecular descriptor values. A double-loop cross-validation procedure was used to provide an unbiased estimate of the prediction accuracy. Variable selection was performed in two phases: first, the descriptors with lowest absolute PLS weight were iteratively removed until only the 25 most important ones remained; second, the same procedure was repeated, but descriptors were kept in the model if removal resulted in an inferior model. The entire double-loop procedure was repeated 100 times for different random partitionings of the data set to enable calculation of confidence intervals of prediction accuracy estimates and model parameters (Table 2).

Table 3.1. Prescription drugs that could potentially cause drug-drug interactions

Compound	Inhibition (%)	Predicted IC_{50} (μM)*	C_{MAX} (μM) †	Protein binding	C_{MAX}/ IC_{50}	Unbound C_{MAX}/ IC_{50}
		Compounds with unbound $IC_{50}/C_{MAX} > 0.1$				
Azlocillin	66.9	9.9	17.3	30%	1.75	1.23
Aztreonam	87.1	5	585	56%	117	51.5
Famotidine	66.9	9.9	308	10%	31.1	28.0
Flufenamic acid	60.6	13.0	24.2	90%	1.9	0.19
Meropenem	65	10.8	256	2%	23.8	23.3
Propafenone	74	7.0	7.9	85%	1.13	0.17
Quinine	90.6	5	10.7	69%	2.15	0.67
Trazodone	94.5	5	7.6	90%	1.53	0.15
Trimethoprim	59.3	13.7	5.9	44%	0.43	0.24
		Compounds with total $IC_{50}/C_{MAX} > 0.1$				
Cilostazol	93.8	5	2.1	95%	0.42	
Emetine	82.7	5	0.6	90%	0.12	
Exemestane	94.5	5	1.4	90%	0.28	
Glimepiride	87.7	5	1.2	99%	0.24	
Imatinib	72.2	7.7	1.2	95%	0.16	
Ketoconazole	93.4	5	1.9	91%	0.38	
Lansoprazole	87.2	5	2.9	97%	0.59	
Leflunomide	50.5	19.6	233	99.3%	11.9	
Omeprazole	64.1	11.2	4.2	95%	0.38	
Prednisolone	67.5	9.6	2.9	70%	0.30	
Rabeprazole	87.3	5	1.3	96%	0.26	
Spironolactone	82.8	5	1.1	93%	0.22	
Telmisartan	81.6	5	2.8	99.5%	0.56	
Valdecoxib	53.6	17.3	2.2	98%	0.13	

* Predicted IC_{50} is calculated based on the percent inhibition values (Materials and Methods).

† C_{MAX} values were obtained from http://www.micromedexsolutions.com/

Table 3.2. Prescription drugs that could inhibit OCT3 in the intestine

Compound	Inhibition (%)	Maximum Dose (mg)	Predicted IC_{50} (μM)*	$C_{Intestine}$ (μM) †
Amiloride	88.3	20	5.0	34.8
Betamethasone	78.1	7.2	5.6	7.3
Buspirone	62	90	12.3	93.4
Camostat	86.7	200	5.0	200.8
Carvedilol	55.5	50	16.0	49.2
Cilostazol	93.8	100	5.0	108.3
Clozapine	54.5	150	16.7	183.6
Dehydroepiandrosterone	78.6	50	5.4	69.3
Diazepam	69.3	10	8.9	14.0
Diphenidol	51.8	50	18.6	64.6
Dipyridamole	85.3	100	5.0	79.3
Doxazosin	93	8	5.0	7.1
Famotidine	66.9	160	9.9	189.7
Flufenamic acid	60.6	400	13.0	568.9
Gossypol	62.9	60	11.8	46.3
Guanabenz	99.4	32	5.0	55.4
Hydrocortisone	65.9	240	10.3	264.9
Ibudilast	86.6	10	5.0	17.4
Imatinib	72.2	400	7.7	324.1
Ketoconazole	93.4	400	5.0	301.1
Lansoprazole	87.2	30	5.0	32.5
Leflunomide	50.5	100	19.6	148.0
Mebeverine	91.7	400	5.0	372.5
Melatonin	61.1	20	12.7	34.4
Methoxsalen	50	70	20.0	129.5
Methylprednisolone	65.8	48	10.4	51.3
Metoclopramide	73.7	15	7.1	17.8
Nefopam	53	60	17.7	94.7
Nylidrin	79.5	12	5.2	16.0
Omeprazole	64.1	20	11.2	23.2
Perospirone	54.7	48	16.6	45.0
Phentolamine	84	80	5.0	113.7
Prazosin	80.2	15	5.0	15.6
Prednisolone	67.5	60	9.6	66.6
Propafenone	74	425	7.0	449.8
Propranolol	82.9	640	5.0	987.1
Quinacrine	55.7	200	15.9	169.2
Quinine	90.6	650	5.0	801.4
Rabeprazole	87.3	20	5.0	22.3
Ritodrine	63.7	40	11.4	49.4
Spironolactone	82.8	400	5.0	384.1
Sulfinpyrazone	74.3	800	6.9	791.1
Tacrine	98.5	160	5.0	322.8
Tegaserod	95.1	6	5.0	8.0
Telmisartan	81.6	80	5.0	62.2
Trazodone	94.5	600	5.0	645.4
Trimethobenzamide	52.2	300	18.3	282.4
Trimethoprim	59.3	200	13.7	275.6

Valdecoxib	53.6	20	17.3	25.4
Verapamil	65.1	480	10.7	422.3

* Predicted IC_{50} is calculated based on the percent inhibition values (Materials and Methods).

† $C_{Intestine}$ represents the maximum expected concentration in the intestinal lumen on the apical side of the enterocytes (0.1 – fold the maximum dose on one occasion / 250 ml)[21].

Table 3.3. Statistics of SAR model

	Internal (confidence interval)		External (confidence interval)	
n components	4.4 ± 0.1	1 - 11		
n variables	45.5 ± 0.6	10 - 73		
AUC	0.82 ± 0.0008	0.75 - 0.86	0.77 ± 0.0008	0.75 - 0.79
MCC	0.32 ± 0.0011	0.23 - 0.40	0.25 ± 0.0015	0.21 - 0.28
Accuracy	0.78 ± 0.0008	0.72 - 0.83	0.76 ± 0.0008	0.74 - 0.78
Balanced accuracy	0.75 ± 0.0007	0.68 - 0.80	0.70 ± 0.0011	0.67 - 0.72
Informedness	0.50 ± 0.0014	0.36 - 0.61	0.40 ± 0.0023	0.33 - 0.45
TPR* precision	0.23 ± 0.0008	0.18 - 0.29	0.20 ± 0.0008	0.18 - 0.22
TNR* precision	0.97 ± 0.0001	0.95 - 0.98	0.96 ± 0.0002	0.95 - 0.96
TPR* recall	0.72 ± 0.0010	0.59 - 0.81	0.62 ± 0.0023	0.56 - 0.68
TNR* recall	0.78 ± 0.0008	0.73 - 0.84	0.77 ± 0.0008	0.75 - 0.80
Average precision	0.60 ± 0.0001	0.18 - 0.98	0.58 ± 0.0003	0.18 - 0.96
Average recall	0.75 ± 0.0001	0.59 - 0.84	0.70 ± 0.0013	0.56 - 0.80

*True positive rate (TPR); true negative rate (TNR).

Figure 3.1

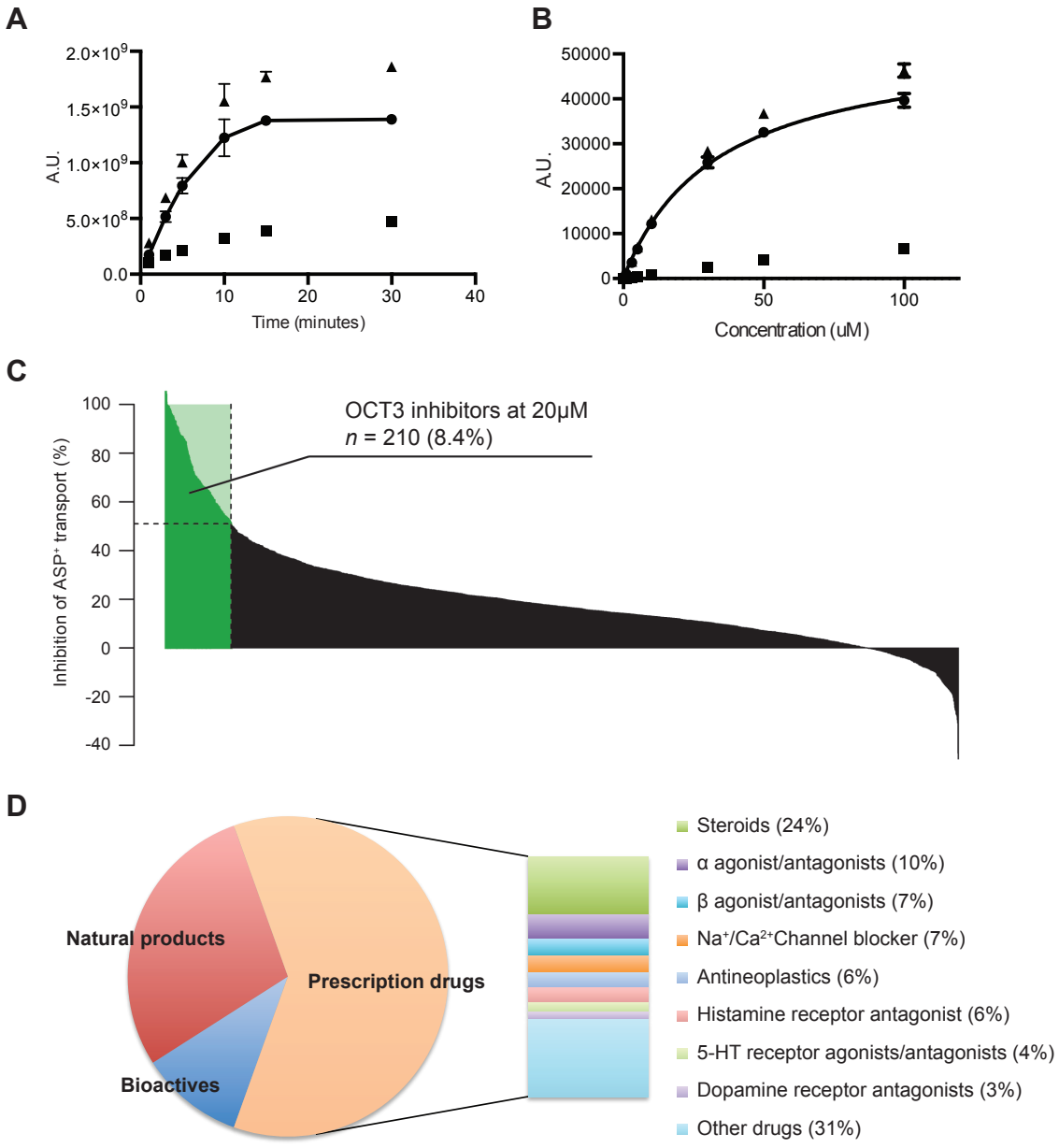

Figure 3.1. HTS of a 2,556 compound library that included prescription drugs and bioactive molecules identified 210 OCT3 inhibitors. (A) Time-dependent ASP^+ uptake in HEK cells overexpressing OCT3 (▲) or empty vector (■), and OCT3-specific ASP^+

uptake (●) given in activity units (A.U.). The uptake was linear for the first 5 minutes. (B) Overexpressing OCT3 increases ASP^+ uptake in HEK cells. ASP^+ uptake studies were conducted in HEK cells overexpressing OCT3 (▲) or empty vector (■). Cells were incubated with increasing concentrations of ASP^+ for 2 minutes. The K_M of OCT3 mediated ASP^+ uptake was determined to be 33.3 μM. The uptake kinetic parameters were calculated using the difference in ASP^+ accumulation between cells overexpressing OCT3 and empty vector cells (●). Data represent mean ± SD, $n = 6$ per data point. (C) 210 inhibitors capable of inhibiting OCT3 activity 50% or more at 20 μM were identified among 2,556 drugs, natural products, and bioactives. (D) The proportions of inhibitors grouped into drug classes.

Figure 3.2

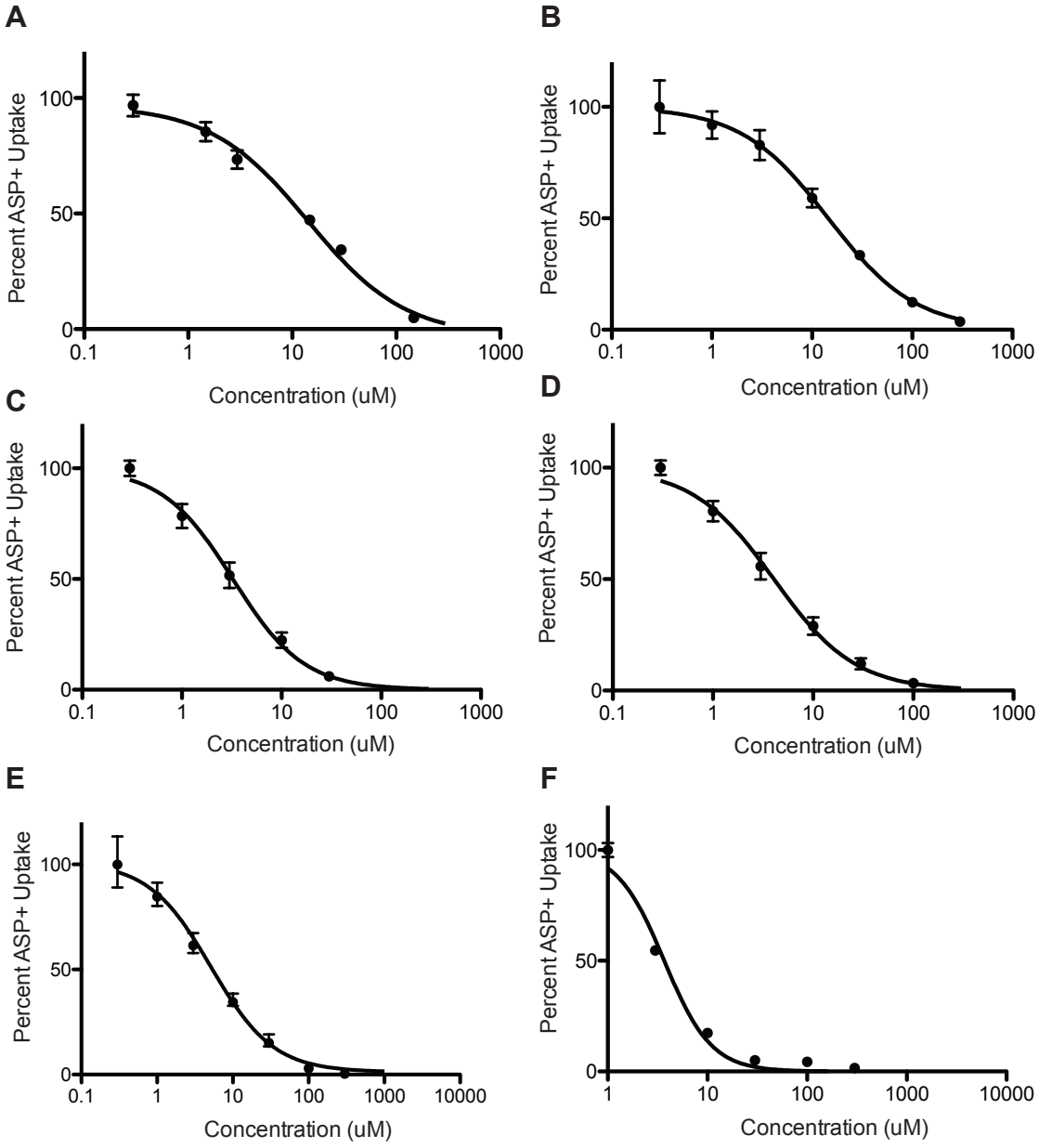

Figure 3.2. Validation of selected inhibitors identified in OCT3 HTS. OCT3 inhibitors identified by HTS were validated by determining their IC_{50} values in inhibition studies, using 2 μM ASP^+ as probe substrates. (A) The IC_{50} of telmisartan was determined to be

12.0 (10.8 ; 13.4) μM. (B) The IC_{50} of amiloride was determined to be 14.5 (12.9 ; 16.4) μM. (C) The IC_{50} of guanabenz was determined to be 3.2 (3.0 ; 3.6) μM. (D) The IC_{50} of papaverine was determined to be 4.1 (3.7 ; 4.4) μM. (E) The IC_{50} of trazodone was determined to be 5.2 (4.6 ; 5.8) μM. (F) The IC_{50} of chlorhexidine was determined to be 3.7 (3.3 ; 4.1) μM. Data represent mean ± SD, n = 6 per data point, 95% confidence limits in parenthesis.

Figure 3.3

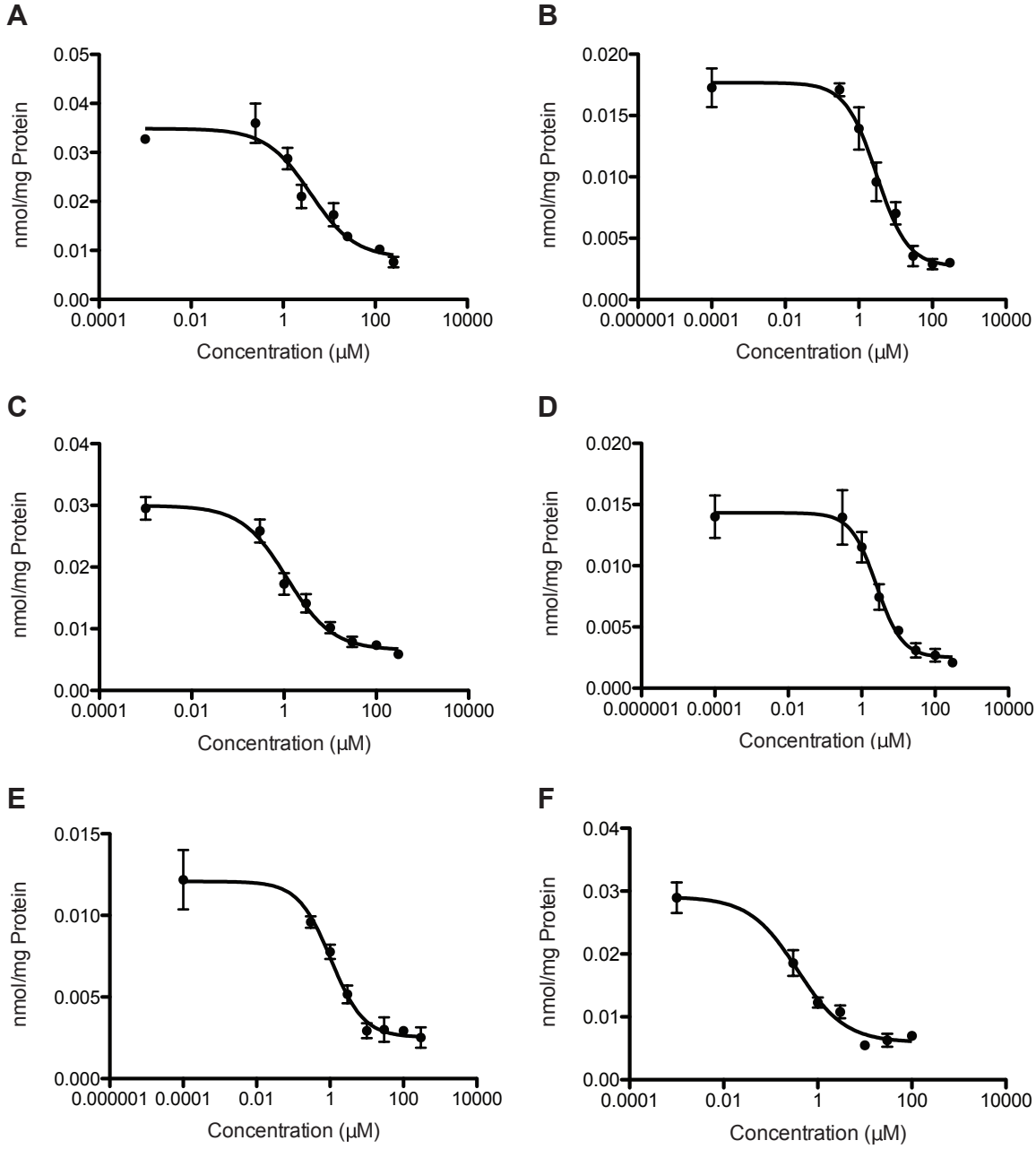

Figure 3.3. Inhibition of OCT3-mediated metformin (1 μM unlabed metformin with 0.5 μCi/ml [^{14}C] metformin) uptake of selected compounds identified in HTS assay. (A) The IC_{50} of telmisartan was determined to be 3.9 (1.7 ; 9) μM. (B) The IC_{50} of amiloride was

determined to be 3.0 (2.1 ; 4.4) μM. (C) The IC_{50} of papaverine was determined to be 1.3 (1.0 ; 1.9) μM. (D) The IC_{50} of doxazosin was determined to be 2.5 (1.7 ; 3.7) μM. (E) The IC_{50} of guanabenz was determined to be 1.1 (0.7 ; 1.6) μM. (F) The IC_{50} of econazole was determined to be 0.4 (0.2 ; 0.7) μM. Data represent mean ± SD, n = 3 per data point, 95% confidence limits in parenthesis.

Figure 3.4

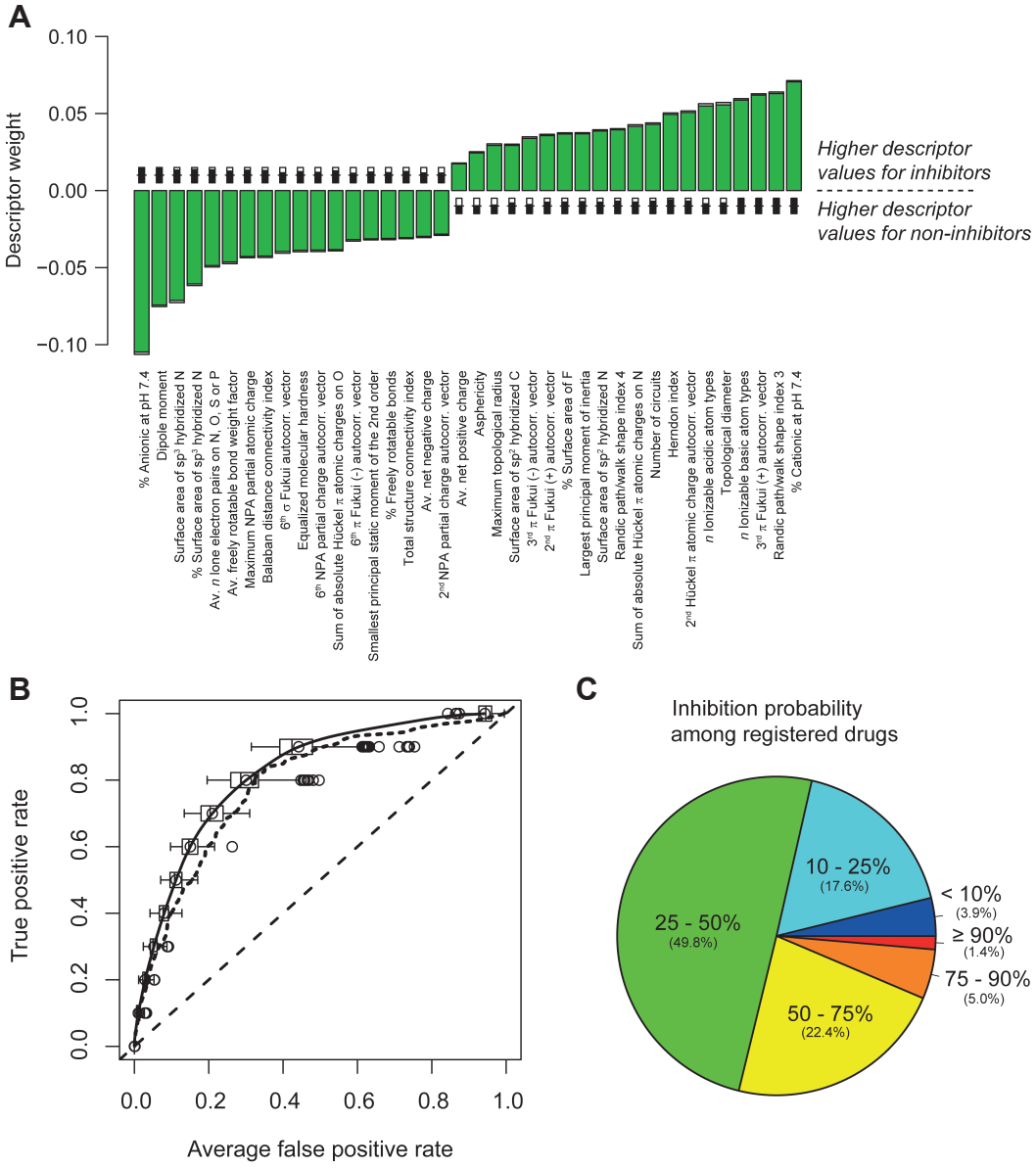

Figure 3.4. SAR model and virtual screening against KEGG drug library. (A) Important molecular descriptors used to classify inhibitors and noninhibitors. Bar shows the mean PLS regression coefficients from cross-validated models. Descriptors with positive coefficient have higher values in inhibitors, and descriptors with negative

values have higher values in noninhibitors. (B) ROC curves for 100 retrospective cross-validation runs. Average ROC curve is shown in solid black line. The AUC for the final SAR model was determined to be 0.77. (C) Inhibition probability result from the virtual screen against registered drugs.

Figure 3.5

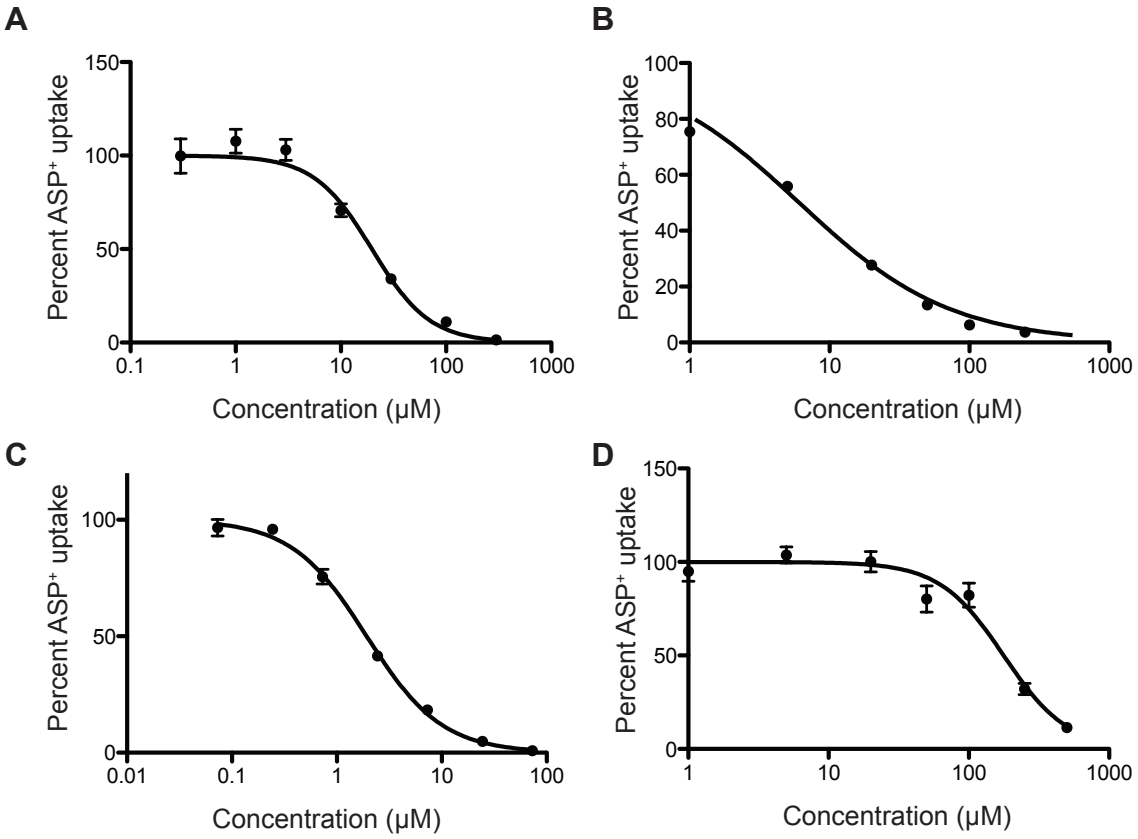

Figure 3.5. *In vitro* validation of the SAR predictions. . OCT3 inhibitors identified by SAR screen were validated by determining their IC_{50} values in inhibition studies, using 2 μM ASP^+ as probe substrates. (A) SAR model predicted carvedilol has an 86% probability of inhibiting OCT3. The IC_{50} was determined to be 19.7 (17.5 ; 22.2) μM. (B) SAR model predicted doxazosin has a 93% probability of inhibiting OCT3. The IC_{50} was determined to be 5.6 (5.0 ; 6.2) μM. (C) SAR model predicted risperidone has an 82% probability of inhibiting OCT3. The IC_{50} was determined to be 1.9 (1.7 ; 2.1) μM.

(D) SAR model predicted desipramine has a 55% probability of inhibiting OCT3 (below 75% cutoff). The IC_{50} was determined to be 177 (148.6, 211.0) μM. Data represent mean ± SD, *n* = 6 per data point, 95% confidence limits in parenthesis.

Figure 3.6

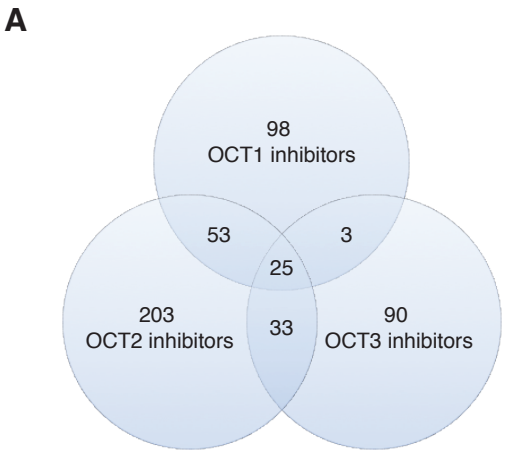

Figure 3.6. Venn diagram showing the overlapping inhibitors for OCT1, OCT2, and OCT3. Based on available HTS data for 717 compounds.

REFERENCE

1. Ogden, C. L., Carroll, M. D., Curtin, L. R., Lamb, M. M. & Flegal, K. M. Prevalence of high body mass index in US children and adolescents, 2007-2008. *JAMA* **303,** 242–9 (2010).

2. Flegal, K. M., Carroll, M. D., Ogden, C. L. & Curtin, L. R. Prevalence and trends in obesity among US adults, 1999-2008. *JAMA* **303,** 235–41 (2010).

3. Boyle, J. G., Salt, I. P. & McKay, G. A. Metformin action on AMP-activated protein kinase: a translational research approach to understanding a potential new therapeutic target. *Diabet. Med.* **27,** 1097–106 (2010).

4. Kirpichnikov, D., McFarlane, S. I. & Sowers, J. R. Metformin: an update. *Ann. Intern. Med.* **137,** 25–33 (2002).

5. Glueck, C. J. *et al.* Sustainability of 8% weight loss, reduction of insulin resistance, and amelioration of atherogenic-metabolic risk factors over 4 years by metformin-diet in women with polycystic ovary syndrome. *Metabolism* **55,** 1582–9 (2006).

6. Pasquali, R. *et al.* Effect of long-term treatment with metformin added to hypocaloric diet on body composition, fat distribution, and androgen and insulin levels in abdominally obese women with and without the polycystic ovary syndrome. *J. Clin. Endocrinol. Metab.* **85,** 2767–74 (2000).

7. Kay, J. P. *et al.* Beneficial effects of metformin in normoglycemic morbidly obese adolescents. *Metabolism* **50,** 1457–61 (2001).

8. Turner, R. C., Cull, C. A., Frighi, V. & Holman, R. R. Glycemic control with diet, sulfonylurea, metformin, or insulin in patients with type 2 diabetes mellitus: progressive requirement for multiple therapies (UKPDS 49). UK Prospective Diabetes Study (UKPDS) Group. *JAMA* **281,** 2005–12 (1999).

9. Villena, J. A. *et al.* Induced adiposity and adipocyte hypertrophy in mice lacking the AMP-activated protein kinase-alpha2 subunit. *Diabetes* **53,** 2242–9 (2004).

10. Blázquez, C., Geelen, M. J., Velasco, G. & Guzmán, M. The AMP-activated protein kinase prevents ceramide synthesis de novo and apoptosis in astrocytes. *FEBS Lett.* **489,** 149–53 (2001).

11. Moreno-Navarrete, J. M. *et al.* OCT1 Expression in adipocytes could contribute to increased metformin action in obese subjects. *Diabetes* **60,** 168–76 (2011).

12. Wild, S., Roglic, G., Green, A., Sicree, R. & King, H. Global prevalence of diabetes: estimates for the year 2000 and projections for 2030. *Diabetes Care* **27,** 1047–53 (2004).

13. Fulton, M. M. & Allen, E. R. Polypharmacy in the elderly: a literature review. *J. Am. Acad. Nurse Pract.* **17,** 123–32 (2005).

14. Ahlin, G. *et al.* Structural requirements for drug inhibition of the liver specific human organic cation transport protein 1. *J. Med. Chem.* **51,** 5932–42 (2008).

15. Kido, Y., Matsson, P. & Giacomini, K. M. Profiling of a prescription drug library for potential renal drug-drug interactions mediated by the organic cation transporter 2. *J. Med. Chem.* **54,** 4548–58 (2011).

16. Cheng, Y. & Prusoff, W. H. Relationship between the inhibition constant (K1) and the concentration of inhibitor which causes 50 per cent inhibition (I50) of an enzymatic reaction. *Biochem. Pharmacol.* **22,** 3099–108 (1973).

17. Zhang, J.-H., Chung, T. & Oldenburg, K. A simple statistical parameter for use in evaluation and validation of high throughput screening assays. *J. Biomol. Screen.* **4,** 67–73 (1999).

18. Pedersen, B. P. *et al.* Crystal structure of a eukaryotic phosphate transporter. *Nature* **496,** 533–6 (2013).

19. Amphoux, A. *et al.* Differential pharmacological in vitro properties of organic cation transporters and regional distribution in rat brain. *Neuropharmacology* **50,** 941–52 (2006).

20. Müller, J. *et al.* Drug specificity and intestinal membrane localization of human organic cation transporters (OCT). *Biochem. Pharmacol.* **70,** 1851–60 (2005).

21. Guideline on the Investigation of Drug Interactions. *European Medicines Agency: CPMP/EWP/560/95/Rev. 1 Corr.** **1,** (2012).

22. Guidance for Industry Drug Interaction Studies. *U.S. Department of Health and Human Services Food and Drug Administration Center for Drug Evaluation and Research (CDER)* (2012). at <http://www.fda.gov/Drugs/DevelopmentApprovalProcess/DevelopmentResources/DrugInteractionsLabeling/ucm093606.htm>

23. Harper, J. N. & Wright, S. H. Multiple mechanisms of ligand interaction with the human organic cation transporter, OCT2. *Am. J. Physiol. Renal Physiol.* **304,** F56–67 (2013).

24. Tweedie, D. *et al.* Transporter studies in drug development: experience to date and follow-up on decision trees from the International Transporter Consortium. *Clin. Pharmacol. Ther.* **94,** 113–25 (2013).

25. Schlessinger, A. *et al.* Structure-based discovery of prescription drugs that interact with the norepinephrine transporter, NET. *Proc. Natl. Acad. Sci. U. S. A.* **108,** 15810–5 (2011).

26. Yamashita, A., Singh, S. K., Kawate, T., Jin, Y. & Gouaux, E. Crystal structure of a bacterial homologue of Na+/Cl--dependent neurotransmitter transporters. *Nature* **437,** 215–23 (2005).

27. Geier, E. G. *et al.* Structure-based ligand discovery for the Large-neutral Amino Acid Transporter 1, LAT-1. *Proc. Natl. Acad. Sci. U. S. A.* **110,** 5480–5 (2013).

28. Kekuda, R. *et al.* Cloning and functional characterization of a potential-sensitive, polyspecific organic cation transporter (OCT3) most abundantly expressed in placenta. *J. Biol. Chem.* **273,** 15971–9 (1998).

29. Chen, L. *et al.* Role of organic cation transporter 3 (SLC22A3) and its missense variants in the pharmacologic action of metformin. *Pharmacogenet. Genomics* **20,** 687–99 (2010).

30. Matsson, P. *et al.* Exploring the role of different drug transport routes in permeability screening. *J. Med. Chem.* **48,** 604–13 (2005).

CHAPTER 4

Discovery of Orthosteric and Allosteric Ligands of the Organic Cation Transporter, OCT1

INTRODUCTION

Organic cation transporter 1 (OCT1, *SLC22A1*), a polyspecific membrane transporter is among the most abundantly expressed transporters in human liver. Localized to the sinusoidal membrane of hepatocytes, OCT1 mediates the hepatic uptake of a diverse array of small positively charged hydrophilic compounds, including many endogenous bioactive amines (e.g., dopamine, histamine, and serotonin). Recently, we identified OCT1 as a high capacity transporter of thiamine in the liver, and showed that the transporter plays a key role in modulating hepatic energy status and lipid content[1].

Although the transporter clearly has important endogenous functions, OCT1 has been characterized primarily as a drug transporter, capable of transporting a wide variety of prescription drugs, including the anti-diabetic drug, metformin, and the opioid analgesic, morphine. Genetic variants of OCT1 with reduced function have been associated with decreased response to metformin[2] as well as high systemic plasma levels of morphine and the active metabolite of the opioidergic drug, tramadol[3]. Further, administration of the calcium channel blocker, verapamil (a potent inhibitor of OCT1), has been shown to reduce response to metformin, presumably through

reducing hepatic drug levels[4]. In recognition of its critical role in drug disposition and response, OCT1 was included in a group of transporters of clinical importance by the International Transporter Consortium[5]. In 2012, the European Medicines Agency (EMA) recommended *in vitro* inhibition studies against OCT1 for investigational drugs in its Guidance on the Investigation of Drug Interactions[6].

Identification of OCT1 inhibitors and the mechanisms of inhibition (competitive/orthosteric or non-competitive/allosteric) is critical to understand and predict clinically important drug interactions with concomitant medications, endogenous metabolites, and dietary constituents. To date, more than 50 inhibitors of OCT1 transport have been identified by *in vitro* inhibition studies using radioactive or fluorescent probe substrates[7,8]. However, these studies have not identified the mechanisms by which inhibitors modulate OCT1 transport. Further, growing evidence suggests that OCT1-mediated transport can be inhibited in a "substrate-dependent" manner due to the presence of multiple, possibly overlapping binding sites on the protein[9].

Characterization of OCT1 ligands and their orthostery or allostery could be facilitated by the availability of an atomic structure. However, the three-dimensional structure of human OCT1 or its mammalian orthologs has not yet been determined. Although several residues important for substrate binding have been reported and rationalized with OCT1 comparative models built using atomic structures of bacterial homologs[10–15], accurate prediction of the binding site(s) remains challenging because of

the low sequence identity between bacterial proteins and human OCT1. Recently, a structure of a high-affinity phosphate transporter (PiPT) from the fungus *Piriformospora indica* was determined by X-ray crystallography[16]. The transporter shares approximately 20% sequence identity with human solute carrier (SLC) transporters, especially within the SLC22 family, thus providing a new opportunity for comparative modeling of OCT1 and virtual screening.

We used a combination of *in silico* and HTS methods to identify prescription drugs and endogenous metabolites that are ligands of OCT1, with the goals of predicting clinical drug interactions and understanding their interaction with OCT1 protein. To this end, we screened a prescription drug library *in silico* for compounds that interact with a predicted binding site on OCT1, using comparative structure modeling and virtual docking. In parallel, we conducted HTS for inhibitors of OCT1-mediated transport of the fluorescent ligand, ASP^+, against the same prescription drug library. We identified 167 ligands in the screened library and predicted 30 orthosteric and 137 allosteric ligands. Moreover, we showed that by combining structure-guided ligand discovery with structure-activity relationship models, orthosteric ligand of OCT1 could be predicted from endogenous and exogenous metabolites.

RESULTS

Comparative model of OCT1 and its validation by docking of known substrates

We modeled human OCT1 based on the 2.9 Å structure of a high-affinity phosphate transporter PiPT, from *Piriformospora* indica, crystallized in an inward-facing occluded state with a bound substrate[16] (Protein Data Bank ID 4J05) (Fig. 4.1A). The best scoring 3-dimensional model was selected using the normalized discrete optimized protein energy (zDOPE) potential[17]. The zDOPE score of -0.22 suggests that 60% of its C-alpha atoms are within 3.5 Å of their correct positions[18]. The model includes all 12 transmembrane helices (TMHs), organized into the N- and C-terminal domains. The following regions were not modeled: a large extracellular loop between TMHs 1 and 2, an intracellular loop between TMHs 6 and 7, and the intracellular N- and C-termini. Because ASP^+ was used as a probe substrate, we first docked ASP^+ into two predicted binding sites and selected the site with the best score (-6.08) for all subsequent docking. Next, we validated the accuracy of the comparative model of the OCT1 transporter by confirming that (1) known OCT1 substrates docked favorably against the predicted binding site and (2) residues implicated in OCT1 transport[10–15] were localized in the predicted binding site, as follows.

First, we docked 15 known OCT1 endogenous and drug substrates against the predicted binding site. Twelve out of fifteen substrates (80%) had favorable (negative) docking scores, ranging from -24.44 for acyclovir to -2.88 for oxaliplatin (Fig. 4.1B and

Table 4.1). Positive scores for the three compounds (e.g., prostaglandins and pentamidine) resulted from steric clashes between ligand and transporter atoms, indicating that either the predicted binding site is too small to accommodate larger OCT1 ligands or that these compounds bind at a different site in the translocation pore. Second, we analyzed favorable docking poses to determine the frequency of predicted hydrogen bonds between binding site residues and substrate molecules. Thirteen residues in TMH 4, 10, and 11 formed hydrogen bonds with substrate molecules (Fig. 4.1A). Previous mutagenesis studies and homology modeling efforts suggested that these residues are important for substrate binding and OCT1-mediated transport in other species[10–15]. In particular, negatively charged D474 is important for interactions with positively charged OCT1 substrates. Additionally, in rat, mutations of Y221 and D474 resulted in the reduced uptake of tetraethylammonium (TEA)[14]. Finally, docked substrates formed non-covalent interactions with W217, T225, I449, and Q447 in TMH 4, 10, and 11. The equivalent residues in rat have also been implicated in ligand-transporter interactions[15].

Prediction of new ligands by virtual screening and validation by HTS

We predicted new ligands of OCT1 by docking each one of the 1,780 compounds in the Pharmakon drug library against the predicted binding site on the OCT1 model. From the 1,780 compounds, 471 putative OCT1 ligands were predicted (normalized docking scores less than -1). These docking predictions were then tested by HTS of the entire Pharmakon library. The HTS assay relied on the uptake of the

fluorescent substrate ASP^+ by OCT1 overexpressing HEK cells to assess the activity of the transporter[8,19]. The uptake of ASP^+ was linear for the first 5 minutes, and the K_m was determined to be 21.2 μM (Fig. 4.2A, B). Thus, a substrate concentration of 2 μM was used to minimize the effect of substrate concentration on the IC_{50} values and an incubation time of 2 minutes was used to measure the initial rate of uptake. An inhibitor was defined as any compound that inhibits 50% or more of ASP^+ uptake at 20 μM. Of the 1,780 Pharmakon compounds, 167 compounds (9%) were determined to be OCT1 inhibitors (Fig. 4.2C). Drugs known to inhibit OCT1 activity at 20 μM were generally confirmed by the screen. The average z-prime score of the HTS was 0.80, indicating an excellent assay[20]. Of the 167 compounds, 30 were also predicted as inhibitors by virtual screening. The overall accuracy of virtual screening was 70%. The sensitivity and specificity of predictions were 77% and 12%. The low specificity is not surprising because the docking pipeline was executed in a fully automated fashion; in contrast, typical structure-based virtual screening involves manual post-docking selection of ligand poses[21–23].

We examined compounds predicted to be OCT1 ligands by the comparative model, but not identified as inhibitors by HTS. In view of the published literature, we identified 13 previously reported substrates and 5 inhibitors of OCT1. Among these predicted ligands, cimetidine (rank #21), metformin (rank #84), and thiamine (rank #200) inhibited OCT1-mediated uptake of ASP^+ by 4.13%, 11.1%, and -1.5%, respectively. The docking poses of all three compounds predicted favorable interaction with the comparative model; in particular, metformin and cimetidine formed hydrogen

bonds with Asp474 (Fig. 4.3A,B). The inability of HTS to identify some of the previously reported ligands can be explained by their OCT1 affinity, which is weaker than that of ASP^+. For example, the reported IC_{50} values of cimetidine and metformin were 149 μM and 1,230 μM, respectively[24,25], and the IC_{50} of thiamine was determined to be 4.1 mM (Fig. 4.4). Because our HTS assay measured inhibition of OCT1 activity by test compounds at 20 μM, it was unable to identify substrates such as cimetidine, metformin, and thiamine.

HTS identified tricyclic antidepressants, antihistamines, and α-adrenergic receptor agonists, agreeing with previously published results[8]. HTS also identified a high proportion of ligands from other drug classes, including calcium channel blockers, β-adrenergic receptor agonists/antagonists, and muscarinic acetylcholine receptor agonists/antagonists (Fig. 4.2D). Finally, HTS identified drugs that were not previously known to interact with OCT1, including carvedilol (an anti-hypertensive medication) and ethopropazine (an anti-Parkinsonian agent). Selected hits not known previously to interact with OCT1 were validated by determining their IC_{50} values *in vitro* (Fig. 4.5). Analysis of the physicochemical properties showed that OCT1 ligands tend to have fewer hydrogen bond donors and acceptors and are less polar, but more lipophilic than non-ligands (Fig. 4.6). As expected, ligands were more likely to be positively charged (Fig. 4.6).

Prediction of orthosteric and allosteric ligands

Thirty of the 1,780 compounds in the library were identified as ligands by both virtual screening and HTS. Because docking was performed against the predicted binding site, it can only identify competitive (orthosteric) inhibitors/substrates. In contrast, HTS can identify both competitive and non-competitive (allosteric) inhibitors/substrates. Thus, the 30 compounds that were identified with both methods are likely to be orthosteric inhibitors or substrates. If docking is accurate, the remaining 137 compounds are likely to bind allosterically. To validate these predictions, Lineweaver-Burk plots were constructed for 2 compounds in each class. First, tacrine and ethopropazine, neither previously known to inhibit OCT1, were confirmed to be competitive inhibitors of ASP^+ uptake by OCT1 (Fig. 4.7A, B). Second, alfuzosin, a previously unknown OCT1 inhibitor, and clotrimazole were confirmed to be non-competitive inhibitors of ASP^+ uptake by OCT1 (Fig. 4.7C, D).

Physicochemical properties of putative orthosteric and allosteric Inhibitors

We analyzed physicochemical properties of 30 putative orthosteric and 137 allosteric ligands. Our analysis revealed that allosteric ligands were significantly larger and more hydrophobic than orthosteric ligands (Fig. 4.8), supporting that the two types of ligands likely bind to different sites on the transporter.

In liver, several Solute Carrier (SLC) transporters participate in uptake of drugs across the sinusoidal membrane into hepatocytes. A comparison of our HTS result with those for two other liver uptake transporters[26], OATP1B1 (SLCO1B1) and

OATP1B3 (SLCO1B3), allowed us to identify OCT1-selective *versus* pan-inhibitors (i.e., compounds that inhibited transport of all three liver transporters). Fifty-one compounds inhibited all three transporters, while 116 inhibited OCT1 only. As expected, differences in charge were significant (Student t-test p-values < 0.05; Fig. 4.9). Additionally, we found that OCT1 inhibitors were significantly smaller and less hydrophobic (Student t-test p-values < 0.05). This result showed that multi-way comparison of HTS data of several transporters can help in identifying compounds that are selective for a specific transporter and underscores the need for HTS of additional SLC transporters.

We next determined the fraction of inhibitors with different predicted inhibitory mechanisms among the OCT1-selective inhibitors and pan-inhibitors. Interestingly, 26 out of 30 predicted orthosteric ligands of OCT1 (87%) were found among the OCT1-selective inhibitors. That is, these 26 were not inhibitors of OATP1B1 or OATP1B3. In contrast, only 4 out 30 predicted orthosteric ligands (13%) were also inhibitors of OATP1B1 and OATP1B3. This finding not only supports the accuracy of our comparative model, but also highlights the importance of combining structure-guided ligand discovery with HTS. By combining experimental HTS with docking against comparative model of OCT1, we can efficiently predict orthosteric OCT1-selective inhibitors with 87% accuracy. Therefore, a structure-guided approach greatly accelerates the identification of selective inhibitors and provides valuable information for drug-drug interaction studies, compared to the conventional trial-and-error approach.

Structure-activity modeling and validation by HTS

To facilitate prediction of orthosteric and allosteric OCT1 ligands from other *in silico* libraries, we constructed a binary structure-activity relationship (SAR) model correlating molecular features of 1,780 compounds with their inhibitory activities, discretized into two classes: ligand and non-ligand. The Random forest (RF) algorithm[27] was employed to build an ensemble classifier of ligand-OCT1 interactions (SAR-I). We evaluated the accuracy of the SAR-I model (i.e., the area under the Receiver Operating Characteristic curve (auROC)), by 100 repeated cross-validation runs (Fig. 4.10A). The average auROC of RF classifiers in this retrospective validation was 0.89±0.30. This accuracy is comparable to the accuracies of retrospective validation of SAR models for other transporters[19,28]. In addition, we estimated the accuracy of RF-based SAR models in prospective validation as follows. First, we used molecular features and inhibitory outcomes of 183 compounds from a small screen[8] to develop a new SAR model (SAR-II). Next, SAR-II was utilized to predict the ligand class of the 1,780 Pharmakon compounds. The auROC for this prospective validation was 0.84 (Fig. 4.10B). Thus, the decrease in accuracy measures between retrospective and prospective validation was only 5%, strongly suggesting that our OCT1 SAR-I model is highly accurate (approximately 84%). We also used SAR-II model to predict the sensitivity and specificity of the classifier at different cutoff values (Fig. 4.10C). The sensitivity and specificity of SAR-II model at a cutoff value of 0.6 were respectively 92% and 43%; at a cutoff value of 0.4, they were 82% and 65%, respectively. Finally, the observed and SAR-II predicted ligand-OCT1 interaction values of the 1,780 Pharmakon compounds

were moderately correlated (Pearson correlation coefficient of 0.50; Fig. 4.10D). These results suggest that SAR models can accurately predict OCT1 ligands by virtual screening.

Virtual screening of endogenous and drug metabolites

In addition to searching for OCT1 ligands among the 1,780 prescription drugs, we applied our structure-based and SAR model methods to predict OCT1 ligands among a larger set of 29,332 endogenous and drug metabolites in the Human Metabolome Database (HMDB)[29]. 868 out of 29,332 (3%) of compounds docked favorably. We then computed ligand-OCT1 interaction values for the 868 compounds using the SAR-I model, allowing us to predict 146 orthosteric ligands (using the definition described above). Among these 146 compounds, 1-Benzyl-1,2,3,4-tetrahydroisoquinoline (1BnTIQ), an endogenous amine present at high level in the cerebrospinal fluid of Parkinson's disease patients[30,31], docked favorably against OCT1 (rank #14) and had an SAR-I inhibition score of 0.48. 1BnTIQ inhibited OCT1 at 82.1 μM, and Lineweaver-Burk plot confirmed that 1BnTIQ inhibited OCT1 competitively (Fig. 4.11A,B). This validation suggests that combined docking and SAR-I virtual screening can accurately predict OCT1 metabolite ligands, in addition to prescription drug ligands.

DISCUSSION

OCT1, a protein of pharmacologic interest, transports a wide array of drugs into and out of the liver, and thus serves as a major determinant of drug metabolism and action. Because of its clinical importance, OCT1 has become a focus of many pharmacogenomics and drug interaction studies, which have prompted the EMA to recommend that all new drugs undergo *in vitro* testing to assess their liability to interact with OCT1[6]. The goals of the current study were (i) to develop robust computational models to predict the interaction of new molecular entities with OCT1, and (ii) to use a combination of experimental and computational approaches to identify prescription drug and metabolite ligands of OCT1. By combining *in silico* and *in vitro* approaches, we sought to gain information about whether a ligand binds orthosterically or allosterically on OCT1.

Three major findings emerged from the current studies. First, a comparative structure model of OCT1 successfully discriminated ligands from non-ligands of the transporter. Second, by combining molecular docking and HTS approaches, we were indeed successful with determining whether a ligand binds orthosterically or allosterically. Third, we identified 30 and 137 prescription drugs as orthosteric and allosteric ligands of OCT1, respectively, including drugs not known to interact with the transporter. We now discuss each one of these findings in turn.

OCT1 ligands can be identified accurately by virtual screening against an OCT1 comparative model

Accurate prediction of inhibitors and substrates of OCT1 is challenging. First, although several atomic structures have been resolved for bacterial members of the Major Facilitator Superfamily of transporters, low sequence identity between bacterial homologs and human OCT1 casts doubt on the accuracy of comparative models built using these structures as templates[14]. Second, OCT1 is considered a polyspecific transporter that transports compounds of different sizes and molecular features. For example, OCT1 mediates the uptake of compounds ranging from small cations such as tetraethylammonium, monoamines (metformin), chemotherapy drugs (oxaliplatin), to hormone-like lipid compounds (prostaglandin E1)[2,32–34]. This polyspecificity may result in inaccurate docking and SAR models. For example, ligand-based models may under-predict ligands, especially in chemical spaces unsampled by the training set. Similarly, docking generally does not consider multiple binding sites, which are characteristic of polyspecific transporters. Docking also depends on the accuracy of the target structure; for example, the large extracellular loop between TMH 1 and 2 of OCT1, which appears to be important for substrate specificity[35], cannot be modeled by relying on structurally defined homologs of OCT1.

Here, we built a comparative model of human OCT1 in an inward-facing occluded conformation, using a recently determined structure of its eukaryotic homolog, a phosphate transporter from *Piriformospora indica* (PipT)[16]. We confirmed

that 80% of known structurally diverse substrates can be docked favorably against the predicted binding site (Table 4.1). The average pairwise Tanimoto coefficient of substrates used to validate the predicted binding site was 0.33, indicating that the compounds were structurally unrelated (Fig. 4.12). In an unbiased validation of the OCT1 comparative model, we docked 1,780 compounds from the Pharmakon library and validated 70% of predicted binders and non-binders *in vitro*. Previous SAR and pharmacophore models of OCT1-ligand interactions identified hydrophobicity and charge as the main physicochemical properties required for inhibition[8,36,37]. Our screening results confirmed that charge and hydrophobicity positively correlated with inhibitory activity of compounds (Fig. 4.5). In addition, ligands had fewer hydrogen bond donors and acceptors and were less polar than non-ligands.

A combination of virtual screening and HTS can determine whether a ligand binds orthosterically or allosterically

It has been frequently assumed that inhibition of SLC-mediated transport is primarily competitive, although some recent studies have challenged this assumption by showing that competitive, noncompetitive, and mixed type inhibition can also occur[9,38–40]. The International Transporter Consortium recently pointed out that the lack of understanding of inhibition mechanisms remains a limiting factor in transporter studies in drug development[41]. We showed that inhibitors of OCT1-mediated ASP^+ transport can be divided into two groups based on their docking scores against the OCT1 model. Predicted competitive (orthosteric) inhibitors of ASP^+ transport are compounds that are identified by experimental screening as well as predicted by virtual

screening against the predicted substrate binding site; our assay and calculation do not distinguish between competitive inhibitors and substrates. In contrast, predicted non-competitive (allosteric) inhibitors are compounds that are identified by experimental screening as well as predicted not to bind by virtual screening. Competitive ligands were significantly smaller and less hydrophobic than the allosteric ligands (Fig. 4.7C). Because we modeled OCT1 in an inward-facing occluded conformation, we predict orthosteric ligands from only those compounds that fit into the compact translocation cavity. As a result, compounds that bind to alternative OCT1 conformations will not be predicted as orthosteric ligands by our docking approach.

Additionally, we showed that 87% of predicted orthosteric ligands were selective for OCT1. In contrast, only 13% of predicted orthosteric ligands were identified among inhibitors of three hepatic uptake transporters OCT1, OATP1B1, and OATP1B3. This result provides further confidence in the accuracy of the comparative model and its ability to predict orthosteric ligands.

To predict orthosteric ligands in the large virtual library of potential ligands, we combined the SAR model (built using our HTS data) and docking against a comparative OCT1 model. Indeed, 146 putative orthosteric ligands among endogenous and exogenous metabolites were predicted in the HMDB library; one of them, 1BnTIQ, was experimentally tested and validated (Fig. 4.6E, F). 1BnTIQ is an endogenous amine detected in human cerebrospinal fluid that accumulates in patients with Parkinson's disease[31] and is able to induce parkinsonism in both mice and monkeys[42,43]. 1BnTIQ

inhibits complex I in the mitochondria and induces dopaminergic death in the same manner as MPP^+, a neurotoxin also known to induce parkinsonism. Structurally similar to MPP^+, 1BnTIQ is hydrophilic and requires an uptake mechanism to enter cells. A likely uptake mechanism is suggested by our identification of 1BnTIQ as an OCT1 ligand.

Novel OCT1 inhibitors can be identified by HTS

Because of the critical role OCT1 plays in drug disposition and response, efforts have been made to identify and characterize OCT1 inhibitors. For example, 20 pharmacologically diverse antidepressants and 14 antipsychotics were screened using an OCT1 mediated radiolabeled MPP^+ uptake assay, identifying drugs that could potentially inhibit 50% or more OCT1 activity in the brain[7]. 191 drugs from various sources were compiled, followed by a medium-throughput identification of 62 inhibitors [8].

In this study, we conducted an extensive HTS of 1,780 drugs that have reached at least clinical trials in the United States or are marketed in Europe and/or Asia. We were able to confirm most of the previously known inhibitors. We also estimate that we identified at least 100 compounds previously unknown to interact with the transporter. Moreover, we grouped the identified OCT1 ligands into therapeutic classes, including tricyclic antidepressants, antihistamines, steroids, and α-adrenergic receptor agonists, all of which were previously reported to be more likely to interact with OCT1[8]. Our HTS also identified additional drug classes that were enriched in OCT1 ligands, including β-

adrenergic receptor agonists/antagonists, calcium channel blockers, and muscarinic acetylcholine receptors agonists/antagonists. Among the inhibitors identified by HTS, select compounds were validated by determining their IC_{50} values (Fig. 4.4). Six of them (bithionol, carbetapentane, carvedilol, erlotinib, griseofulvin, and ketoconazole) had IC_{50} values that were at least 10% of their maximum plasma concentrations achieved after therapeutic doses of the drug (Table 4.2) These estimates suggest the possibility of clinical drug-drug interactions with OCT1 substrates. Further OCT1 inhibitors may potentially have beneficial effects on hepatic steatosis[1]. With the exception of erlotinib and ketoconazole, the drugs noted here were newly identified OCT1 ligands.

In conclusion, we developed a comparative structural model of OCT1 that discriminates ligands from non-ligands, and used the model together with an *in vitro* HTS assay. By combining the two approaches, we were able to predict whether a ligand binds orthosterically or allosterically. The structure-guided approach also accurately predicted inhibitors specific to OCT1 rather than two other hepatic drug transporters, OATP1B1 and OATP1B3. Finally, we conducted a virtual screen against a metabolite library using both comparative and SAR models built from HTS data, and accurately identified and validated the parkinsonism-producing neurotoxin, 1BnTIQ, as a competitive inhibitor of OCT1.

METHODS

Chemicals

The MicroSource Pharmakon compound library (Gaylordsville, CT) was obtained through the Small Molecular Discovery Center at University of California, San Francisco (San Francisco, CA). 4-(4-(Dimethylamino)styryl)-N-methylpyridinium iodide was purchased from Molecular Probes (Grand Island, NY). All other chemicals were purchased from Sigma-Aldrich (St. Louis, MO). All cell culture media and supplements were purchased from Life Technologies (Carlsbad, CA) except fetal bovine serum, which was purchased from GE Healthcare Life Sciences (South Logan, UT).

Cell culture

Human embryonic kidney (HEK-293) cell line stably overexpressing OCT1 was established previously in our laboratory [2]. The cells were maintained in Dulbecco's Modified Eagle's Medium (DMEM H-21) supplemented with 75 μg/ml of hygromycin B, penicillin (100 U/ml), streptomycin (100 mg/ml), and 10% fetal bovine serum in a humidified atmosphere with 5% CO_2 at 37°C.

In vitro uptake studies

HEK-293 cells overexpressing OCT1 were seeded in black, clear bottom poly-D-lysine coated 96-well plates (Greiner Bio-One, Monroe, NC) and allowed to grow for 48 hours until approximately 90% confluency. For uptake kinetics study, cells were

incubated with HBSS containing serial dilution of ASP^+ for 2 minutes at 37°C. At the end of experiments, the media were aspirated and the cells were washed twice with ice-cold HBSS containing 50 μM spironolactone. The K_m and V_{max} were calculated by fitting the data to Michaelis-Menten equations. For time course study, cells were incubated with HBSS containing 2 μM ASP^+ at 37°C. At various time points, the experiment was stopped as previously described. For IC_{50} determination, cells were incubated with HBSS containing 2 μM ASP^+ and serial dilution of inhibitors for 2 minutes at 37°C. IC_{50} was determined using appropriate curve fitting. For Lineweaver-Burk plots, cells were incubated with HBSS containing serial dilution of ASP+ and the inhibitor of interest at 4 different fixed concentration for 2 minutes at 37°C. The reciprocal value of ASP^+ uptake at each inhibitor concentration was fitted with linear regression. The signal of ASP^+ was measured using an Analyst AD plate reader (Molecular Devices, Sunnyvale, CA) with excitation and emission filters tuned at 485 and 585 nm wavelength, respectively. All statistical analysis and curve fitting were done using GraphPad Prism software (La Jolla, CA).

High-throughput screening

The high throughput screen was performed at the Small Molecule Discovery Center at the University of California, San Francisco. HEK-293 cells overexpressing OCT1 were seeded in black, clear bottom poly-D-lysine coated 96-well plates (Greiner Bio-One, Monroe, NC) and allowed to grow for 48 hours until approximately 90% confluency using methods established previously[19]. Cells were incubated with HBSS containing 2mM ASP^+ and 20 μM of test compounds at ambient temperature for

approximately 2 minutes. At the end of the experiment, media were aspirated and cells were washed twice with HBSS containing 50 μM spironolactone. Nonspecific transport was determined in wells on each assay plate using 100 μM spironolactone as OCT1 inhibitor. The screen was carried out with a Biomek FXp liquid handler (Beckman Coulter, Brea, CA). Fluorescence was measured as previously described.

OCT1 structure modeling and docking

Human OCT1 was modeled based on the 2.9 Å structure of a high-affinity phosphate transporter PiPT, from *Piriformospora indica*, crystallized in an inward-facing occluded state with bound phosphate [16]. The template was selected based on the shared MFS fold assignment [44], structure quality, sequence similarity to OCT1, and the ligand-bound conformation. The sequence alignment was obtained by a manual refinement of gaps in the output from the PROMALS3D [45] and MUSCLE [46] servers. One hundred models were generated using the "automodel" class of MODELLER 9.14 [47], and the normalized discrete optimized protein energy (zDOPE) potential [17]. The top scoring model was used to predict putative binding sites with the FTMap web server [48]. Two of the predicted bindings sites were identified in the translocation cavity between the two domains [16]. ASP^+ probe substrate was docked against the two binding sites with UCSF DOCK 3.6. [49,50]. The pose with the best docking score was used as the template for another round of comparative modeling by MODELLER 9.14, generating 100 new models of OCT1. The best scoring model was used for subsequent virtual screening. Compounds in the Pharmakon library were downloaded from the ZINC database [51] and docked against the predicted binding site on the comparative model,

using UCSF DOCK 3.6. Negative DOCK score predicts a favorable interaction with the transporter, while a positive score predicts unfavorable (or unlikely) intermolecular interaction. Normalized docking scores were computed by subtracting from the docking score of a compound the average docking score of all compounds (including the nonbinders) and dividing by the standard deviation of all docking scores.

Structure-activity relationship modeling of OCT1 inhibition

Two-dimensional structure files of the1,780 compounds from the Pharmakon library were also downloaded from the ZINC database [51]. 2,900 molecular descriptors and charge (pH 7.4) for each compound were computed using PaDEL software [52] and ChemAxon cxcalc program (http://www.chemaxon.com), respectively. Non-informative descriptors (i.e., molecular descriptors with near zero variance and redundant descriptors defined by a correlation higher than 0.95 to an accepted descriptor) were removed. Next, information content and correlation between descriptor values and percent inhibition of 1,780 compounds were computed with the cfs filtering algorithm in the FSelector package [53] in R and 21 most informative descriptors were retained for further modeling. Percent inhibition values determined by HTS were discretized into two outcomes. Values of at least 50% were mapped to '1' (i.e., ligand) and values of less than 50%, including negative values, were mapped to '0' (i.e., non-ligand). Binary SAR models were built with the RF algorithm [27]. Their accuracy was estimated using a double loop five-fold cross-validation [19] protocol in the caret package [54] in R. To evaluate the accuracy of models, the average area under the

Receiver Operating Characteristic curve (auROC) [55] was computed from 100 repeated double-loop cross-validation runs.

For prospective validation, 21 molecular descriptors for 183 compounds [8] were computed and SAR models were optimized by repeated 5-fold cross-validation. The model was employed to predict inhibition values for the 1,780 compounds in the Pharmakon library.

For virtual screening, molecular structure files of the HMDB compounds were downloaded from the ZINC database [51] and 21 molecular features were computed for each compound. The ligand score ranging between 0 and 1 was computed for each compound by SAR-I. Compounds with the ligand score higher than 0.4 were labeled as ligands.

Pairwise compound similarity computation and clustering

The MayaChemTools (http://www.mayachemtools.org) package was used to compute two-dimensional Extended Connectivity Fingerprints (ECFP) and pairwise Tanimoto coefficients. The *hclust* function from the *stats* library [53] was used to perform hierarchical compound clustering.

Table 4.1. Summary of 15 substrates used to validate OCT1 docking site.

CID	Name	Smiles	DOCK score
2022	Acyclovir	C1=NC2=C(N1COCCO)NC(=NC2=O)N	-24.44
4091	Metformin	CN(C)C(=N)N=C(N)N	-21.64
39484	MPP+	C[N+]1=CC=C(C=C1)C2=CC=CC=C2	-20.29
3454	Ganciclovir	C1=NC2=C(N1COC(CO)CO)NC(=NC2=O)N	-18.71
457	N(1)-methylnicotinamide	C[N+]1=CC=CC(=C1)C(=O)N	-14.24
5816	Epinephrine	CNCC(C1=CC(=C(C=C1)O)O)O	-11.49
305	Choline	C[N+](C)(C)CCO	-11
5413	TEA	CC[N+](CC)(CC)CC	-10.47
681	Dopamine	C1=CC(=C(C=C1CCN)O)O	-6.40
5333955	ASP+	C[N+]1=CC=C(C=C1)C=CC2=CC=C(C=C2)N(C)C.[I-]	-6.08
439260	Norepinephrine	C1=CC(=C(C=C1C(CN)O)O)O	-5.69
6857599	Oxaliplatin	C1CC[C@H]([C@@H](C1)N)N.C(=O)(C(=O)O)O.[Pt+2]	-2.88
4735	Pentamidine	C1=CC(=CC=C1C(=N)N)OCCCCCOC2=CC=C(C=C2)C(=N)N	103.78
5280363	Dinoprost	CCCCCC(C=CC1C(CC(C1CC=CCCCC(=O)O)O)O)O	128.26
5280360	Dinoprostone	CCCCCC(C=CC1C(CC(=O)C1CC=CCCCC(=O)O)O)O	171.01

Table 4.2. Identified OCT1 inhibitors that could cause drug-drug interactions.

Name	IC_{50}*, μM	C_{MAX} †, μM	$C_{Portal\ Vein}$ ‡	C_{MAX} / IC_{50}
Bithionol	2.2	1.0	N.A.	0.45
Carbetapentane	1.6	0.2	N.A.	0.12
Carvedilol	3.4	0.4	0.7	0.12
Erlotinib	16.2	4.8	7.0	0.30
Griseofulvin	7.3	4.5	4.6	0.62
Ketoconazole	2.6	6.6	10.0	2.54

* IC_{50} is the estimated half maximal inhibitory concentration.

† C_{MAX} values were obtained from http://www.micromedexsolutions.com/

‡ $C_{Portal\ Vein}$ values were calculated based on equation 1 in reference [56].

Figure 4.1

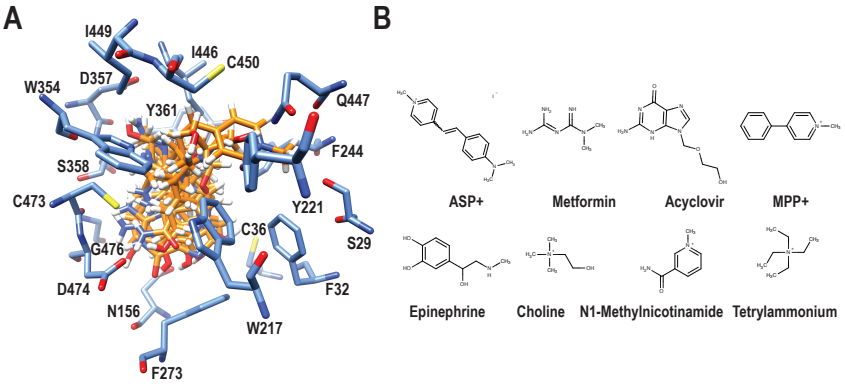

Figure 4.1. Predicted binding site of OCT1 and representative substrates. (A) Thirteen residues (S29, F32, C36, N156, Y221, F273, W354, Y361, I446, S358, C450, C473, and D474) formed hydrogen bonds with docked substrate molecules. Six residues in the predicted binding site, W217, F244, I449, D357, Q447, and G476 participated in non-covalent and/or polar substrate-transporter interactions. OCT1 residues are shown as cornflower blue sticks. Structures of 12 favorably docked known OCT1 substrates are shown as orange sticks. Oxygen, nitrogen, sulfur, and hydrogen atoms are depicted in red, dark blue, yellow, and white, respectively. (B) 2D structures of representative OCT1 substrates are drawn using MarvinView 14.7.7.0 (Chemaxon).

Figure 4.2

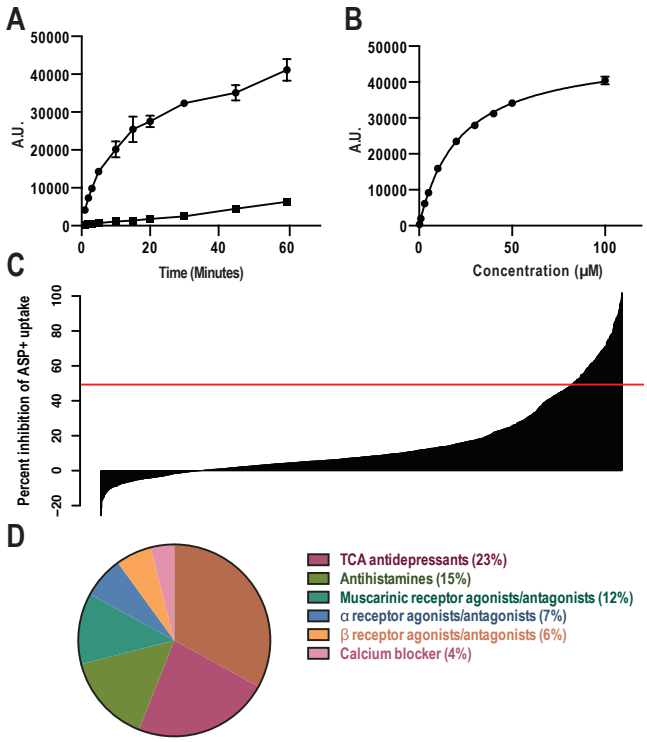

Figure 4.2. Uptake of ASP^+ and HTS screening data. (A) Time-dependent ASP^+ uptake in HEK cells overexpressing OCT1 (●) or empty vector (■). (B) Overexpressing OCT1 increases ASP^+ uptake in HEK cells. ASP^+ uptake studies were conducted in HEK cells overexpressing OCT1 or empty vector. Cells were incubated with increasing concentrations of ASP+ for 2 minutes. The uptake kinetic parameters (Results) were calculated using the difference in ASP+ accumulation between cells overexpressing OCT1 and empty vector cells. Data represent mean ± SD, n = 6 per data point. (C) Distribution of inhibition values from HTS of 1,780 compounds. A total of 167 Inhibitors were identified among the 1,780 Pharmakon compounds. (D) The distribution of the 167 inhibitors in various pharmacological classes.

Figure 4.3

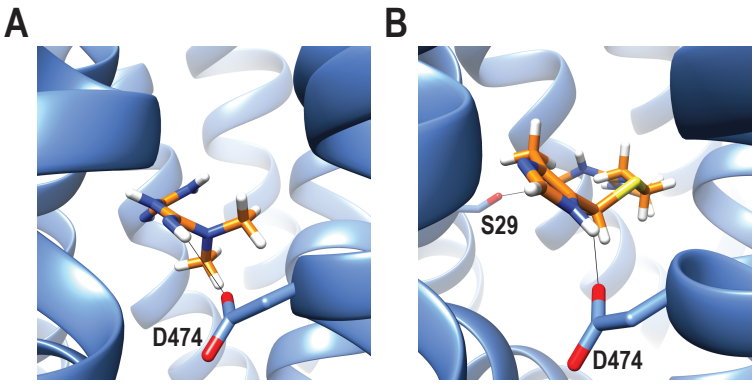

Figure 4.3. Docking results of known OCT1 substrates. Compounds are shown in orange sticks and hydrogen bonds as black dotted lines. (A) The predicted pose of metformin and its hydrogen bond with aspartic acid residue 474. (B) Predicted pose of cimetidine and its hydrogen bonds with D474 and S29.

Figure 4.4

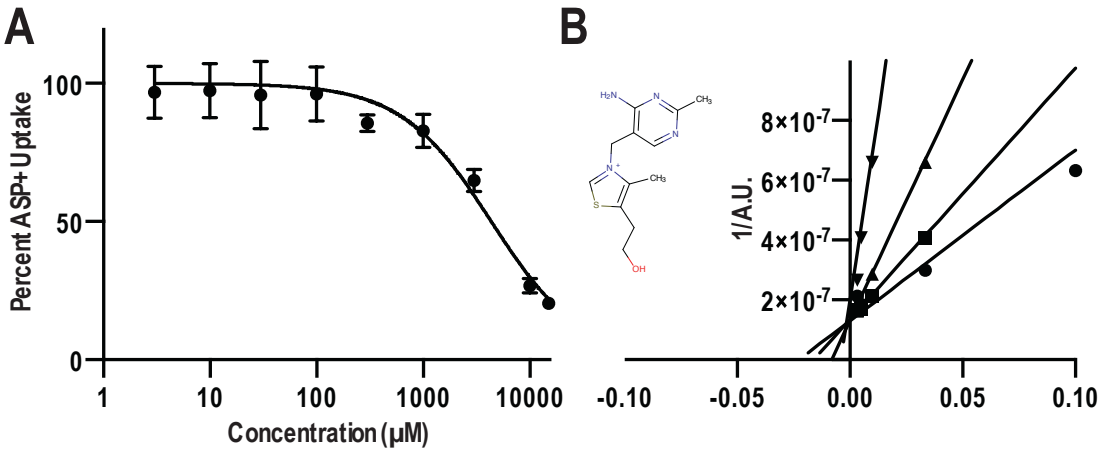

Figure 4.4. The effect of thiamine on the uptake of ASP^+ by OCT1. (A) Thiamine inhibited ASP^+ uptake by OCT1 and the IC_{50} was determined at 4.1 mM. (B) The inhibitory effect of thiamine at at 0 μM (●), 20 μM (■), 1000 μM (▲), 5 mM (▼) against increasing concentrations of ASP^+ showed that thiamine inhibited OCT1 competitively**.** Data represent mean ± SD, *n* = 3 per data point.

Figure 4.5

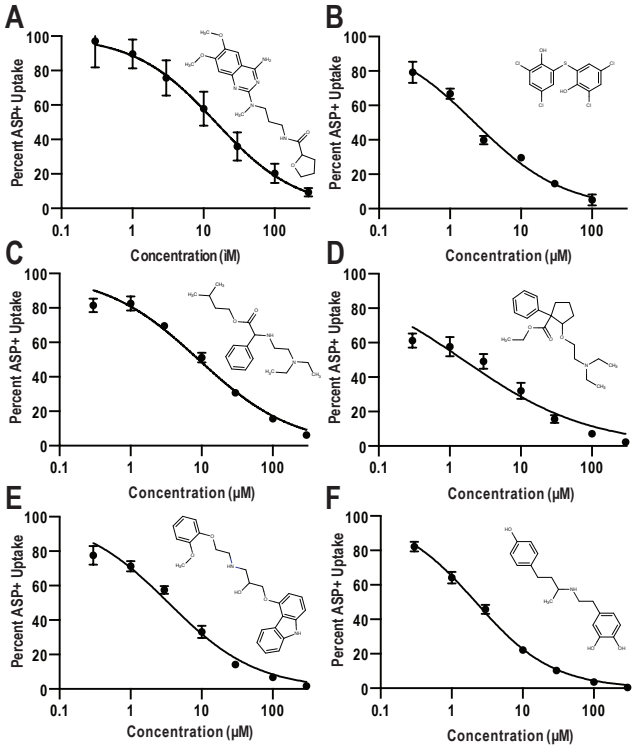

Figure 4.5. Selected inhibition studies of previously unknown OCT1 ligands and their estimated half maximal inhibitory concentration (IC_{50}), with 95% confidence limits in parenthesis. (A) Alfuzosin, an α_1 receptor antagonist. IC_{50}= 14.9 (11.9; 18.5) μM. (B) Bithionol, an anthelmintic. IC_{50}= 2.2 (2.0; 2.5) μM. (C) Camylofine, an anti-muscarinic. IC_{50}= 9.1 (8.0; 2.5) μM. (D) Carbetapentane, an antitussive. IC_{50}= 1.6 (1.2; 2.0) μM. (E) Carvedilol, a nonselective β/α_1 antagonist. IC_{50}= 3.4 (3.0; 3.9) μM. (F) Dobutamine, a Sympathomimetic. IC_{50}= 2.2 (2.1; 2.3) μM. Data represent mean ± SD, *n* = 6 per data point.

Figure 4.6

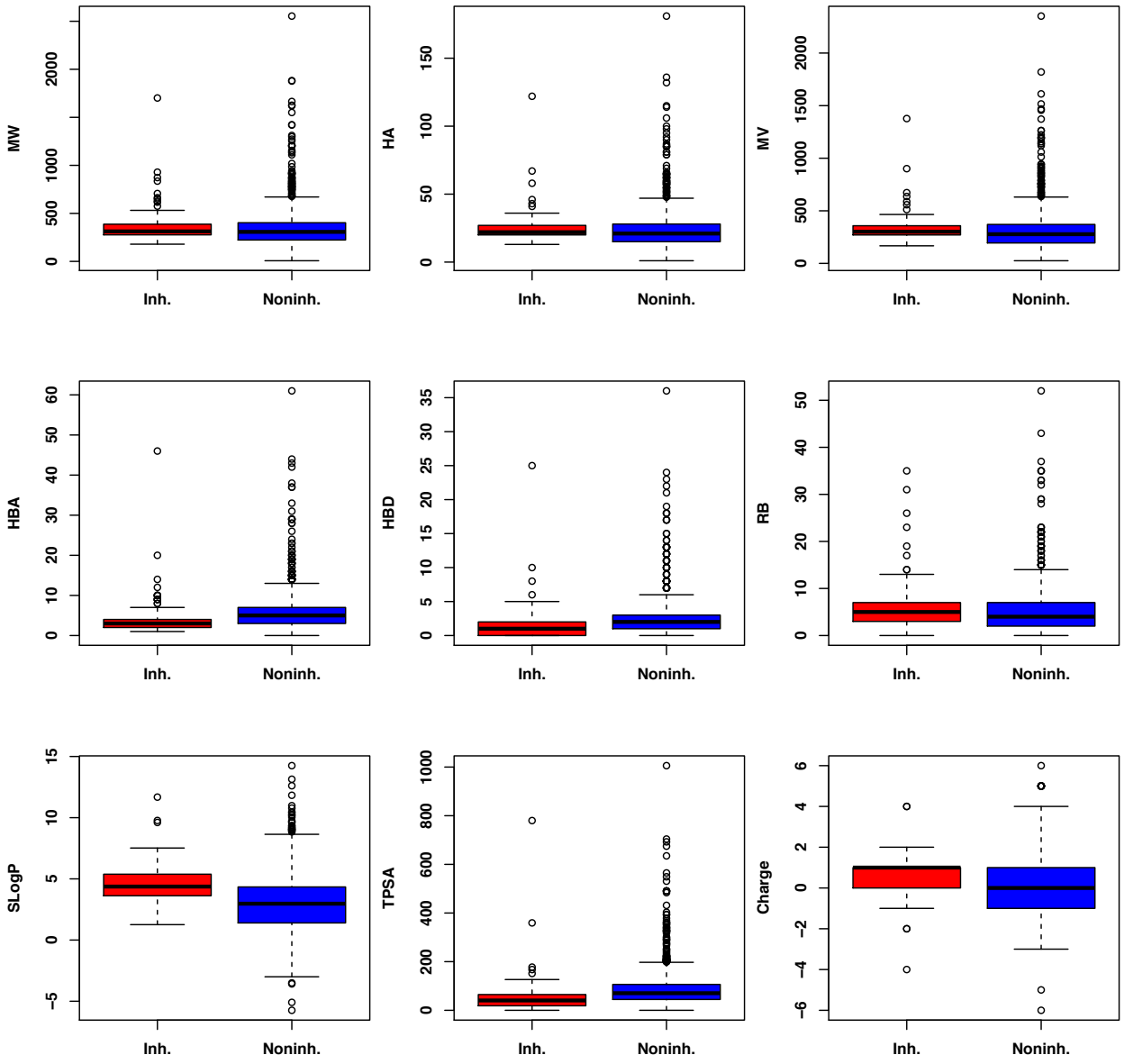

Figure 4.6. Differences in physicochemical properties of 167 inhibitors and 1,613 nonhibitors. Boxplots of MW: molecular weight, HA: number of heavy atoms, MV: molecular volume, HBD: number of hydrogen bond donors, HBA: number of hydrogen bond acceptors, RB: number of rotable bonds, SLogP: calculated log of the

octanol/water partition coefficient, TPSA: total polar surface area, and Charge at pH 7.4. Statistically significant differences were estimated using Student's t-test. Distributions of HBD, HBA, SLogP, TPSA, and charge were significantly different between inhibitors and noninhibitors (p-value < 0.0001).

Figure 4.7

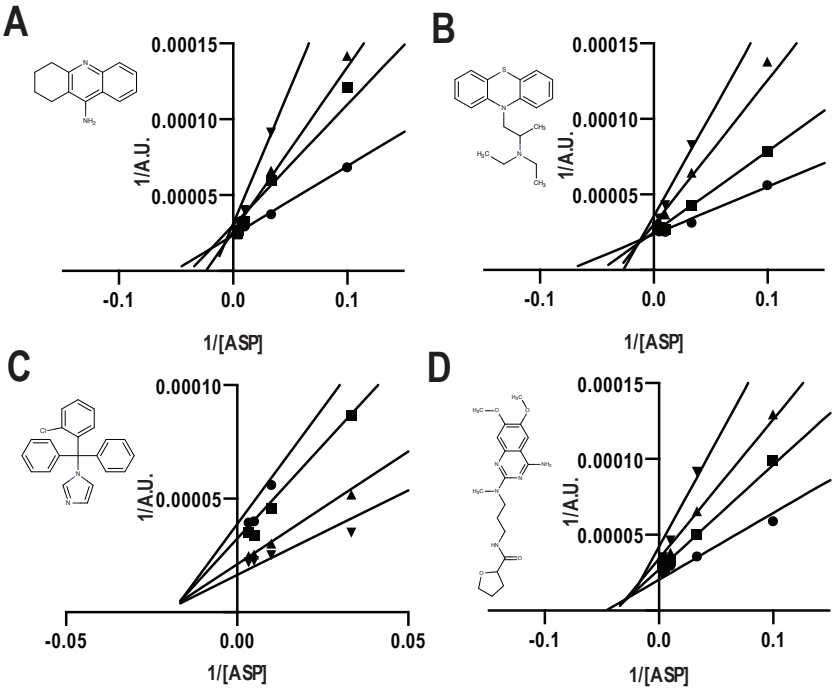

Figure 4.7. Lineweaver-Burk plots for discriminating between competitive and non-competitive inhibitors of OCT1. The inhibitory effects of selected inhibitors at various concentrations (●<■<▲<▼) were measured with increasing concentration of ASP^+. (A) The inhibitory effect of tacrine on ASP^+ uptake by OCT1 indicated competitive inhibition. (B) The inhibitory effect of ethopropazine on ASP^+ uptake by OCT1 indicated competitive inhibition. (C) The inhibitory effect of alfuzosin on ASP^+ uptake by OCT1 indicated noncompetitive inhibition. (D) The inhibitory effect of clotrimazole on ASP^+ uptake by OCT1 indicated noncompetitive inhibition. Data represent mean values. Error bars were not plotted in the other panels because they would obscure the data points.

Figure 4.8

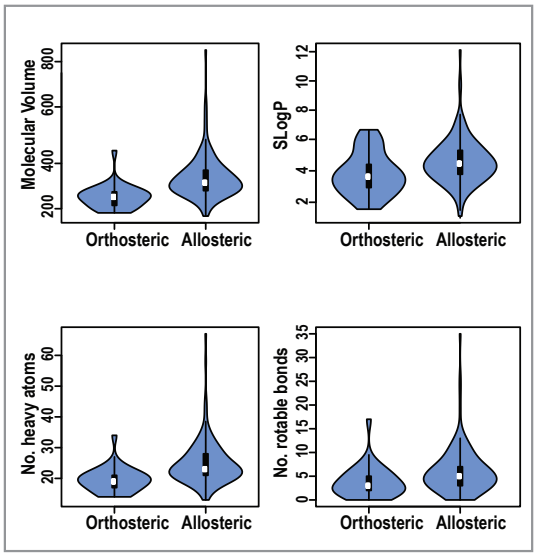

Figure 4.8. Physiochemical properties of OCT1 ligands in the Pharmakon library. Differences in distribution of physicochemical properties for predicted orthosteric (n=30) and allosteric (n=137) inhibitors of OCT1. Only significantly different distributions are shown (Student t-test p-value < 0.05). Width of the figures indicates relative distribution of compounds within each group.

Figure 4.9

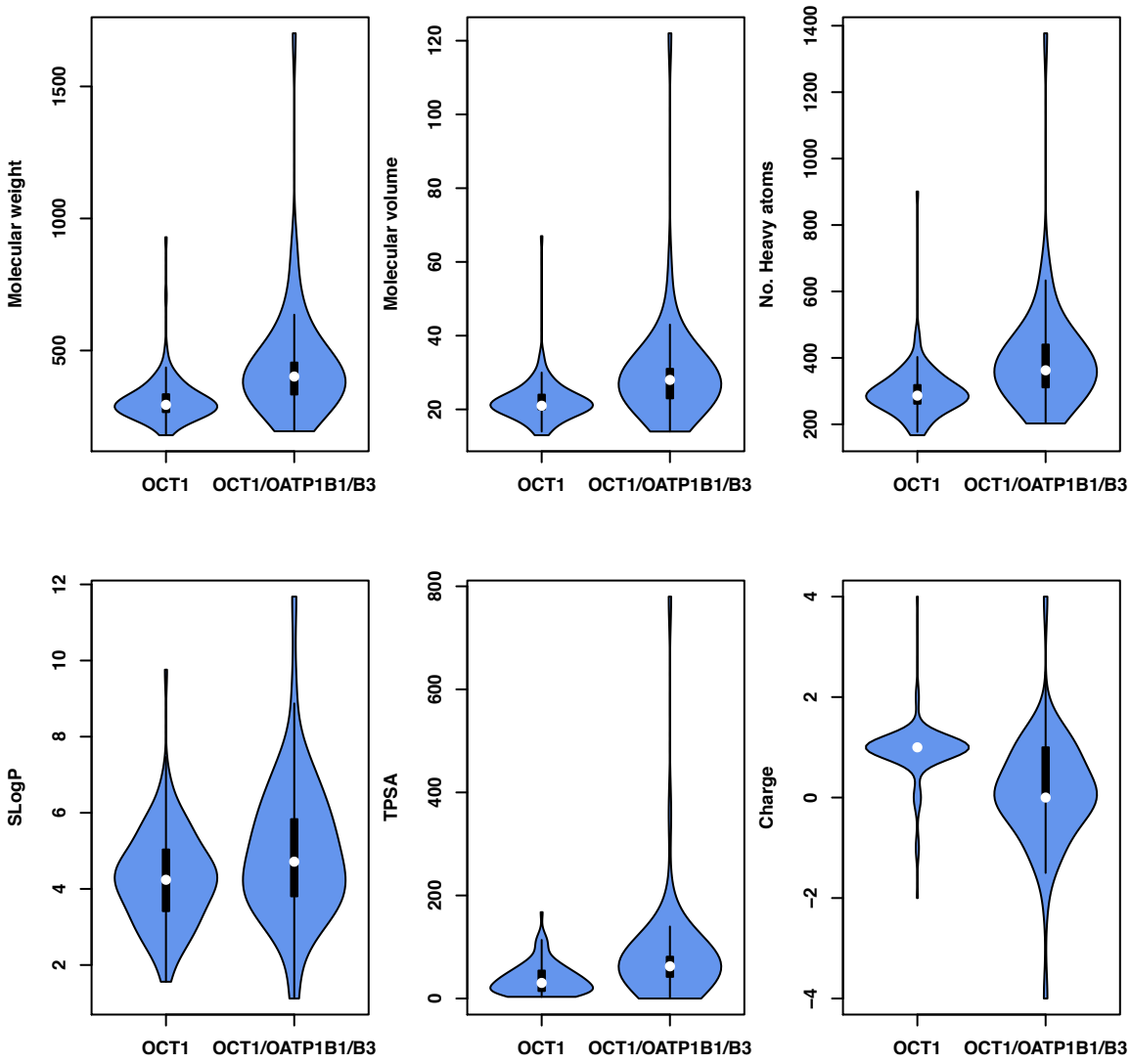

Figure 4.9. Differences in physicochemical properties of OCT1-selective inhibitors and paninhibitors. Only the distributions of statistically significant properties are shown (Student t-test p-value < 0.05).

Figure 4.10

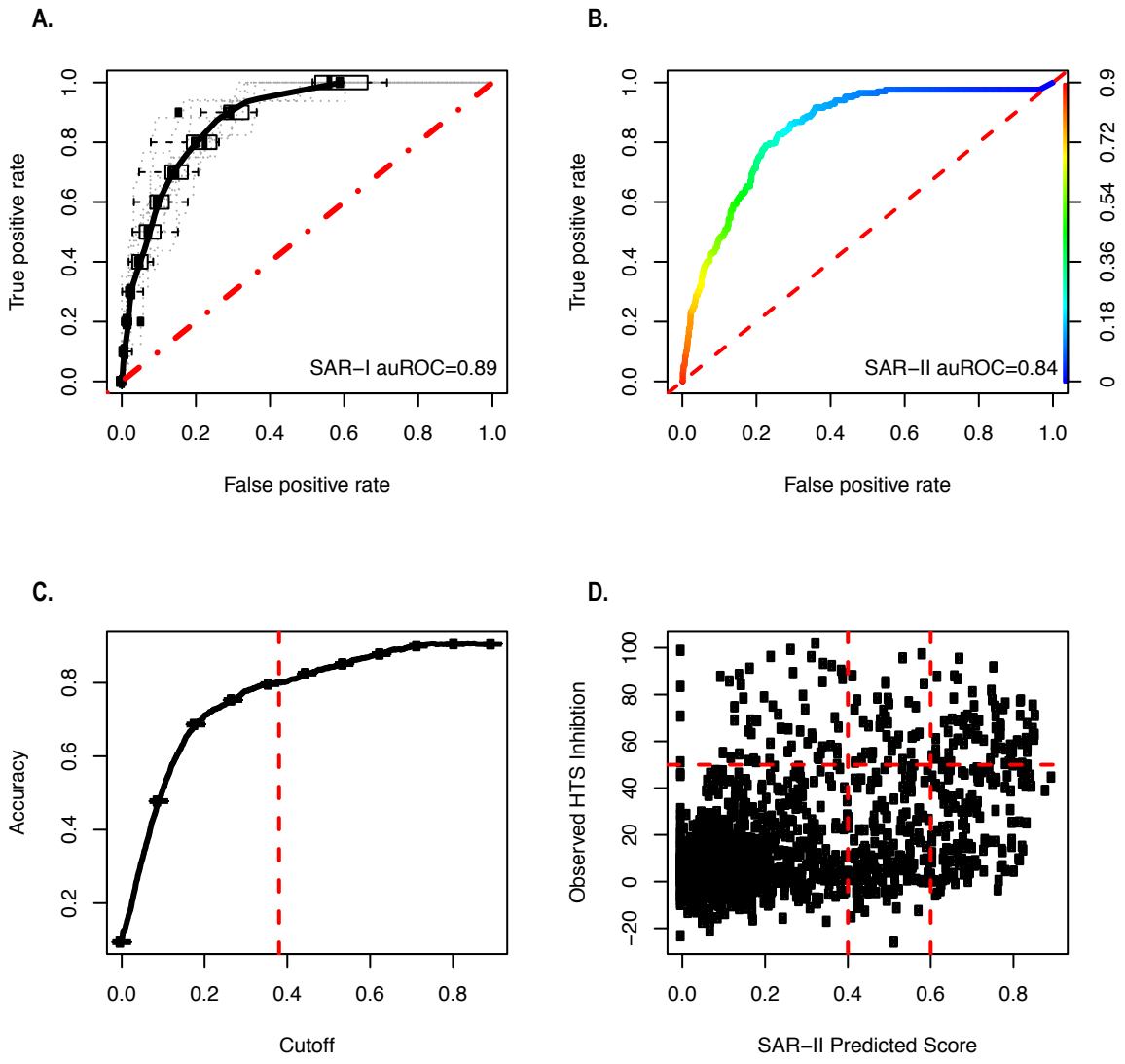

Figure 4.10. Results of structure-activity relationship modeling. (A) ROC curves for 100 retrospective cross-validation runs. Average ROC curve is shown in black. ROC curve of a random classifier is shown as a red dotted line. (B) ROC curve for the SAR model tested in prospective validation of 1,780 predicted inhibition values. Performance at different cutoff values (shown on the right y-axis) are indicated by rainbow colors. (C)

Accuracy of classification of 1,780 compounds using SAR-II model as a function of cutoff. A cutoff of 0.38 is indicated by the red dotted line. (D) Observed vs. predicted inhibition values for 1,780 compounds. Two classification cutoffs are drawn vertically and HTS classification cutoff is drawn horizontally.

Figure 4.11

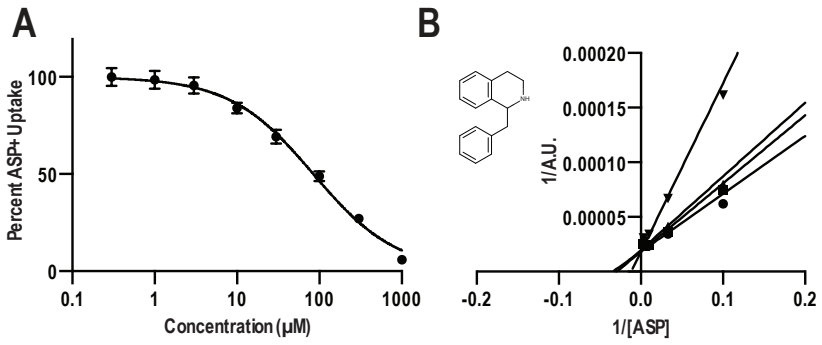

Figure 4.11. 1BnTIQ is a competitive inhibitor of OCT1. (A) 1BnTIQ inhibited ASP^+ uptake by OCT1 and the IC_{50} was determined to be 82.1 μM. (B) The inhibitory effect of 1BnTIQ at various concentrations (●<■<▲<▼) on ASP^+ uptake by OCT1 indicated competitive inhibition. Data represent mean values, except in panel A where data represent mean ± SD, n = 3 per data point. Error bars were not plotted in the other panels because they would obscure the data points.

Figure 4.12

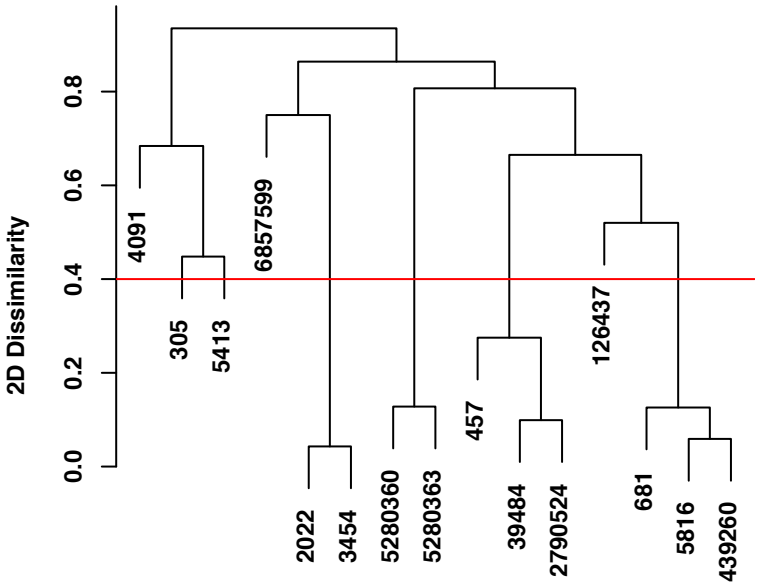

Figure 4.12. 2D dissimilarity clustering of 15 known substrates of OCT1. Dissimilarity (i.e., 1 – pairwise Tanimoto similarity) between substrates is shown on the y-axis. Compounds with dissimilarity score less than 0.4 (shown by the red line) are considered similar.

References

1. Chen, L. *et al.* OCT1 is a high-capacity thiamine transporter that regulates hepatic steatosis and is a target of metformin. *Proc. Natl. Acad. Sci. U. S. A.* **111,** 9983–8 (2014).

2. Shu, Y. *et al.* Effect of genetic variation in the organic cation transporter 1 (OCT1) on metformin action. *J. Clin. Invest.* **117,** 1422–31 (2007).

3. Tzvetkov, M. V. *et al.* Genetically polymorphic OCT1: another piece in the puzzle of the variable pharmacokinetics and pharmacodynamics of the opioidergic drug tramadol. *Clin. Pharmacol. Ther.* **90,** 143–50 (2011).

4. Cho, S. K., Kim, C. O., Park, E. S. & Chung, J.-Y. Verapamil decreases the glucose-lowering effect of metformin in healthy volunteers. *Br. J. Clin. Pharmacol.* **78,** 1426–32 (2014).

5. Giacomini, K. M. *et al.* Membrane transporters in drug development. *Nat. Rev. Drug Discov.* **9,** 215–36 (2010).

6. Guideline on the Investigation of Drug Interactions. *European Medicines Agency: CPMP/EWP/560/95/Rev. 1 Corr.** **1,** (2012).

7. Haenisch, B. *et al.* Interaction of antidepressant and antipsychotic drugs with the human organic cation transporters hOCT1, hOCT2 and hOCT3. *Naunyn Schmiedebergs Arch. Pharmacol.* **385,** 1017–23 (2012).

8. Ahlin, G. *et al.* Structural requirements for drug inhibition of the liver specific human organic cation transport protein 1. *J. Med. Chem.* **51,** 5932–42 (2008).

9. Belzer, M., Morales, M., Jagadish, B., Mash, E. A. & Wright, S. H. Substrate-dependent ligand inhibition of the human organic cation transporter OCT2. *J. Pharmacol. Exp. Ther.* **346,** 300–10 (2013).

10. Koepsell, H. Polyspecific organic cation transporters: their functions and interactions with drugs. *Trends Pharmacol. Sci.* **25,** 375–81 (2004).

11. Zhang, X., Shirahatti, N. V., Mahadevan, D. & Wright, S. H. A conserved glutamate residue in transmembrane helix 10 influences substrate specificity of rabbit OCT2 (SLC22A2). *J. Biol. Chem.* **280,** 34813–22 (2005).

12. Koepsell, H. Substrate recognition and translocation by polyspecific organic cation transporters. *Biological Chemistry* **392,** 95–101 (2011).

13. Gorboulev, V., Shatskaya, N., Volk, C. & Koepsell, H. Subtype-specific affinity for corticosterone of rat organic cation transporters rOCT1 and rOCT2 depends on three amino acids within the substrate binding region. *Mol. Pharmacol.* **67,** 1612–9 (2005).

14. Popp, C. *et al.* Amino acids critical for substrate affinity of rat organic cation transporter 1 line the substrate binding region in a model derived

from the tertiary structure of lactose permease. *Mol. Pharmacol.* **67,** 1600–11 (2005).

15. Volk, C., Gorboulev, V., Kotzsch, A., Müller, T. D. & Koepsell, H. Five amino acids in the innermost cavity of the substrate binding cleft of organic cation transporter 1 interact with extracellular and intracellular corticosterone. *Mol. Pharmacol.* **76,** 275–89 (2009).

16. Pedersen, B. P. *et al.* Crystal structure of a eukaryotic phosphate transporter. *Nature* **496,** 533–6 (2013).

17. Shen, M.-Y. & Sali, A. Statistical potential for assessment and prediction of protein structures. *Protein Sci.* **15,** 2507–24 (2006).

18. Eramian, D., Eswar, N., Shen, M.-Y. & Sali, A. How well can the accuracy of comparative protein structure models be predicted? *Protein Sci.* **17,** 1881–93 (2008).

19. Kido, Y., Matsson, P. & Giacomini, K. M. Profiling of a prescription drug library for potential renal drug-drug interactions mediated by the organic cation transporter 2. *J. Med. Chem.* **54,** 4548–58 (2011).

20. Zhang, J.-H., Chung, T. & Oldenburg, K. A simple statistical parameter for use in evaluation and validation of high throughput screening assays. *J. Biomol. Screen.* **4,** 67–73 (1999).

21. Schlessinger, A. *et al.* High selectivity of the γ-aminobutyric acid transporter 2 (GAT-2, SLC6A13) revealed by structure-based approach. *J. Biol. Chem.* **287,** 37745–56 (2012).

22. Schlessinger, A. *et al.* Structure-based discovery of prescription drugs that interact with the norepinephrine transporter, NET. *Proc. Natl. Acad. Sci. U. S. A.* **108,** 15810–5 (2011).

23. Carlsson, J. *et al.* Ligand discovery from a dopamine D3 receptor homology model and crystal structure. *Nat. Chem. Biol.* **7,** 769–78 (2011).

24. Minematsu, T., Iwai, M., Umehara, K.-I., Usui, T. & Kamimura, H. Characterization of human organic cation transporter 1 (OCT1/SLC22A1)- and OCT2 (SLC22A2)-mediated transport of 1-(2-methoxyethyl)-2-methyl-4,9-dioxo-3-(pyrazin-2-ylmethyl)- 4,9-dihydro-1H-naphtho[2,3-d]imidazolium bromide (YM155 monobromide), a novel sma. *Drug Metab. Dispos.* **38,** 1–4 (2010).

25. Bourdet, D. L., Pritchard, J. B. & Thakker, D. R. Differential substrate and inhibitory activities of ranitidine and famotidine toward human organic cation transporter 1 (hOCT1; SLC22A1), hOCT2 (SLC22A2), and hOCT3 (SLC22A3). *J. Pharmacol. Exp. Ther.* **315,** 1288–97 (2005).

26. Gui, C., Obaidat, A., Chaguturu, R. & Hagenbuch, B. Development of a cell-based high-throughput assay to screen for inhibitors of organic anion

transporting polypeptides 1B1 and 1B3. *Curr. Chem. Genomics* **4,** 1–8 (2010).

27. Svetnik, V. *et al.* Random forest: a classification and regression tool for compound classification and QSAR modeling. *J. Chem. Inf. Comput. Sci.* **43,** 1947–58 (2003).

28. Wittwer, M. B. *et al.* Discovery of potent, selective multidrug and toxin extrusion transporter 1 (MATE1, SLC47A1) inhibitors through prescription drug profiling and computational modeling. *J. Med. Chem.* **56,** 781–95 (2013).

29. Wishart, D. S. *et al.* HMDB 3.0--The Human Metabolome Database in 2013. *Nucleic Acids Res.* **41,** D801–7 (2013).

30. Kotake, Y. [Tetrahydroisoquinoline derivatives as possible Parkinson's disease-inducing substances]. *Yakugaku Zasshi* **122,** 975–82 (2002).

31. Kotake, Y., Tasaki, Y., Makino, Y., Ohta, S. & Hirobe, M. 1-Benzyl-1,2,3,4-tetrahydroisoquinoline as a parkinsonism-inducing agent: a novel endogenous amine in mouse brain and parkinsonian CSF. *J. Neurochem.* **65,** 2633–8 (1995).

32. Zhang, L., Schaner, M. E. & Giacomini, K. M. Functional characterization of an organic cation transporter (hOCT1) in a transiently transfected human cell line (HeLa). *J. Pharmacol. Exp. Ther.* **286,** 354–61 (1998).

33. Zhang, S. *et al.* Organic cation transporters are determinants of oxaliplatin cytotoxicity. *Cancer Res.* **66,** 8847–57 (2006).

34. Kimura, H. *et al.* Human organic anion transporters and human organic cation transporters mediate renal transport of prostaglandins. *J. Pharmacol. Exp. Ther.* **301,** 293–8 (2002).

35. Keller, T. *et al.* The large extracellular loop of organic cation transporter 1 influences substrate affinity and is pivotal for oligomerization. *J. Biol. Chem.* **286,** 37874–86 (2011).

36. Bednarczyk, D., Ekins, S., Wikel, J. H. & Wright, S. H. Influence of molecular structure on substrate binding to the human organic cation transporter, hOCT1. *Mol. Pharmacol.* **63,** 489–98 (2003).

37. Moaddel, R., Ravichandran, S., Bighi, F., Yamaguchi, R. & Wainer, I. W. Pharmacophore modelling of stereoselective binding to the human organic cation transporter (hOCT1). *Br. J. Pharmacol.* **151,** 1305–14 (2007).

38. Harper, J. N. & Wright, S. H. Multiple mechanisms of ligand interaction with the human organic cation transporter, OCT2. *Am. J. Physiol. Renal Physiol.* **304,** F56–67 (2013).

39. Ekins, S., Polli, J. E., Swaan, P. W. & Wright, S. H. Computational modeling to accelerate the identification of substrates and inhibitors for

transporters that affect drug disposition. *Clin. Pharmacol. Ther.* **92,** 661–5 (2012).

40. Martínez-Guerrero, L. J. & Wright, S. H. Substrate-dependent inhibition of human MATE1 by cationic ionic liquids. *J. Pharmacol. Exp. Ther.* **346,** 495–503 (2013).

41. Tweedie, D. *et al.* Transporter studies in drug development: experience to date and follow-up on decision trees from the International Transporter Consortium. *Clin. Pharmacol. Ther.* **94,** 113–25 (2013).

42. Abe, K. *et al.* Biochemical and pathological study of endogenous 1-benzyl-1,2,3,4-tetrahydroisoquinoline-induced parkinsonism in the mouse. *Brain Res.* **907,** 134–8 (2001).

43. Kotake, Y. *et al.* Chronic administration of 1-benzyl-1,2,3,4-tetrahydroisoquinoline, an endogenous amine in the brain, induces parkinsonism in a primate. *Neurosci. Lett.* **217,** 69–71 (1996).

44. Schlessinger, A. *et al.* Comparison of human solute carriers. *Protein Sci.* **19,** 412–28 (2010).

45. Pei, J., Kim, B.-H. & Grishin, N. V. PROMALS3D: a tool for multiple protein sequence and structure alignments. *Nucleic Acids Res.* **36,** 2295–300 (2008).

46. Edgar, R. C. MUSCLE: multiple sequence alignment with high accuracy and high throughput. *Nucleic Acids Res.* **32,** 1792–7 (2004).

47. Sali, A. & Blundell, T. L. Comparative protein modelling by satisfaction of spatial restraints. *J. Mol. Biol.* **234,** 779–815 (1993).

48. Brenke, R. *et al.* Fragment-based identification of druggable "hot spots" of proteins using Fourier domain correlation techniques. *Bioinformatics* **25,** 621–7 (2009).

49. Fan, H., Irwin, J. J. & Sali, A. *Computational Drug Discovery and Design*. 105–126 (Springer New York, New York, NY, 2012).

50. Huang, N., Shoichet, B. K. & Irwin, J. J. Benchmarking sets for molecular docking. *J. Med. Chem.* **49,** 6789–801 (2006).

51. Irwin, J. J., Sterling, T., Mysinger, M. M., Bolstad, E. S. & Coleman, R. G. ZINC: a free tool to discover chemistry for biology. *J. Chem. Inf. Model.* **52,** 1757–68 (2012).

52. Yap, C. W. PaDEL-descriptor: an open source software to calculate molecular descriptors and fingerprints. *J. Comput. Chem.* **32,** 1466–74 (2011).

53. R Core Team (2013). *R: A language and environment for statistical computing.* (R Foundation for Statistical Computing, Vienna, Austria. 2013), http://www.R-project.org/.

54. Kuhn, M. Building Predictive Models in R Using the caret Package. *J. Stat. Softw.* **28,** 1–26 (2008).

55. Hanley, J. a & McNeil, B. J. The meaning and use of the area under a receiver operating characteristic (ROC) curve. *Radiology* **143,** 29–36 (1982).

56. Ito, K. *et al.* Which concentration of the inhibitor should be used to predict in vivo drug interactions from in vitro data? *AAPS PharmSci* **4,** E25 (2002).

CHAPTER 5

Conclusion and Perspective

Metformin is a widely prescribed antidiabetic drug in the biguanide class. Given its negligible metabolism and plasma protein binding[1] as well as low lipophilicity[2], metformin is unlikely to enter cells through passive diffusion, suggesting transporter mediated uptake and efflux. Indeed, studies from our laboratory and others have shown that two members of the organic cation transporters, OCT1 and OCT2, are capable of transporting metformin, and genetic variations in these transporters affect the pharmacokinetics of metformin[3–5]. The glycemic control effect of metformin is generally attributed to decreased gluconeogenesis in the liver, and increased glucose utilization in peripheral tissues[6]. While OCT1 was determined to be the major metformin transporter in the liver, transporter(s) responsible for the peripheral uptake of metformin remain to be discovered.

In contrast to *OCT1* and *OCT2*, expression of *OCT3* is ubiquitous across all tissues, with highest expression in skeletal muscle and adipose tissue. Studies from our laboratory have shown that OCT3 is a low affinity, high capacity metformin transporter comparable to OCT1 and OCT2[7], suggesting that it may be important in the peripheral uptake of metformin. The major goals of this research are to determine the role of OCT3 in metformin disposition and response, identify OCT3 inhibitors that could potentially result in clinical drug-drug interactions when co-administered with

metformin, and develop a method to predict competitive and non-competitive inhibitors of transporters.

In chapter 2, we determine the role of OCT3 in the pharmacokinetics and pharmacodynamics of metformin using *Oct3* knockout mice. Our major findings were that OCT3 played a critical role in both the pharmacokinetics and pharmacodynamics of metformin. In terms of pharmacokinetics, we used both intravenous and oral doses, and concluded that OCT3 has a route-dependent effect on systemic plasma concentrations in mice. That is, after intravenous administration, deletion of *Oct3* resulted in decreased clearance and accumulation of metformin in various tissues, particularly in skeletal muscle and adipose tissue. The decreased clearance was associated with higher systemic plasma levels of the drug. In contrast, after oral administration, Oct3 deletion resulted in no effects on the systemic plasma levels of metformin. In particular, we observed a decreased bioavailability in the Oct3 knockout mice, which together with the decreased clearance resulted in no changes in the systemic plasma levels of metformin. The results suggest an important role of OCT3 in the absorption as well as the elimination of metformin. In terms of pharmacodynamics, our studies demonstrated that *Oct3* knockout mice have reduced response to metformin, as indicated by a reduced effect on oral glucose tolerance tests. In addition, we showed that the effects of metformin on AMPK phosphorylation and glucose transporter 4 expression were significantly reduced in the adipose tissue of *Oct3* knockout mice. Finally, we showed that healthy volunteers with a reduced function 3'UTR variant of *OCT3* also have a reduced response to metformin during an

oral glucose tolerance test. Taken together, our findings establish a major role of OCT3 in the pharmacological action of metformin in both mice and humans.

Given the relevance of OCT3 to metformin disposition and response established in chapter 2, inhibitors of OCT3 could potentially cause drug-drug interactions with metformin and alter its pharmacologic response. To identify potent OCT3 inhibitors, we developed a high-throughput screen (HTS) for OCT3 inhibitors using ASP^+ uptake as a measurement of OCT3 activity in a cell line overexpressing the transporter. We performed the HTS against a library of 2,556 drugs, natural products, and bioactives, and identified 210 compounds that can inhibit ≥ 50% OCT3 activity at 20 μM. Based on predicted IC_{50} values and observed C_{MAX} after therapeutic doses, our data suggest that 23 prescription drugs may potentially cause drug-drug interactions with metformin at clinically relevant concentrations. We then generated a structure-activity relationship (SAR) model capable of discriminating inhibitors and noninhibitors. Using the SAR model, we screened 2,643 registered drugs *in silico*, and identified additional OCT3 inhibitors. Our HTS results validated a valuable methodology for future *in vivo* drug interaction studies, and the predictive SAR model we developed could inform *in vitro* and *in vivo* studies during drug development.

Recently, the U.S. Food and Drug Administration and the European Medicines Agency included transporters in their guidelines for drug interaction studies[8,9], and in the future there will be an increasing demand for detailed studies of inhibitors and substrates of transporters. Thus, tools such as HTS and predictive models can inform

and accelerate *in vitro* as well as *in vivo* studies during drug development. However, as noted in chapter 3, current methods have serious limitations. First, the HTS and SAR models cannot distinguish inhibitors from substrates. Second, the methods do not provide any information on the mechanism of inhibition (competitive *versus* non-competitive). The International Transporter Consortium also commented in 2013 that the knowledge of inhibition mechanisms is currently lacking in the transporter field[10]. Although experimental methods are available to determine the mechanisms of inhibition, the methods are time-consuming and require multiple concentrations of both inhibitor and substrate to accurately understand the kinetic constants and mechanism of interaction. Clearly, a predictive model could greatly accelerate the process. To this end, we attempted to develop a method capable of distinguishing between competitive and non-competitive inhibitors.

In chapter 4, we developed an approach combing *in silico* structure-based modeling and *in vitro* HTS that can accurately predict the mechanism of transporter inhibition. As a proof of concept, we used our method to screen against a prescription drug library for OCT1 inhibitors. Among the 1,780 drugs screened, we identified 30 competitive (orthosteric) inhibitors and 137 non-competitive (allosteric) inhibitors. Select inhibitors from both groups were experimentally tested and the mechanism of inhibition was validated. To demonstrate the utility of our approach beyond current drug space, we conducted a virtual screening of 29,332 endogenous and exogenous metabolites against the structure-based model and a SAR model generated using the HTS data. A total of 146 competitive inhibitors of OCT1 were predicted, one of which,

1-Benzyl-1,2,3,4-tetrahydroisoquinoline (1BnTIQ), was experimentally validated. 1BnTIQ is an endogenous neurotoxin found at higher levels in the cerebrospinal fluid of patients with Parkinson's disease. However, future studies are needed to assess the role of OCT1 in the toxic effects of this metabolite in the brain.

In summary, this dissertation provides evidence for an important role of OCT3 in the pharmacokinetics and pharmacodynamics of metformin, particularly via modulation of metformin accumulation and action in the peripheral tissues. In addition, we developed a novel approach combining *in vitro* and *in silico* methods to characterize the mechanism of inhibition for ligands of membrane transporters. Our results reinforced the idea that membrane transporters are capable of modulating disposition of drugs, but also the pharmacological response. The result also highlighted the need to measure drug levels in target organs and tissues in addition to their systemic concentrations. Future studies are needed to explore the emerging role of membrane transporters in the therapeutic effects of drugs. Additionally, developing new assays and predictive models capable of discerning substrates and inhibitors of transporters in a high-throughput manner could greatly enhance our understating of the mechanisms of transporter-drug interactions and enable the discovery of transporter-targeting or transporter-delivered drugs.

REFERENCES

1. Bailey, C. J. & Turner, R. C. Metformin. *N. Engl. J. Med.* **334,** 574–9 (1996).

2. Graham, G. G. *et al.* Clinical pharmacokinetics of metformin. *Clin. Pharmacokinet.* **50,** 81–98 (2011).

3. Chen, Y. *et al.* Effect of genetic variation in the organic cation transporter 2 on the renal elimination of metformin. *Pharmacogenet. Genomics* **19,** 497–504 (2009).

4. Shu, Y. *et al.* Effect of genetic variation in the organic cation transporter 1 (OCT1) on metformin action. *J. Clin. Invest.* **117,** 1422–31 (2007).

5. Shikata, E. *et al.* Human organic cation transporter (OCT1 and OCT2) gene polymorphisms and therapeutic effects of metformin. *J. Hum. Genet.* **52,** 117–22 (2007).

6. Boyle, J. G., Salt, I. P. & McKay, G. A. Metformin action on AMP-activated protein kinase: a translational research approach to understanding a potential new therapeutic target. *Diabet. Med.* **27,** 1097–106 (2010).

7. Chen, L. *et al.* Role of organic cation transporter 3 (SLC22A3) and its missense variants in the pharmacologic action of metformin. *Pharmacogenet. Genomics* **20,** 687–99 (2010).

8. Guideline on the Investigation of Drug Interactions. *European Medicines Agency: CPMP/EWP/560/95/Rev. 1 Corr.** **1,** (2012).

9. Guidance for Industry Drug Interaction Studies. *U.S. Department of Health and Human Services Food and Drug Administration Center for Drug Evaluation and Research (CDER)* (2012). at <http://www.fda.gov/Drugs/DevelopmentApprovalProcess/DevelopmentResources/DrugInteractionsLabeling/ucm093606.htm>

10. Tweedie, D. *et al.* Transporter studies in drug development: experience to date and follow-up on decision trees from the International Transporter Consortium. *Clin. Pharmacol. Ther.* **94,** 113–25 (2013).

Publishing Agreement

It is the policy of the University to encourage the distribution of all theses, dissertations, and manuscripts. Copies of all UCSF theses, dissertations, and manuscripts will be routed to the library via the Graduate Division. The library will make all theses, dissertations, and manuscripts accessible to the public and will preserve these to the best of their abilities, in perpetuity.

I hereby grant permission to the Graduate Division of the University of California, San Francisco to release copies of my thesis, dissertation, or manuscript to the Campus Library to provide access and preservation, in whole or in part, in perpetuity.

Author Signature  Date December 27th, 2014